

FINAL REPORT

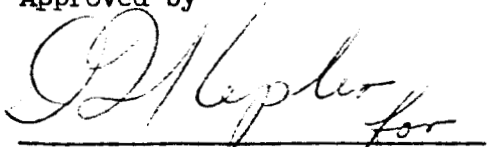
INVESTIGATION OF IN-FLIGHT ROLL
CONTROL TECHNIQUES FOR SOUNDING ROCKETS

Contract No. NAS 5-9628

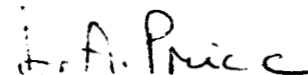
LMSC L-31-65-1

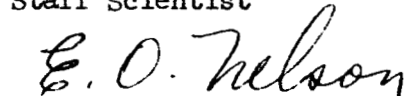
31 December 1965

Approved by


R. L. Nelson
Senior Member
Flight Mechanics
Aerospace Sciences Laboratory

Written by


D. A. Price
Staff Scientist


E. O. Nelson
Research Specialist


J. E. Torrillo
Research Specialist

Prepared by

LOCKHEED MISSILES AND SPACE COMPANY
A Group Division of Lockheed Aircraft Corporation
Palo Alto, California

for

Goddard Space Flight Center
Greenbelt, Maryland

FOREWORD

The work described in this report was performed by Lockheed Missiles and Space Company for the National Aeronautics and Space Administration under Contract No. NAS 5-9628, Investigation of In-Flight Roll Control Techniques for Sounding Rockets. This document represents the final report on the study which was carried out from August through December 1965. The study was conducted for the Sounding Rocket Branch (Code 671) of the Goddard Space Flight Center (GSFC), under the technical cognizance of Mr. J. T. Lawrence.

The purpose of the study was to investigate techniques for maintaining roll control of sounding rockets in the presence of configurational, mass and thrust asymmetries. Three methods for control of roll rate were investigated: Reaction Impulse, Aerodynamic Surface Deflection, and Center of Gravity Shift. The objective of the work was to evaluate the relative merits of these methods for roll control upon the basis of simplicity, weight, size and adaptability to operational and development vehicles and to recommend the most promising approach for further development.

This work represents an outgrowth of the understanding of the roll resonance phenomena experienced by sounding rockets and the establishment of the sources and mechanisms leading to roll lock-in developed in a previous study - The Aerobee 150A Roll Lock-In Study, Contract No. NAS 5-9061 - also conducted for GSFC by LMSC.

The following persons were engaged in the study and their individual contributions are gratefully acknowledged.

R. L. Nelson	Program Director
E. O. Nelson	Reaction and C.G. Shift Analysis
J. E. Torrillo	Aerodynamic Control Surface Analysis
J. D. Vosti	Technical Computation

ABSTRACT

The results of an investigation into techniques for controlling roll rate during the flight of sounding rockets in the presence of configurational, mass and thrust asymmetries are presented. Such asymmetries cause coupling between the pitch and roll modes leading to roll lock-in. Means for maintaining roll control were devised by (1) overpowering the asymmetry effects with auxiliary roll driving moments and (2) reducing the effects of the asymmetries.

Three methods were studied: Reaction Impulse, Aerodynamic Surface Deflection, and Center of Gravity Shift. The relative merits of these methods were evaluated through preliminary design upon the basis of simplicity, weight, size and adaptability to operational and development vehicles.

Tip ailerons mounted on two fins emerged as the most promising roll control device, especially when coupled with a wind driven gyro actuator for programming to nearly constant roll rates. This device is recommended for further development.

The auxiliary roll moment technique and devices which were devised and evaluated for recovery from roll lock-in and catastrophic growth of the angle of attack provide an attractive feature for all flights. A very significant reduction in angle of attack (by a factor of two or three) during passage through roll resonance accrues for

combinations of asymmetries less than the lock-in tolerances. This angle of attack control will provide decreased attitude and trajectory dispersions in the presence of mass, configurational and thrust asymmetries.

TABLE OF CONTENTS

Section	Page
FOREWORD	i
ABSTRACT	iii
TABLE OF CONTENTS	v
LIST OF ILLUSTRATIONS	vi
NOMENCLATURE	viii
1.0 INTRODUCTION	1-1
1.1 Background	1-1
1.2 Study Objectives	1-2
1.3 Technical Approach	1-3
1.4 Plan of Report	1-4
2.0 EVALUATION OF ROLL CONTROL TECHNIQUES	2-1
2.1 Review of Roll Lock-In Phenomena	2-1
2.2 Motion Control Methods	2-5
2.3 Asymmetry Tolerance Contour Improvement	2-8
2.4 Timing Criteria	2-9
2.5 Angle of Attack Control	2-19
3.0 DESIGN EVALUATION	3-1
3.1 Performance Requirements	3-1
3.2 Sensing Requirements	3-2
3.3 Packaging Requirements	3-3
3.4 Mechanization Schemes	3-4
3.5 Description of Control Devices Evaluated	3-8
3.6 Design Comparison	3-15
3.7 Development Plan	3-16
4.0 CONCLUSIONS AND RECOMMENDATIONS	4-1
5.0 REFERENCES	5-1
FIGURES	

LIST OF ILLUSTRATIONS

Figure No.

- 2-1 Axis System and Nomenclature
- 2-2 Pitch Rolling Trim Characteristics
- 2-3 Roll Trim and Asymmetry Tolerances
- 2-4 Motion Control Methods and Tolerance Contour Improvement
- 2-5 Roll Lock-In Equilibrium Equations
- 2-6 Tolerance Contour Comparison
- 2-7 Limiting Trim Asymmetry
- 2-8 Timing Criteria for Roll Control Mode
- 2-9 Breakout Demonstration with Roll Reaction
- 2-10 Breakout Demonstration with Tip Ailerons
- 2-11 Breakout Demonstration with C. G. Shift
- 2-12 Timing Criteria for Pitch Mode
- 2-13 Breakout Demonstration with Pitch Reaction Impulse
- 2-14 Effect of Roll Rate Limit
- 2-15 Verification of Tolerance Contours with Tip Aileron Deflection
- 2-16 Verification of Tolerance Contours with Tip Aileron Deflection
 δ_a Programmed for 2 rps
- 2-17 Tolerance Contours - Fin Tip Aileron
- 2-18 Tolerance Contour Boundary - Pitch Reaction Control
- 2-19 Tolerance Contours for Total Angle of Attack
- 2-20 Demonstration of Angle of Attack Control

LIST OF ILLUSTRATIONS (CONT'D)

Figure No.

- 3-1 Acceleration Environment
- 3-2 Reaction Control Mechanization
- 3-3 C. G. Shift Roll Control Mechanization
- 3-4 Aerodynamic Surface Mechanization
- 3-5 Reaction Impulse Design
- 3-6 C. G. Shift Design
- 3-7 Aerodynamic Glove Design
- 3-8 Tip Aileron Design
- 3-9 Trailing Edge Spoiler Design
- 3-10 Gyro Aileron Design
- 3-11 Spin Rate Programming with Gyro Aileron
- 3-12 Design Comparison

NOMENCLATURE

A	Reference area and cross-sectional area of vehicle, square feet
a	Nozzle offset, inches
b	$R (\bar{q}A/mV\omega) [C_{L_{\alpha}} (1-v) - \sigma (C_{m_q} + C_{n_{p\alpha}})]$
C_{ℓ}	Roll moment coefficient
$C_{\ell\delta}$	Roll moment coefficient due to a differential fin cant, δ , on each fin
$C_{\ell p}$	Roll damping coefficient based on $pd/2V$
$C_{m_{\alpha}}$	Pitch moment coefficient derivative
C_{m_q}	Pitch damping moment coefficient based on qd/V and referred to the center of gravity
$C_{L_{\alpha}}$	Lift coefficient derivative
$C_{N_{\alpha}}$	Normal force coefficient derivative
$C_{n_{p\alpha}}$	Magnus moment coefficient derivative
C_{ℓ_I}	Induced roll moment coefficient
C_A	Axial force coefficient
C_{m_0}	Moment coefficient representing an aerodynamic asymmetry
d	Reference length and diameter, feet
g	Acceleration of gravity, feet per second squared
h	Altitude, feet
I	Pitch moment of inertia, slug-feet squared
I_x	Roll moment of inertia, slug-feet squared
I_{sp}	Specific impulse, seconds
K	Aileron effectiveness ratio, $(1 + \Delta\delta/\delta)$

m	Mass, slugs
PM	Reaction pitch moment, foot-pounds
p	Roll rate, degrees per second
\bar{q}	Dynamic pressure, pounds per square feet
R	57.3 degrees per rad
RM	Reaction roll moment, foot-pounds
r_e	Distance from center of gravity to nozzle throat, feet
r_o	$\sqrt{r_e^2 - (I/m)}$
T	Sustainer thrust as a function of time, pounds
T_o	Time of initiation of control moment, seconds
t_f	Time of termination of control moment, seconds
t_B	Time of sustainer burnout, seconds
V	Velocity, fps
α	Angle of attack in body XZ plane, degrees
α_T	Total angle of attack, degrees
α_{Tmax}	Maximum angle of attack of RPM program, degrees
α_{ST}	Static trim angle of attack, degrees
α^*	Angle of attack for which C_{L_I} changes sign
β	Angle of attack in body XY plane, degrees
Γ	Angle defining the orientation of the center of gravity offset, degrees
ΔCG	Center of gravity offset, inches
Δm	Center of gravity shift, inches
δ	Fin cant angle, degrees
δ_a	Aileron deflection angle, degrees
δ_p	Aerodynamic surface pitch deflection, degrees

$\Delta\delta$	Effective increase in fin cant angle, degrees
ϵ_T	Equivalent angular thrust misalignment, $Ra/12\lambda_0$, degrees
θ	Angle defining the orientation of the thrust misalignment, degrees
λ	Angle defining the orientation of the geometric asymmetry
ν	I_x/I
σ	md^2/I
ϕ	Arctan β/α
ψ	Phase angle ($\lambda - \phi$), degrees
ω	Natural frequency, $R \sqrt{-C_{m\alpha} \bar{q}Ad/I}$, degrees per second

Section 1 INTRODUCTION

1.1 Background to the Study

Roll rate programs are usually introduced in sounding rockets in order to reduce trajectory dispersion caused by vehicle asymmetries and to maintain attitude control. The use of passive means such as differential fin cant introduces an additional requirement for successfully negotiating roll resonance in the presence of configurational, mass and thrust asymmetries. These asymmetries can lead to roll lock-in and subsequent catastrophic growth of the angle of attack, as was demonstrated in the Aerobee 150A Roll Lock-In Study of Reference 1. An explanation of the mechanisms of the resulting roll resonance and angle of attack divergence was developed upon the basis of the equilibrium trim response of the spinning vehicle. It was then possible to specify tolerances on asymmetry combinations (e.g., lateral center of gravity offset and aerodynamic or thrust pitch trim) yielding recovery from roll resonance and subsequent convergence of angle of attack. The evaluation of the influence of the timevarying environment and vehicle dynamic response demonstrated that the criteria based on equilibrium or steady state solutions yield conservative and realistic tolerances.

However, the asymmetry tolerances defined in this manner are difficult to assess with current pre-flight checkout and balancing

procedures. Hence, investigation of means for positive control of the dynamic behavior during flight represented a natural outgrowth of the understanding of the roll resonance phenomena experienced by sounding rockets. Identification of the sources and establishment of the mechanisms leading to roll lock-in suggested several promising techniques for in-flight control of the motion. With this background the present study was embarked upon.

1.2 Study Objectives

This report describes the work accomplished under Contract No. NAS 5-9628, In-Flight Roll Control Techniques for Sounding Rockets, during the period from August through December 1965. The study was performed for the Sounding Rocket Branch (Code 671) of Goddard Space Flight Center, National Aeronautics and Space Administration (NASA), under the technical cognizance of Mr. J. T. Lawrence, Technical Officer.

The purpose of the study is to investigate techniques for maintaining roll control of sounding rockets in the presence of configurational, mass and thrust asymmetries. Three methods for control of the roll rate are being investigated: (1) Reaction Impulse, (2) Aerodynamic Surface Deflection, and (3) Center of Gravity Shift. The objective of the work is to evaluate the relative merits of these methods for roll control upon the basis of simplicity, reliability, weight, size and adaptability to operational and development vehicles and to recommend the most promising approach for further development.

1.3 Technical Approach

The methods of analysis developed in the Roll Lock-In Study of Reference 1 were utilized for the analysis of the roll control techniques. The primary emphasis is placed on dynamic motion response at small angles of attack. The motion behavior control requirements were examined on the basis of the equilibrium trim response for a spinning vehicle. The influence of vehicle dynamics and time varying environment was evaluated numerically with the Roll-Pitch Motion (RPM) program developed for the roll lock-in study and described in Reference 2. This approach proved to be invaluable in the cited study for establishing the sources and mechanisms leading to lock-in and for specifying realistic, conservative asymmetry tolerances. Since the principal forces and moments causing roll lock-in are body-fixed or oriented, corrective measures can be established and executed in the body-referenced axis system. Because of the high pitch damping inherent in current sounding rocket design, dynamic motions about trim are small and well damped. Therefore, dynamic motion effects do not influence the principal trim response to and correction for the asymmetries.

The merit of a given control technique was determined by the amount of improvement in the pre-flight asymmetry tolerances. Mechanization schemes were devised to yield the simplest and most reliable system with minimum interference to the existing rocket design. Although the Aerobee 350 vehicle was used as the basis for evaluation of these schemes, adaptability to other sounding rockets represented a very important consideration.

Preliminary designs were then developed for the Aerobee 350 which provided equivalent improvement in the asymmetry tolerances in order to place the comparison of each device upon a common basis.

1.4 Plan of Report

The results of the investigation are presented in the subsequent sections. The development of the effectiveness of various control techniques, including timing requirements and operational limitations, is presented in Section 2. Section 3 describes the design evaluation made for the mechanization scheme which evolved from the study including a suggested development plan. Principal conclusions drawn from the study and recommendations for further development of the most promising device are presented in Section 4.

Section 2

EVALUATION OF ROLL CONTROL TECHNIQUES

2.1 Review of Roll Lock-In Phenomena

In order to place the present study into the proper perspective, a brief review of the roll lock-in problem is in order. Roll lock-in is construed here to mean maintenance of roll resonance throughout the atmospheric portion of the trajectory. The studies of References 1 and 2 clearly demonstrate that the body-fixed asymmetries such as aerodynamic trim or thrust misalignment and lateral center of gravity offset are the primary sources of roll resonance phenomena.

The definition of these asymmetries and orientation in the body-fixed axis system is illustrated in Figure 2-1. The standard NASA notation for axes, angle of attack, body rates and aerodynamic characteristics is adopted. Pitch trim asymmetries are defined such that the static trim angle of attack, α_{ST} , appears in the first quadrant. The orientation, ϕ , of the total angle of attack, α_T , is measured clockwise from the positive y axis.

The pitch response of the spinning vehicle sets the stage and provides the primary source of energy for loss of roll control. The well known resonant response of the trim angle of attack is reviewed in Figure 2-2 for the Aerobee 350 vehicle. The static trim angle of attack α_{ST} , resulting from a configurational or mass asymmetry, is greatly

magnified in the vicinity of resonance (i.e., $p \approx \omega$), where the aerodynamic stability is reduced or cancelled by the "gyroscopic" stability (Fig. 2-2a). The peak amplification which is determined by the effective damping changes with time along the trajectory as indicated in the figure. Note that large amplitudes are reached only in close proximity to resonance. For sounding rockets such as the Aerobee 150A or 350, the peak occurs virtually at $p=\omega$. The trim angle of attack is greatly reduced for spin rates above resonance $p > \omega$, tending toward zero for large p/ω . The relative orientation of the trim angle of attack with respect to the static trim undergoes a radical shift during passage through resonance as depicted in Figure 2-2b. At resonance, a phase shift ψ close to 90 degrees is encountered and approaches 180 degrees for large p/ω . This phase angle is seen to undergo a large change in the close proximity to resonance ($\pm 5\%$) while the amplification changes little. Thus, large resultant angles of attack (70% of peak amplification) are maintained over a phase shift of ± 45 degrees about resonance.

Coupling between the resultant trim normal force and lateral c.g. offset, plus the induced roll moment from body-fin flow interactions, can then cause serious degradation of the roll moment from fin cant. For sufficiently large pitch asymmetry, induced roll moment in itself can cause roll lock-in. With trim asymmetries smaller than this value, increasing magnitude of lateral center of gravity offset is required to cause roll lock-in.

By using the peak trim angle of attack derived from the equilibrium resonance response for $p=\omega$, the orientation of the body-fixed asymmetries causing the maximum roll rate degradation can be prescribed uniquely.

This arrangement is shown in Figure 2-3a for large angles of attack where the circled signs indicate the direction of the induced roll moment term. The longitudinal asymmetry C_{m_0} (or ϵ) causes a static trim α_{ST} which rotates ninety degrees and grows to $\alpha_T = \alpha_{ST}/b$ at resonance. The resulting normal force and the lateral c.g. orientation combine with the negative induced roll moment to cause the greatest roll moment degradation with this orientation in the body.

This coupling is illustrated in Figure 2-3b for two times in the flight as a function of proximity to resonance. The total rolling moment coefficient resulting from fin cant and damping ($\delta C_{l_\delta} + C_{l_p} p d/2V$), induced roll (C_{l_T}) and normal force-lateral c.g. coupling ($\Delta CG C_{N_\alpha} \alpha_T$) is given as functions of the spin parameter p/ω . Only fin damping is varied with flight time in this example, as depicted by the change in slope. Early in the flight, the fin cant driving moment can be cancelled by induced roll moment alone (point C_1), lateral c.g. offset alone (C_2), or the combined effects of induced roll and c.g.-normal force coupling (C_3). With increasing time, the intersections move from C_1 , C_2 , and C_3 to D_1 , D_2 , and D_3 , respectively, at the peak magnification of the trim angle of attack. If the peak trim angle of attack and, hence, the peak asymmetry rolling moment coefficient C_{l_T} (points D), grows faster than the fin cant line rotates, roll resonance continues throughout the atmospheric portion of the flight (i.e., roll lock-in). When the fin cant line rotates above the peak D, only the solution B exists, and hence, breakout from roll resonance occurs. Thus, the tangency point D_3 represents the maximum allowable asymmetries for breakout from roll resonance. Because the magnitude of the induced roll moment and the c.g.-normal force coupling depend upon angle of attack, points D can also be utilized for specifying

asymmetry tolerances in order to limit the angle of attack to a predetermined maximum.

With this "worst condition" arrangement for peak α_T , c.g. location and C_{L_T} , the lateral c.g. offset required to maintain roll resonance (i.e., $p=\omega$) is known throughout the trajectory for a given magnitude of the pitch trim asymmetry (C_{m_0} or ϵ). Evaluation of an appropriate range of trim asymmetries yields the maximum angle of attack and roll lock-in tolerance contours depicted in Figure 2-3c for a given vehicle and specified trajectory. Asymmetry combinations below and to the left of the tolerance contours will always break out from roll resonance or not exceed the angle of attack limitation. However, significant motion disturbances may occur. The angle of attack limit will be exceeded or lock-in will occur for some arrangement of the asymmetry combinations lying above or to the right of the corresponding tolerance contour.

The intercept (i.e., $\Delta CG = 0$) occurs at the resonance time for the nominal roll rate program. Time of breakout from roll resonance then increases with higher magnitudes of ΔCG . In essence, for asymmetry combinations along the contour, roll resonance begins at the intercept time and continues until the time of breakout indicated (e.g., 42 seconds for $\Delta CG = 1.0$ inch). It should also be noted that along the lock-in contour the angle of attack is everywhere equal to the critical value α^* where the induced roll moment changes sign (Ref. 1,2,5).

Now the contours of Figure 2-3c represent the asymmetry tolerances that must be observed in pre-flight preparation and checkout of the sounding rocket to avoid roll lock-in or an angle of attack limit. While current estimates of thrust misalignment magnitudes (about 0.1 degree from

the geometric centerline) are well within the tolerance contours for a fin cant of 0.3 degree, the region is severely restricted for 0.15 degree cant. In addition, if the thrust misalignment is measured from the vehicle centerline, an additional thrust asymmetry is introduced by the c.g. offset. In other words, the thrust asymmetry is specified with respect to the center of gravity position.

2.2 Motion Control Methods

Two methods are available for breaking out from roll resonance for combinations of asymmetry above the asymmetry tolerance depicted in Figure 2-3c. These are: (1) overpower the asymmetry roll moment or (2) reduce the asymmetry roll moment directly. The former can be accomplished by an auxiliary roll moment to increase the roll driving moment from the fin cant. The latter method can be accomplished by reducing angle of attack or displacing the c.g. appropriately. The three techniques for in-flight roll control investigated represent different hardware approaches to these two methods or combinations thereof. The three main categories of roll control techniques studied were (a) reaction impulse, (b) aerodynamic surface deflection, and (c) lateral center of gravity displacement.

The mechanism for accomplishing the roll rate increase or angle of attack reduction is illustrated in Figure 2-4 in terms of the total rolling moment coefficient. The conditions represented by the tolerance contours are reproduced here from Figure 2-3b by the solid curves. If the asymmetry combination exceeds the tolerance contour, roll resonance occurs at point E_1 and will remain locked in throughout the entire flight (point E_2).

Application of a rolling moment ($A \rightarrow B$) by means of a reaction moment (RM) or tip aileron deflection (δ_a) will increase the effective fin driving moment above the asymmetry moment and provide breakout to point F. With removal of the auxiliary roll moment at a later time ($G \rightarrow H$), the solution will gravitate toward point F'. Since breakout will occur for the tangency condition, the applied moment can overcome a larger magnitude of either ΔCG or C_{m_0} and ϵ depicted by point E_3 .

In a similar manner, the application of a pitching moment (PM) or a lateral c.g. shift can reduce the magnitude of the asymmetry roll moment as shown in Figure 2-4b. The pitch moment (PM) reduces the angle of attack, thereby decreasing the magnitude of the normal force and the induced roll moment C_{L_T} . The c.g. shift (Δm) acts directly on the normal force coupling ($\Delta CG - \Delta m$). In either case, the nominal fin driving moment exceeds that caused by the asymmetries and drives the roll rate toward point F. When the auxiliary moments are released, the solution gravitates toward point F'. Again, the applied moments can overcome a larger asymmetry combination of ΔCG , C_{m_0} or ϵ equivalent to raising point E_3 to D_3 .

This is exactly the procedure used to establish the tolerance contours of References 1 and 2. Therefore, a new tolerance contour can be established by considering the aileron deflection, reaction moment, or c.g. shift to be acting throughout the entire trajectory, as depicted in Figure 2-4c. A typical point on the original contour shifts from A to A' for a c.g. shift, reaction roll moment impulse or aileron deflection, and to A'' for a reaction pitch impulse or a pitch aerodynamic surface deflection (δ_p). This solution technique can be applied equally well to the limit angle of attack contours or the roll lock-in contours. As a matter

of fact, in the process of assessing the roll lock-in contours, the angle of attack limit contours are determined also. The orientation of the "worst condition" is altered by 45 degrees to account for the change of sign of induced roll moment at angles of attack smaller than the critical value α^* .

The equations used to compute the improved tolerance contours are presented in Figure 2-5. With the arrangement of asymmetries shown in Figure 2-3a, the equations of motion (Ref. 1,2) reduce to a particularly simple form under the assumption of roll resonance ($p=\omega$). The first equation in Figure 2-5 represents the lateral c.g. offset necessary to maintain roll rate at the pitch natural frequency for the resonant trim angle of attack of the second equation. The reaction roll moment RM and pitch moment PM have been incorporated into the ΔCG and α_T equations, respectively. Aerodynamic surface deflections were treated as an effective change in δ for roll and C_{m_0} for pitch control. Center of gravity displacement is represented by an effective change in thrust asymmetry ϵ and a bias of ΔCG . When $\Delta CG \equiv 0$, the intercept solutions reduce to particularly simple forms as illustrated by the lower formulae. Note that all quantities in the equations are known for a given vehicle and trajectory profile. Furthermore, no restriction on vehicle and aerodynamic characteristics other than small angle linearity has been imposed. Hence, determination of the allowable asymmetries becomes a straightforward process for either roll lock-in or maximum angle of attack limit with a fixed magnitude of control moment applied throughout the trajectory.

2.3 Asymmetry Tolerance Contour Improvement

The improvement in the roll lock-in tolerance contours for representative control moment magnitudes are summarized in Figure 2-6a for aerodynamic trim asymmetry and in Figure 2-6b for thrust asymmetry individually. Combined aerodynamic and thrust trim asymmetry effects were shown in References 1 and 2. Magnitudes of the applied control moments have been selected to yield about equivalent improvement in the tolerance contours. Very significant increase in tolerable asymmetry levels to avoid roll lock-in is evident. For example, a roll reaction impulse increases the aerodynamic trim asymmetry intercept by 41 percent from 0.83 to 1.17 and the thrust asymmetry by 60 percent from 1.55 to 2.48. With a center of gravity offset of 0.9 inch, the corresponding increase is 138 percent and 186 percent for C_{m_0} and ϵ , respectively. In Figure 2-6a, the roll reaction impulse and pitch aerodynamic surface deflection are seen to essentially shift the original contour to a higher C_{m_0} . The c.g. shift technique raised the original contour an amount equivalent to the c.g. displacement less the effect of the induced thrust misalignment. The pitch reaction impulse yields an increasingly larger C_{m_0} with larger ΔCG because of the greater effectiveness of the reaction impulse with decreasing dynamic pressure later in the trajectory. In Figure 2-6b, the roll and pitch reaction moments were selected to yield an identical improvement in the ϵ intercept. In this case, the pitch moment (PM) provides a shift in the original contour to larger ϵ . The c.g. shift technique again raises the original contour to a higher ΔCG but also shifts to a lower ϵ by the amount of the induced thrust misalign-

ment. The tip roll aileron is seen to be more effective for smaller ΔCG levels while the pitch surface deflection appears equivalent to the roll reaction impulse.

2.3.2 Limiting Trim Asymmetry

The improved contours shown in Figure 2-6 were developed for somewhat arbitrary magnitudes of control moments. These results suggest unlimited improvement with increasing control magnitudes. However, trajectory and vehicle characteristics limit the improvement as illustrated in Figure 2-7 for the intercept trim asymmetries, C_{m_0} or ϵ . The value of the intercept depends only upon the time of resonant altitude (for $\delta = 0.3$ degree, $t = 32$ seconds, so that $C_{m_0} = 0.82$ and $\epsilon = 1.53$). Application of a roll moment yields a new resonance time ($t = 29$ seconds for $R_m = 500$ ft/lb, for example), resulting in $C_{m_0} = 1.17$ and $\epsilon = 2.47$ degrees from Figure 3-7. This corresponds to the intercept magnitudes shown in Figure 2-6a and b for $R_m = 500$ ft/lb. This procedure suggests that for sufficiently large control magnitudes it may be possible to eliminate tolerances altogether. However, operational limits such as maximum roll rate within the atmosphere or maximum vacuum roll rate will restrict the usable increase as discussed later.

2.4 Timing Criteria

The timing criteria depends upon the magnitude of improvement in the tolerance contours desired (C_{m_0} or ϵ) and the absolute value of ΔCG to be accommodated. The timing criteria adopted are summarized in

Figure 2-8 for the roll control mode and in Figure 2-12 for the pitch control mode. Breakout demonstrations with these criteria are presented in Figure 2-9 through 2-11 for the roll mode and in Figure 2-13 for the pitch mode.

2.4.1 Roll Control Mode

Consider the improved tolerance contour shown in Figure 2-8a for which roll lock-in would obviously occur without the applied control. Since $\alpha_T = \alpha^*$ everywhere along the contour, a particular trajectory time is associated with each trim asymmetry magnitude (C_{m_0} or ϵ). Hence, constant time contours are vertical such as depicted for points 3 and 5.

For the sake of clarity, the development of the roll control mode criteria will be traced for an effective change of fin cant angle from δ_1 to δ_2 . The new intercept trim asymmetry (say $C_{m_{02}}$) corresponds to an earlier time t_2 , the time at which nominal resonance occurs for a fin cant of δ_2 . The rolling trim angle of attack response with the new intercept magnitude for the fin cant angles δ_1 and δ_2 is depicted in Figure 2-8b. The point AA establishes the intercept trim asymmetry since $\alpha_{Tmax} = \alpha^*$. The variation of α_{Tmax} and α^* with time are shown by the dashed contours. Application of the control impulse at t_2 is inherently conservative since α_T cannot increase above α^* due to the increase of the roll rate above resonance. However, for equilibrium conditions, the control impulse can be applied at any time where $\alpha_T = \alpha^*$ such as point BB. The trim condition after control application is point CC on the response curve for δ_2 . But this timing is no longer conservative "a priori" because of the over-

shoot of the dynamic motion response possibly exceeding α^* as depicted by the dash-dot curve. The condition yielding minimum overshoot is point EE which was selected as the initiation time criteria. This time of crossover of the response curves t_0 is a unique function of the resonance times t_1 and t_2 and independent of the magnitude of the trim asymmetry. The resultant trim response is then illustrated by the cross-hatched curve.

The termination time t_f selection is illustrated in Figure 2-8 for the c.g. asymmetry magnitude ΔCG_3 . The angle of attack response for the corresponding C_{m02} on the new tolerance contour, as indicated by the heavy solid lines, would reach α_{Tmax} at t_2 (AA) if the fin cant δ_2 were applied throughout the trajectory. During resonance, the peak magnitude α_{Tmax} grows to α^* at t_4 , at which time breakout from resonance and subsequent reduction of α_T (DD) occurs. However, at this time in the trajectory with C_{m04} , the allowable magnitude of lateral c.g. offset is ΔCG_6 corresponding to point 6 on the original contour without control. Therefore, the control must be maintained until the time corresponding to ΔCG_3 on the original contour.

When the fin cant δ_2 is applied at t_0 (EE), the angle of attack response follows the cross-hatched contour until release at t_f (CC). The trim jumps to point BB where the α_T must be less than $\alpha^* \Delta CG_3 / \Delta CG_5$. This amounts to maintaining the applied control until at least t_3 , corresponding to ΔCG_3 on the nominal tolerance contour. The combined roll disturbance at point BB is then less than that required to yield $p=\omega$.

The contour improvements were verified with dynamic solutions via the RPM computer program utilizing the timing criteria illustrated in

Figure 2-8. The results are indicated by the symbols spotted on Figure 2-6. The open symbol depicts breakout from roll resonance while the solid symbol indicates roll lock-in. A reduced degree of conservatism is shown for control application contours by comparison with the proximity of the closed symbols to the original contours.

Representative breakout cases with roll reaction moment applied are presented in Figure 2-9. Figures 2-10 and 2-11 demonstrate recovery from roll resonance for typical points on the improved contours for the tip aileron and c.g. shift techniques, respectively. All cases are seen to develop the familiar growth of angle of attack until breakout from roll resonance occurs when the peak angle of attack magnification is reached for the dynamic response. The total angle of attack response is not greatly altered but the phase orientation is significantly improved by the applied roll control moment or the reduced roll coupling resulting from the c.g. displacement. In general, the dynamic motions with applied control exhibit the same characteristics observed for those cases along the original contours without control.

The range of times used in Figure 2-9 indicates that the initiation time based on equilibrium criteria is not critically sensitive to variations in nominal roll rate history and pitch stability (i.e., ω). The response to tip aileron roll moment shown in Figure 2-10 demonstrates a significant reduction in the angle of attack response for the equilibrium trim criteria. The roll rate response (Figure 2-10c) exhibits a short duration recapture to resonance until final breakout occurs at 33 seconds. Note in the α - β locus of Figure 2-10a that a similar trim growth occurs but displaced about 90 degrees in phase.

The c.g. shift case of Figure 2-11 exhibits a slightly different response than the direct application of roll moment. In this case, the c.g. is prepositioned in order to utilize the resonant trim force to increase roll rate. Hence the angle of attack response is changed little--only the coupling is reduced to yield breakout. The oscillation of the resultant angle of attack about the new trim well above resonance (point CC of Figure 2-8b) is clearly demonstrated in Figures 2-10a and 2-10b. The roll rate response departs only momentarily from the nominal profile as shown in Figure 2-10c.

2.4.2 Pitch Control Mode

The timing criteria for the pitch control mode is similarly illustrated in Figure 2-12. The initial time t_0 is determined by the intersection of the resonant response curves for the nominal resonance time t_1 and the psuedo resonance time t_2 corresponding to the intercept $C_{m_{o2}}$ in Figure 2-12a. The angle of attack then follows the cross-hatched contour of Figure 2-12b. This yields a peak $\alpha_T = \alpha^*$ at t_1 for the applied control moment with consequent breakout from roll resonance. The termination time again depends upon the magnitude of c.g. tolerance to be accommodated (e.g., ΔCG_3). With the asymmetry combination of point 4 acting, the angle of attack response follows the curve labeled $C_{m_{o4}}$ in Figure 2-12c until t_0 , when the pitch control moment is applied. Thereafter the response follows the curve for $C_{m_{o3}}$, breaking out of resonance at t_3 and with subsequent reduction of angle of attack to point CC. Release of the control moment at t_f causes a jump to point BB. The angle of attack α_T must be less than $\alpha^* \Delta CG_3 / \Delta CG_5$ at point BB in order to prevent reoccurrence of

roll resonance due to the c.g.-normal force coupling. This corresponds to maintaining the pitch control moment until at least t_3 .

The verification for this pitch mode timing criteria is illustrated in Figure 2-13 for a pitch reaction moment applied at several times encompassing the equilibrium criteria. Figures 2-13a and 2-13b show the angle of attack response follows the trim equivalent to the reduced trim asymmetry (C_{m03} of Figure 2-12). A slight increase in magnitude occurs due to the change in pitch stability and damping with flight time. Roll resonance of Figure 2-13c is little changed with PM until breakout occurs.

2.4.3 Effect of Roll Rate Limitations

The duration of the control moment application for the improved tolerance contours of Figures 2-6a and 2-6b were sufficient to handle a maximum ΔCG of 1.0 inch. Reduction of the duration to minimize energy requirements (e.g., reaction impulse) or to satisfy an operational limit such as maximum roll rate can lead to a significant restriction of the usable improvement in the contours. The effects of a roll rate limitation upon the maximum contour improvement is illustrated in Figures 2-14 through 2-16 for the tip aileron roll control technique. The spin limit is based on the roll rate attained at termination of the roll control with no asymmetries acting.

By increasing the magnitude of the applied control to the equivalent of fin cant angle of 1.0 degree, a fourfold increase in the $\Delta CG-C_{m0}$ tolerance contour can be achieved. The comparison is shown in Figure 2-14. The intercept magnitude of 4.47 corresponds a new resonant time of 16.5 seconds indicated by the upper plot of equilibrium spin rate and aero-

dynamic pitch frequency. Utilizing a 1.5 degree fin cant would appear to yield an infinite intercept tolerance, since at booster burnout the roll rate is already above resonance. However, since the roll rate history in both cases parallels the aerodynamic pitch frequency, an extended period of resonance could occur for small differences in fin cant or pitch stability. Hence, fin cant angles up to 1.0 degree (or the equivalent for other techniques) probably represent a reasonable upper limit.

It is immediately apparent from Figure 2-14 that imposition of a maximum roll rate limit of 2 rps, for example, will constrain the usable improvement in the tolerance contour. Along the original contour for $\delta = 0.3$ degree, the intercept C_{m_0} of 0.83 occurs at 32.1 seconds (point EE). The equilibrium roll rate reaches 2 rps at 45.8 seconds (FF), which corresponds to $\Delta CG = 1.35$ inches on the tolerance contour. Hence, the Aerobee 350 vehicle can accommodate a range of $C_{m_0} = 0.83$; $\Delta CG = 0$ to $C_{m_0} = 0.15$; $\Delta CG = 1.35$ inches with no control application under the constraint of a maximum roll rate of 2 rps. Application to other deflections yields the 2 rps spin rate boundary shown in Figure 2-14.

With a deflection from $\delta = 0.3$ degree to $\delta = 0.5$ degree (point AA to BB) as prescribed by the initiation timing criteria of Figures 2-8 and 2-12, limiting roll rate is reached at 36 seconds (CC). Release of the control deflection to point DD corresponds to an allowable ΔCG of 0.4 inch on the original contour rather than 1.12 inches on the control contour for $\delta = 0.5$ degree. Since the angle of attack is equal to α^* along any of the contours, the ΔCG of point CC would cause roll resonance again. Hence, a ΔCG of 0.4 inch represents the maximum allowable along the control contour (point DD'). The asymmetry contour is then represented by

EE' to DD' (on the $\delta = 0.5$ degree curve) to DD (at constant ΔCG) through FF (on the original contour). Thus, in order to accommodate a ΔCG of 0.83 inch, the control application of $\delta = 0.5$ degree must be maintained until 42 seconds, which results in a maximum roll rate of 2.75 rps.

If the 2 rps constraint is applied to the fin cant of 1.0 degree, the value of the control is completely negated. This is illustrated in Figure 2-14 by the points labeled ABCD. After fin deflection from A to B, the roll rate attains 2 rps at C (20.5 seconds). Return to $\delta = 0.3$ degree (D) returns the roll rate to below resonance with subsequent roll lock-in after point EE, because the asymmetry combination is well above the original contour. In order to handle the $\Delta CG = 0.83$ inch and $C_{m_0} = 2.75$ combination, the control application must again be maintained until 42 seconds.

This requirement is illustrated in Figure 2-15 for an intermediate asymmetry combination of $C_{m_0} = 1.5$ and $\Delta CG = 0.83$ inch. In Figure 2-15a a termination time $t_f = 20.5$ seconds, corresponding to point C of Figure 2-14, merely returns the roll rate to well below resonance (point D in Figure 2-14) with subsequent roll lock-in. Increasing t_f to 33 seconds returns the roll rate to just above resonance, where it is immediately locked in. Not until $t_f = 42$ seconds does the roll rate remain above resonance and continue to grow. However, the roll rate has significantly exceeded the vacuum roll rate for $\delta = 0.3$ degree as well as the 2 rps limit within the atmosphere. The α - β locus of Figure 2-15b illustrates an identical growth and phase change toward the new trim until the control is released. For $t_f = 20.5$ seconds, the angle of attack converges to the below resonance trim and subsequently grows in the familiar pattern

during roll resonance. For $t_p = 33$ seconds, the immediate return of the roll rate to slightly above resonance causes a growth of the angle of attack in a clockwise direction to the equilibrium orientation midway between the fins. When held until $t_p = 42$ seconds, the angle of attack continues to converge to the trim value well above resonance after release of the control deflection. Figure 2-15c depicts the resultant angle of attack behavior compared to the equilibrium trim response. The initial growth above trim is caused by the nearly 180 degrees phase shift to the new trim for $\delta = 1.0$ degree, which is well above resonance. This trim change causes the dynamic motion about the new trim observed in Figure 2-15b. Release of the control deflection at $t_p = 20.5$ seconds then allows growth of the trim toward 20 degrees at nominal resonance. For $t_p = 33$ seconds, the angle of attack again grows from a very small magnitude toward the resonant trim value ($\alpha_T > 20$ deg) and locks in because of the large asymmetry combination. But with $t_p = 42$ seconds, the roll rate is sufficiently far above resonance to prevent return to roll resonance.

The resulting asymmetry contour in Figure 2-14 is then given by points C' to C (on the $\delta = 1.0$ degree curve) to GG' (at constant ΔCG) and through FF (on the $\delta = 0.3$ degree curve). Thus, it is seen that the usable improvement in the contour is determined by the maximum ΔCG desired. The roll rate limitation then determines the increase of C_{m_0} or ϵ possible.

Thus, the simple impulse application of the roll control can result in very high roll rates within the atmosphere and hence restrict the amount of improvement possible in the asymmetry tolerances. However, with fin deflection programming to maintain 2 rps roll rate, the major portion of this potential improvement can be regained. This procedure

is demonstrated in Figure 2-16 for the asymmetry combinations designated by the diamond symbols in Figure 2-14. For the trim asymmetry of $C_{m_0} = 1.5$, it was necessary to reduce the ACG from 0.83 inch (on the 2 rps boundary) to 0.7 inch to obtain breakout from roll resonance, as shown in Figure 2-16a. The case with $C_{m_0} = 1.0$ being well below the 2 rps boundary exhibited the predicted breakout behavior. The explanation for the lock-in case is found in the roll rate response. For these cases, the fin deflection program was based on the equilibrium roll response. Consequently, the dynamic roll rate attained only 1.92 rps due to lag effects as shown in Figure 2-16b. The case which locked in ($ACG = 0.83$ inch, $C_{m_0} = 1.5$) is well above the 1.9 rps boundary, whereas the two cases which broke out from roll resonance are either on or below this curve. Hence, by appropriately adjusting the roll deflection program to provide 2 rps in the dynamic case will yield the same effectiveness as the fixed deflection with no roll rate limit.

2.4.4 Usable Tolerance Contour Improvement

The asymmetry tolerance contours for various roll rate limitations can be constructed from information such as presented in Figure 2-14. Example tolerance contours for fin tip aileron deflections are given in Figure 2-17a for aerodynamic trim and in Figure 2-17b for thrust asymmetries. The spin limit curves represent the usable tolerance combinations for fin deflection programming, as indicated by the cross-hatching for 2 rps and $\delta = 1.0$ degree. With a fixed fin deflection to 0.75 degree and a 3 rps spin limit, the lower boundary results -- a considerable

reduction of the allowable asymmetry tolerances.

The final tolerance contours with pitch control follow a similar pattern but without a roll rate limit other than the roll rate compatibility with the nominal fin cant. The maximum desired ΔCG tolerance establishes the termination time t_f (e.g., point DD of Figure 2-14). The resulting tolerance boundary for the pitch reaction moment of 4000 ft-lb is illustrated in Figures 2-18a and 2-18b for aerodynamic trim and thrust asymmetries, respectively, with a ΔCG tolerance of 0.5 inch. The corresponding boundaries for other techniques can be similarly constructed.

2.5 Angle of Attack Control

The control procedures described thus far have been applied to breakout from roll resonance in order to avoid roll lock-in. While these analyses provide a spectacular demonstration of the efficacy of the control techniques, large motion disturbances and angles of attack are generated in the process.

The same control procedures will apply equally well to maintaining the angle of attack to within a prescribed limit. The roll lock-in tolerance contours are determined for the condition where $\alpha_T = \alpha^*$, which varies throughout the trajectory. The corresponding contours are evaluated for the appropriate worst condition arrangement (i.e., negative induced roll moment) at the selected angle of attack.

Significant improvement in the tolerance contours for a four degree angle of attack limit is achieved by means of a fin deflection to 0.5 degree, as illustrated in Figure 2-19. A twofold increase in the trim

asymmetry intercept magnitude is obtained for C_{m_0} while an almost three-fold increase results for ϵ .

Similarly, the timing criteria developed for the roll lock-in case applies directly to angle of attack control. In addition, the initial timing criteria of Figure 2-8 (point EE) provides an angle of attack significantly less than the prescribed limit. This reduced angle of attack response is illustrated in Figure 2-20 for the C_{m_0} and ϵ intercept. The peak angle of attack for the nominal roll program ($\delta = 0.3$ degree) is 6.3 degrees or 57 percent above the limit due to dynamic lag effects. With roll control, the peak response is reduced to 2.2 degrees or to 55 percent of the limit (four degrees).

Thus, the control techniques designed to decrease susceptibility to roll lock-in can provide a powerful means for controlling angle of attack within acceptable limits for every flight.

Section 3

DESIGN EVALUATION

The objective of the design evaluation is to provide a relative comparison of weight, complexity, size and adaptability to operational and development vehicles. The analysis was carried to sufficient depth to clearly demonstrate the relative merits of each method of roll control in order to recommend the most promising approach for further development.

3.1 Performance Requirements

The approach was to select the performance requirements for each technique based on a representative and significant improvement in the asymmetry contours as discussed in Section 2. The performance capability described in Figure 2-6 for each method has been selected for design comparison. The sizing of the applied moment was adjusted to yield a common intercept magnitude of the trim asymmetry. For example, the control magnitude for roll reaction moment equivalent to an effective fin cant increase of 0.2 degree is $RM = 1372 \text{ ft-lb}$. The corresponding equivalent magnitudes for each technique are shown in the following table, column I in terms of an 0.2 degree fin cant increment and column II with respect to a 500 ft-lb roll reaction moment.

Technique	I	II
Roll aileron, $\Delta\delta_a$ -deg	0.2	0.10
Roll reaction, RM-ft-lb	1372	500
Pitch reaction, PM-ft-lb	11,000	4,000
C.G. shift, Δm -inch	0.62	0.30
Pitch aileron, $\Delta\delta_p$ -deg	0.25	0.125

It is seen that significant differences in performance requirements can occur depending upon the standard of comparison. On this basis, the values listed in column II were selected for the design comparison.

3.2 Sensing Requirements

The impulse roll control technique, whether reaction or aerodynamic surface, requires only a timer for initiation of the control action if no roll rate limitation is imposed. With a maximum roll rate limit, a termination time signal is required in addition. The pitch control and c.g. shift roll control techniques require, in addition, a determination of the orientation of the pitch trim asymmetry.

The most direct measure of the trim asymmetry is the resulting trimmed normal force. By adequate filtering or damping of the sensor, the motions about trim can be eliminated. The magnitude of the trim normal acceleration is sufficiently large as depicted in Figure 3-1 for an assumed one degree trim angle of attack to distinguish from the centripetal acceleration from roll or even to provide direct actuation of the control mechanism. For example, at the nominal resonance time of 32

seconds, the aerodynamic normal force acceleration is 15 g's per degree angle of attack compared to about 4 g's centripetal at the fin tips.

The roll moment method requires only timing signals to initiate and terminate the roll reaction impulse or aerodynamic surface deflection of fixed magnitude. For a selected nominal roll rate program and given control magnitude, the timing can be preset. Since the direction of the applied control moment is known (i.e., to aid the fin cant moment), knowledge of the orientation of the trim asymmetry and c.g. offset is unnecessary. On the other hand, use of pitch control and c.g. shift require determination of the arrangement of the trim asymmetry early in the flight (i.e., prior to resonance). The roll moment augmentation method appears most attractive from this viewpoint because of reduced complexity.

3.3 Packaging Requirements

Two locations within the Aerobee 350 vehicle have been selected for placement of the control device: (1) a one-diameter body extension immediately forward of the sustainer pressurization tank (Sta. 110.0 of Space General Drawing No. 1102000) and (2) within the fins. Location 1 has the advantages of unencumbered volume, good pitch moment arm, and close to the electrical umbilical from the service tower. It has the disadvantages of added structural weight, increasing vehicle length and small roll moment arm.

Location 2 has the advantages of a large moment arm in both roll and pitch, minimum additional structure and no configuration change. Its disadvantages are restricted volume and distance from electrical umbilical.

The basic ground rule being observed for the design evaluation is that no changes to the launching facility be required, especially concerning fin span.

3.4 Mechanization Schemes

A number of preliminary mechanization schemes are presented in Figure 3-2 for the reaction impulse technique, Figure 3-3 for the center of gravity shift technique, and in Figure 3-4 for the aerodynamic surface deflection technique.

Reaction jets can be mounted in either a body extension or on the trailing edge of the fins, as shown in Figure 3-2a for roll and in Figure 3-2b for pitch control. Only two diametrically opposed nozzles are needed for roll since the desired direction of the control moment is known. Stored gas units were considered but eliminated upon the basis of weight since a hydrogen peroxide cold gas system would weigh about one-third more than solid motors due to the lower specific impulse. Packaging the roll impulse device in the body extension increases the propellant weight by a factor of about four due to the smaller moment arm available.

The pitch reaction system of Figure 3-2b was eliminated from contention on the basis of preliminary weight estimates alone. With a fin-mounted unit, a thrust level of about 330 pounds is required for the 4000 lb-ft pitch moment. The corresponding propellant weight is then 23 pounds for one thruster. Since four units are required to accommodate any orientation of the trim asymmetry, a total weight on the order of 200 pounds is required, including inert and sensor weights. About 25 percent smaller weight is required for the thruster units when mounted

in the body extension due to the increase in moment arm about the center of gravity. Therefore, only the roll reaction mechanization schemes of Figure 3-2a were evaluated.

Possible mechanization schemes for the c.g. shift technique are shown in Figure 3-3a for stored pressure actuation and in Figure 3-3b for acceleration actuation. The body-mounted arrangement consists of a tube with the transfer weight initially restrained slightly offset from the vehicle centerline. The resulting pendulum effect aligns the tube with the normal acceleration caused by the pitch trim asymmetry early in the flight. For a given acceleration threshold, the transfer weight is released and slides to the end of the tube where it bursts a diaphragm. Pressurized gas from the storage tank then expands into the cylinder and forces the control mass to the opposite end of the tube and also locks the tube orientation. This shifts the vehicle center of gravity such that during passage through resonance the c.g.-normal force coupling increases the roll rate. Relative low pressure in the tube is required to transfer the control mass. For example, at nominal resonance (32 seconds) with the maximum trim asymmetry (α^*), a pressure of 61 psi will provide a 1 g acceleration to the control mass in a three-inch diameter tube.

By utilizing the same transfer methods in the fin location, assuming mercury as the control mass, the weight can be reduced by about 77 percent due to the longer transfer distance. However, since transfer in the plane of the fins or midway between fins only can be achieved, the control mass allowance must be doubled. Hence, only a 55 percent reduction in weight over the body mounting can be attained with the fin tip arrangement. Another possible control mass transfer method is to utilize

a piston to develop differential pressure on the mercury tanks in the fins, as shown in Figure 3-3b. The acceleration of the mercury and piston is made up of the sum and difference of the centripetal and normal acceleration on opposing fins. The resulting pressure difference then transfers the mercury to the opposite tank. A means for latching the pistons after transfer is required to prevent backflow with rotation of the trim normal acceleration vector in the body. Some increase in weight for the pistons is required for this method.

Several schemes for aerodynamic surface deflection are shown in Figure 3-4. The glove technique of Figure 3-4a provides a roll impulse by detaching appropriate trailing edge sections of the fin. The original symmetrical fin contour is maintained until the initiation time (t_0) when the right side glove on the upper fin (left-hand side on lower fin) is detached to provide an effective tip aileron deflection. At the selected termination time (t_p), the opposite glove on each fin is removed, returning the fin to symmetry and nearly the original roll rate programming. The weight will be in proportion to the area of the glove to the fin's area and weight. Another approach is to place the glove over the complete fin tip without any alteration to the existing fin. This thickening of the fin tip may interfere with the launch tower, however.

A second scheme for roll control is the fin tip aileron or trailing edge flap of Figure 3-4b. The spring-loaded tip aileron can be triggered for an increased roll deflection at the specified initiation time. At the termination time, this spring is released, allowing a secondary spring load to return the aileron to zero deflection. A two-event timer and pin puller device are required. A small stored gas actuator could be

used in place of a mechanical spring. Relative small aileron deflection is required to achieve the selected contour improvement. For example, with an aileron area of six percent of the total fin area, a deflection angle of about 1.5 degrees is required to yield an effective fin cant increase of 0.1 degree. A trailing edge flap of the same area would require about 2.8 degrees deflection angle. It may be possible to eliminate the spring or gas actuation by using unbalanced flaps deflected by the normal acceleration, as indicated with the bottom fin in Figure 3-4b. For roll control, the deflection is allowed in one direction, which requires a split unbalance mass.

Pitch control can be handled by the same size ailerons or flaps as for the roll control. The unbalanced canard or fin surfaces, as shown in Figure 3-4c, can provide a proportional deflection for the static trim asymmetry (i.e., zero roll rate). The balance mass distribution is indicated by the small dot and arrow. Body-mounted canard could utilize an internal mass pendulum and two shafts working against a spring torsion. Adequate damping is needed to filter out the motion about trim. A ratchet or clamping arrangement maintains the control deflection to offset the trim asymmetry. The direction of the deflection is accounted for by the normal force orientation and no timing or auxiliary actuation mechanism is needed. This method appears quite attractive for proportional angle of attack control.

A method for roll rate programming has been devised, as depicted in Figure 3-4d. A mechanical governor device operated by the spin rate is shown on the left. The flap or tip aileron is normally deflected to provide an effective fin cant of one degree, for example. When the roll

rate limit (say 2 rps) is reached, the centripetal acceleration rotates the pendulum and through linkage reduces the flap or aileron deflection. Because of excellent roll damping, no deflection for negative roll acceleration is needed. The large effect of normal force on the governor eliminated this scheme from further consideration. A simple airstream-driven gyro can be used in the same manner, as illustrated in the right-hand sketch. The roll rate input to the gyro causes a proportional output torque to reduce the initial aileron deflection as the roll rate approaches the desired magnitude. This technique is currently used on the Navy Sidewinder missile.

The mechanization schemes described are examined in greater detail to establish comparative weights, complexity and adaptability to existing sounding rockets in the following sections.

3.5 Description of Control Devices Evaluated

Six particular control devices were examined in greater detail with the results presented in Figures 3-5 through 3-10. It will be noted that all of these devices are fin mounted and provide an auxiliary roll driving moment, except for the center of gravity displacement mechanism.

Reaction Impulse

The roll reaction impulse mechanization, as illustrated in Figure 3-5, represents perhaps the most straightforward approach in terms of operational simplicity. The end burning solid propellant rocket is mounted on the trailing edges of two of the Aerobee 350 fins, with the right angle nozzle placed near the tip (3.5 foot moment arm). A thrust level of 70 pounds

and burning time of 14 seconds are required. The basis for this design is the Atlantic Research Corporation "Metroc" motor with a fiberglass case. Its characteristics are listed below.

Diameter	3.0 inch
Length	39.0 inch
Thrust	130 lb
Burn Time	17.5 sec
Total Impulse	1930 lb-sec
Weight	14 lb

In order to assess the weight for application to the roll control mechanization, this motor was simply cut in half, a right angle nozzle incorporated, and the thrust reduced to retain the same burn time. Obviously, motor development is required, particularly for the right angle nozzle, for which it is probably best to start from scratch rather than attempt to alter the Metroc motor (Ref. 6). An additional 0.5 lb was included for the nozzle revision. Brackets and attachments accounted for 0.5 lb on each fin. The battery (Yardney-Silvercells), timer (AGASTAT-solid state model 1716), and wiring account for 0.6 lb. This weight for the power source and timer was used for all devices where required. The total weight of 17 lb looks fairly attractive. Since only one timing event is required for motor ignition, excellent reliability should result. Only impulsive roll moment additions are possible so that high roll rates can result.

C.G. Shift

A relatively simple mechanism for the center of gravity displacement scheme emerged during the design as presented in Figure 3-6. Mercury

is contained in flasks at the tip of each fin. The acceleration resulting from the static trim normal force causes the mercury to burst the appropriate diaphragm (e.g., Calmec part no. 567-16A). The release of the mercury then shifts the center of gravity in the proper direction to increase the roll moment during resonance. This scheme avoids the use of a pressure source and tubes passing near the sustainer nozzles required for positive transfer scheme of Figure 3-3. No timing device or power source is required. However, the system is very heavy (100 pounds for 0.3 inch c.g. shift) and was not carried any further.

Aerodynamic Glove

The remaining mechanisms represent variations of aerodynamic surface deflection techniques. The "glove" concept was evaluated for a tip aileron arrangement on two fins shown in Figure 3-7. The two halves of the glove hook around the trailing edges of the fin and are secured at the leading edge by explosive separation devices such as the Hi-Shear Corporation, Model SN-1100-2, separation nut. The right-hand side is ejected at the initial time to yield an effective tip deflection for positive roll moment. The left-hand side is retained by the strap which hooks around the right trailing edge. At the final time, the second separation nut releases the strap and the left-hand side is stripped away by the airstream. The construction details of the Aerobee 350 fins were assumed for the glove (0.1 inch aluminum skin). With the two event timer and battery a total weight of 27 pounds results for two fins. The principal operational disadvantage of increased fin thickness is increased drag and possible interference with the launch tower.

Tip Aileron

The movable tip aileron of Figure 3-8 provides the most effective aerodynamic surface arrangement. The existing fin tip has been utilized with additional bracing at the joint. The cast aluminum pivots are interlocked to provide widely spaced bearing surfaces. The pivot shaft is pinned to the aileron. The hinge line is placed aft of the center of pressure (at the 2D location). When the pin puller (such as the Hi-Shear Corporation Model SP 1106) releases the pivot at the initial time, the positive aerodynamic hinge moment deflects the aileron against the return actuator. A five-degree deflection angle is shown. The aileron is prevented from deflecting in the negative roll direction by the limit stop. The actuator (such as Hi-Shear Model SF 2012-4 thruster) returns the aileron to zero deflection at the second signal from the two event timer. A light weight of ten pounds for two fins results, mainly due to the use of the existing fin structure. A damper would enhance the operation and suppress oscillations due to rapid roll rate changes. This design appears very attractive from the standpoint of weight, simplicity and roll effectiveness. In addition, aeroelastic bending increases the effectiveness of the tip aileron.

Trailing Edge Spoiler

Trailing edge flaps and spoiler provide essentially the same roll effectiveness. However, the spoiler can be incorporated in the Aerobee 350 fin with almost no alterations, whereas the trailing edge flap involves changes similar to the tip aileron. Therefore, the spoiler arrangement shown in Figure 3-9 was evaluated in lieu of a trailing edge flap. The spoiler slides on two guides mounted in the trailing edge channel. The

frame-mounted lower pin puller releases the spoiler blade at the initial time. The preloaded actuator spring deflects the spoiler into the air-stream as illustrated. At the final time the spoiler mounted upper pin puller releases the actuation spring collar and allows the smaller spring to return the blade to the closed position. Details of the arrangement of the springs and pin puller are shown in the insert. Gas generator actuators such as the Hi-Shear Model SF 2012-4 thruster could be used in place of the springs. The spoiler shown here yields the lowest weight for two fins of about six pounds. However, this is probably somewhat optimistic since the actuation mechanisms must be protected from the sustainer exhaust plume during boost. Also the size may increase to account for decrease in effectiveness due to aeroelastic bending. The spoiler is easily adaptable to any thick trailing edge fin.

Gyro-Aileron

The devices described above yield an impulsive roll moment or asymmetry reduction and, hence, are subject to any roll rate limitation. The mechanism of Figure 3-10 consisting of a tip aileron with a wind-driven-gyro actuator shows great promise for roll programming. This type of system is used on the Sidewinder missile (Ref. 7 and 8) and has been examined in detail for application to glide bombs (Ref. 9) and other missiles (Ref. 10 and 11). The torsion spring preload deflects the aileron against the stop at five degrees for the design shown. (The spring unloads at eight degrees deflection.) The gyro wheel spins at a rate proportional to velocity (Ref. 8 indicates a peripheral wheel speed of about 40 to 45 percent of the air speed). The vehicle roll motion torques the gyro which precesses and deflects the aileron in the direction to reduce roll

rate. The spring preload is set to equal the gyro precession torque at the desired spin rate, at which time the aileron just begins to come off the stop. The increasing wheel spin rate continues to reduce the aileron deflection throughout the flight. A limit pin can also be used to restrict negative deflections. The device applied to two fins is fairly light (13 pounds including a one-pound damper). A two-pound wheel with speeds up to 60,000 rpm appears satisfactory for nearly constant roll rate programming. No timer or power source is required if passage through resonance with the deflected aileron at an earlier time is satisfactory. A pin puller could be used to maintain zero aileron deflection until the initial time criteria in order to reduce the angle of attack response. The additional weight would be about 1.1 pounds for two fins.

The predicted steady roll rate performance for gyro spin rate proportional to velocity is illustrated in Figure 3-11. The spring preload condition is determined by the aileron deflection angle and the nominal spin rate required. For example, with a $K = 1.67$ and 2 rps, an unloaded aileron deflection of $K = 2.66$ is required. The spin rate response without the deflection stop is shown by the dashed line up to 2 rps at 35.8 seconds increasing to about 2.06 rps maximum and dropping below 2 rps after 45.5 seconds. This second point is selected by the ΔCG tolerance to be accommodated (see Section 2.4). With a deflection limit at $K = 1.67$ the roll response is depicted by the heavy curve for which resonance occurs at 26.5 seconds. If the aileron is restrained at zero deflection until 30 seconds, the roll rate response indicated by the hatched lines results. With a larger aileron deflection (e.g., $K = 1.0$), 2 rps roll rate is reached earlier at 20.5 seconds, increasing to a maximum of 2.3 rps.

Thus, very reasonable roll rate programs can be achieved even for large deflections. The roll rate responses of Figure 3-11 suggests the use of the gyro-aileron to program roll rate above resonance immediately, such as depicted by the curve for $\delta_0 = 2.3$ ($K = 7.68$). This program represents essentially a continuation of the booster roll programming. Large aileron cant angles are required but the loads experienced are mild. For example, in order to yield 600 deg/sec roll rate in five seconds, a constant aileron force of 13 pounds is required for two fins.

The suggested roll program can accrue very large benefits in terms of the asymmetry tolerance improvement. Theoretically, the tolerances are infinite since the roll rate is always above resonance, and the rolling trim angle of attack is zero. In actual practice, however, normal fin cant deviations, etc., can yield roll rates closer to resonance, resulting in a rolling trim angle of attack other than zero with consequent roll coupling. But since the aerodynamic damping is large in this flight regime, angle of attack amplification at resonance is relatively small and roll resonance may not be especially objectionable. The asymmetry tolerances to breakout from resonance can be easily defined by methods of Section 2. An additional feature of the roll programming by the gyro aileron is the reduction of roll rate late in the flight. While the flight vehicle cannot respond to the steady state roll rates depicted in Figure 3-11 due to lag at high altitudes, reasonably low roll rates can be expected.

This gyro aileron retains all of the advantages of the tip aileron (i.e., high roll effectiveness, low weight and simplicity), in addition to providing the advantages of roll programming. The wind-driven-gyro actua-

tion has been demonstrated in operational vehicles. The adaptation to sounding rockets consists primarily of incorporating the spring preload. Adapting the gyro wheel to thin fins does not appear to present any unsurmountable problems.

3.6 Design Comparison

The principal characteristics of the devices described in Section 3.5 are summarized in Figure 3-12 for direct comparison. A pitch reaction mechanization is included also for reference although no design details are presented. The c.g. shift can be eliminated from further consideration upon the basis of weight alone. The pitch reaction device requires four thrusters and an additional device for sensing the proper direction to thrust. Two extra thrusters must be carried along for the ride since thrust direction is fixed, essentially doubling the weight. Hence, the pitch reaction device was eliminated from contention.

The fixed deflection aerodynamic surfaces (glove, spoiler and tip aileron) requires a two event time signal. The relatively high weight of the glove and the decrease in roll effectiveness of the spoiler due to its trailing edge location and aeroelastic bending tend to favor the tip aileron. The weight difference between the spoiler and tip aileron is not considered significant enough for selection of the aileron on the basis of weight alone with the type of design evaluation made here.

The selection of the tip aileron over the roll reaction device appears justified on the basis of weight and the requirement for a new motor development with a right angle nozzle.

Thus, the selection of the most promising control device evolves

to tip aileron and its method of actuation. The timing requirement can be eliminated completely or reduced to one event by use of the gyro actuation. The potential advantage for virtual elimination of asymmetry tolerances by roll rate programming and maintaining roll rate within reasonable limits make the gyro aileron the most promising device.

Therefore, the gyro aileron roll control mechanization is recommended for further development.

3.7 Development Plan

The development of the gyro aileron control device should be a fairly straightforward analysis and design procedure. The principal problem appears to be limiting the gyro wheel speed to within load capacity of available ball bearings. The simple saw tooth wheel design of References 7 to 9 indicates wheel peripheral speeds of about 40 percent of the air-stream. For a fully exposed wheel of two-inch diameter, a spin rate of 368,000 rpm at the Aerobee 350 burnout velocity of 8000 fps would result. Wheel design, location and air ducting need careful consideration to yield wheel speeds within reasonable mechanical limits. Wind tunnel tests would be helpful to verify the wheel design, aileron hinge moment and damper characteristics prior to flight testing on the Aerobee 350 development vehicles.

The following program plan is suggested for development and flight demonstration of the gyro aileron roll control device.

1. Evaluate roll rate performance characteristics to
 - a. Establish aileron sizing
 - b. Gyro wheel response

- c. Roll rate programming
- 2. Design wind tunnel tests to
 - a. Assess gyro wheel performance and response
 - b. Verify tip aileron aero-characteristics
 - c. Demonstrate free spin control
- 3. Perform detail design for application to
 - a. Thick finned vehicles (e.g., Aerobee 350)
 - b. Thin finned vehicles (e.g., Nike-Apache)
- 4. Flight performance tests
 - a. Modify existing Aerobee 350 fins
 - b. Fabricate gyro aileron
 - c. Define instrumentation requirement
 - d. Perform evaluation of test data
- 5. Final Development
 - a. Modify design based on flight test performance
 - b. Prepare fabrication plans

Section 4
CONCLUSIONS AND RECOMMENDATIONS

The following conclusions can be drawn from the motion analysis and design studies conducted during the course of the investigation.

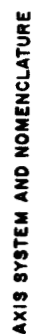
1. Significant improvement in the asymmetry tolerance contours for maximum angle of attack and roll lock-in can be obtained with roll and pitch control. The magnitude of the improvement is directly proportional to the size of the applied control moment.
2. Roll control yields the most simple system. The direction of the applied moment is known a priori, eliminating in-flight measurement of the orientation of the asymmetries. Angle of attack response to asymmetries is greatly reduced due to high rate of passage through resonance.
3. Control capability and timing criteria based on equilibrium trim response provides realistic and conservative criteria. Timing criteria is relatively insensitive to operational and vehicle deviations.
4. Operational restrictions such as a maximum roll rate limitation can severely restrict the usable tolerance contour improvement for impulsive fixed magnitude control moments. Roll rate programming can regain most of the potential improvement based on equilibrium trim response.

5. Asymmetry tolerances can be virtually eliminated by programming roll rate above resonance immediately off the booster.
6. Mechanization of reaction, weight shift and aerodynamic surface roll control devices yielding light weight (10 to 17 pounds) have been examined in sufficient detail for realistic comparison. Fin tip mounted devices proved most effective due to the large roll moment arm.
7. The gyro-actuated tip aileron device is recommended for further development because of its light weight (13 pounds), high roll effectiveness, simplicity of operation, adaptability and, most importantly, its capability for roll rate programming.
8. It is recommended that development of the gyro-aileron device be initiated promptly for flight test on the Aerobee 350 performance flights during 1966 and 1967.

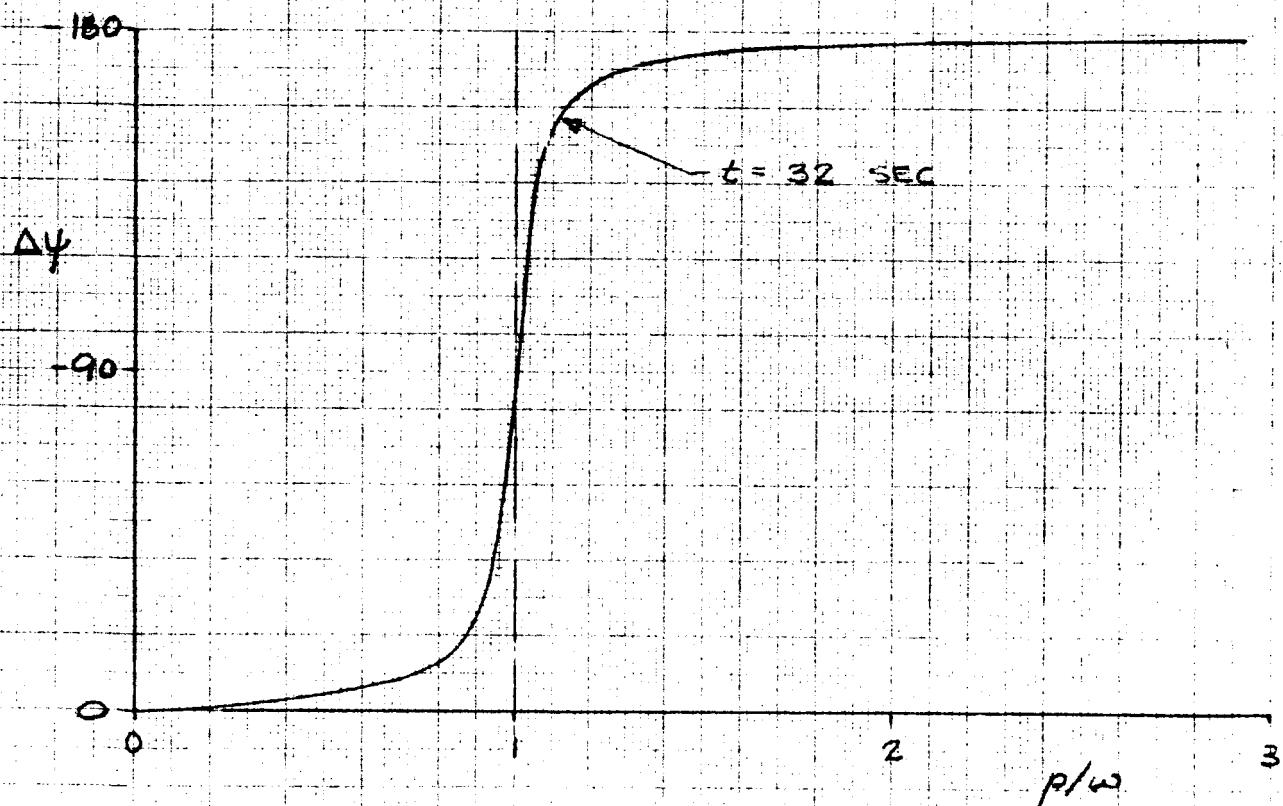
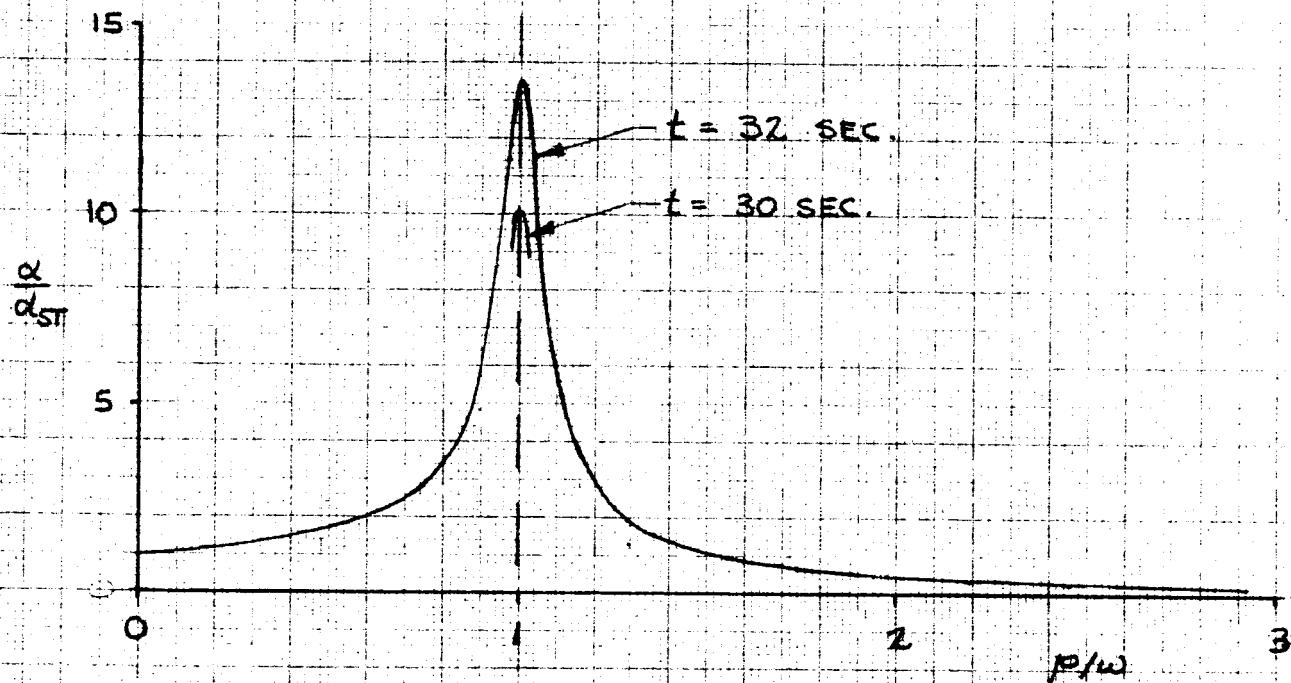
Section 5
REFERENCES

1. Price, D. A., and Nelson, E. O., Final Report for the Aerobee 150A Roll Lock-In Study, Contract No. NAS 5-9061, Lockheed Missiles and Space Company, Palo Alto, California, March 1965.
2. Price, D. A., and Nelson, E. O., Final Report for the Aerobee 350 Roll Lock-In Study, Extension to Contract No. NAS 5-9061, Lockheed Missiles and Space Company, Palo Alto, California, June 1965.
3. McNeal, D. R., Description and Users Manual for Roll-Pitch Motion Digital Computer Program, LMSC Report No. M-60-64-2, Lockheed Missiles and Space Company, Palo Alto, California, March 1965.
4. Technical Proposal, Investigation of In-Flight Roll Control Techniques for Sounding Rockets, LMSC-894018, Lockheed Missiles and Space Company, Palo Alto, California, March 1965.
5. Price, D. A., Nelson, E. O., and Torrillo, J. E., Progress Report No. 1, Investigation of In-Flight Roll Control Techniques for Sounding Rockets - Contract No. NAS 5-9628, Lockheed Missiles and Space Company, Palo Alto, California, August 1965.
6. Private communication - J. Rhinehart, LMSC Propulsion Engineering, (Dept. 55-11) to D. A. Price, Jr.

7. La Berge, B., and Donnkwater, W. D., Preliminary Evaluation of a Simplified Roll Rate Stabilization System, NAVORD Report 1269 (NOTS 339), US Naval Ordnance Test Station (Inyokern, California), 8 January 1951.
8. Nason, M. L., Brown, C. A., and Rock, R. S., An Evaluation of a Rollenon-Roll-Rate Stabilization System for a Canard Missile Configuration at Mach Numbers from 0.9 to 2.3, NACA RM L55C22, 1955.
9. Sanderson, D. L., and Millevolte, P. L., Aero-Mechanical Control Device for Glider Bomblets - Final Summary Report, Contract DA 18-064-CML-2765, Minneapolis-Honeywell Regulator Company, Hopkins, Minnesota, 1962.
10. Zaronsky, J., and Gardiner, R. A., Flight Investigation of a Roll Stabilized Missile Configuration at Varying Angles of Attack at Mach Numbers Between 0.8 and 1.79, NACA TN 3915, 1957.
11. Jepps, G., Roll Dynamics of a Gyro-Tab with Applications to Aerodynamic Test Vehicles, TN HSA-91, Weapons Research Establishment, Adelaide, Australia, March 1962.

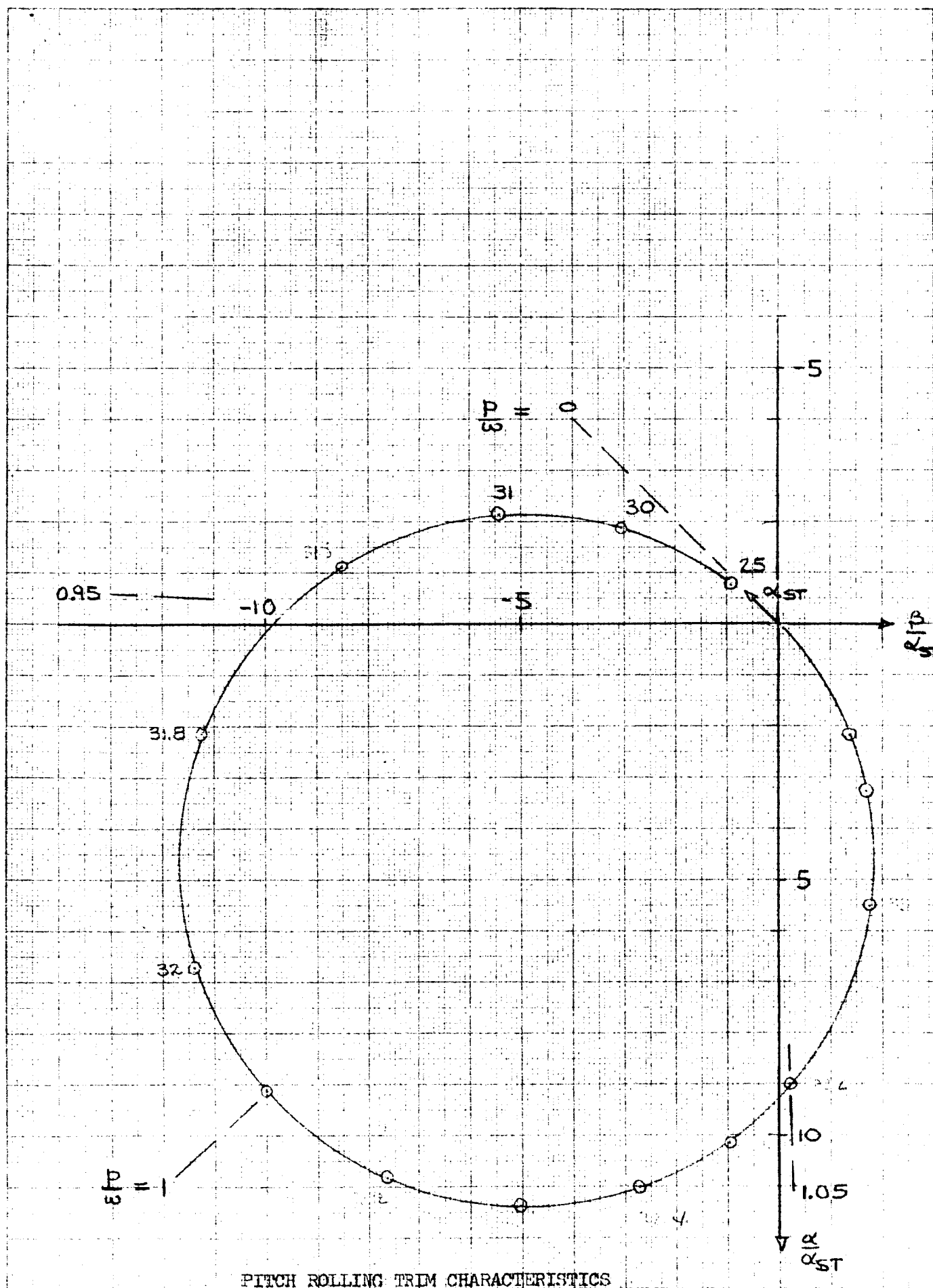


8



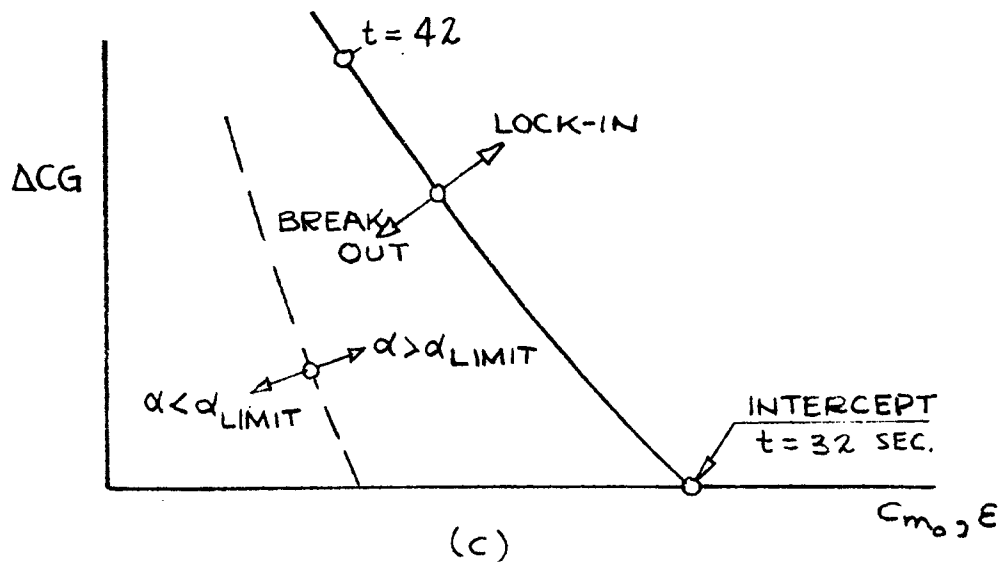
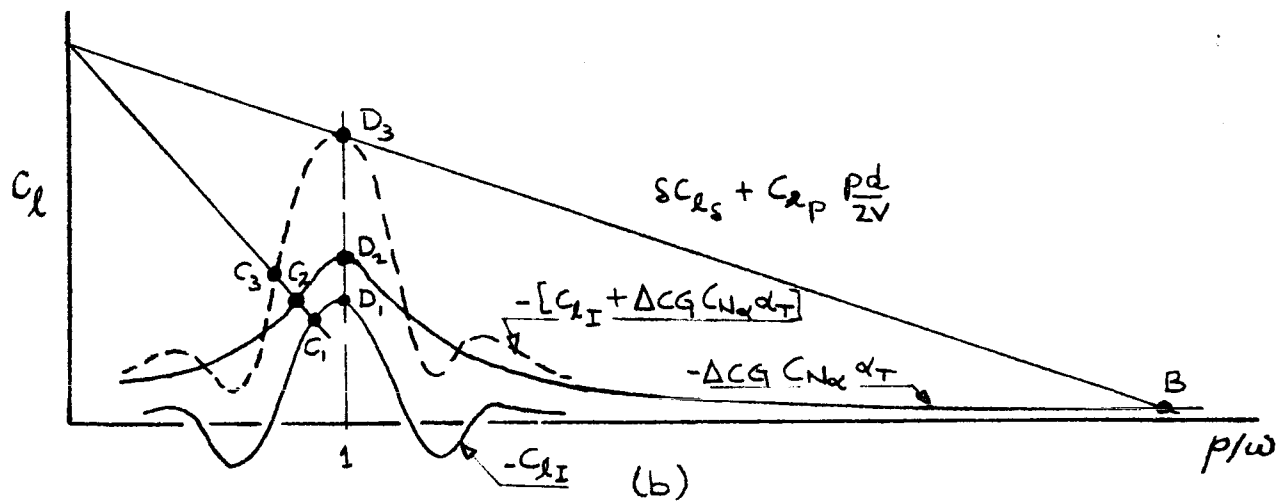
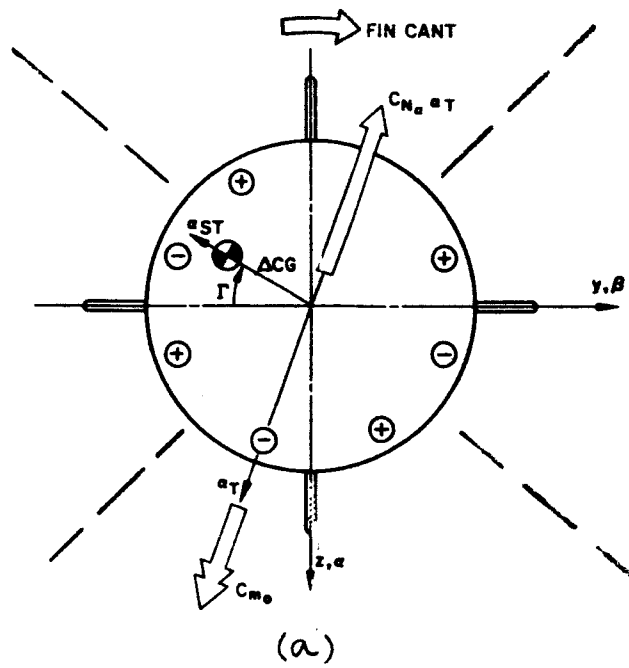
PITCH ROLLING TRIM CHARACTERISTICS

Fig. 2-2a

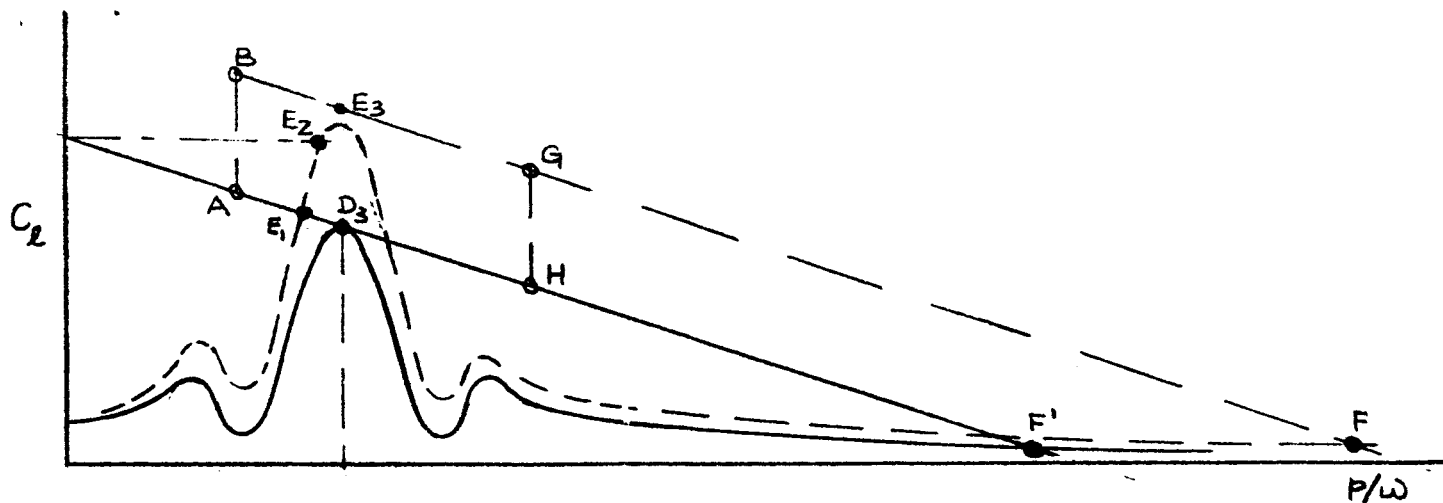


PITCH ROLLING TRIM CHARACTERISTICS

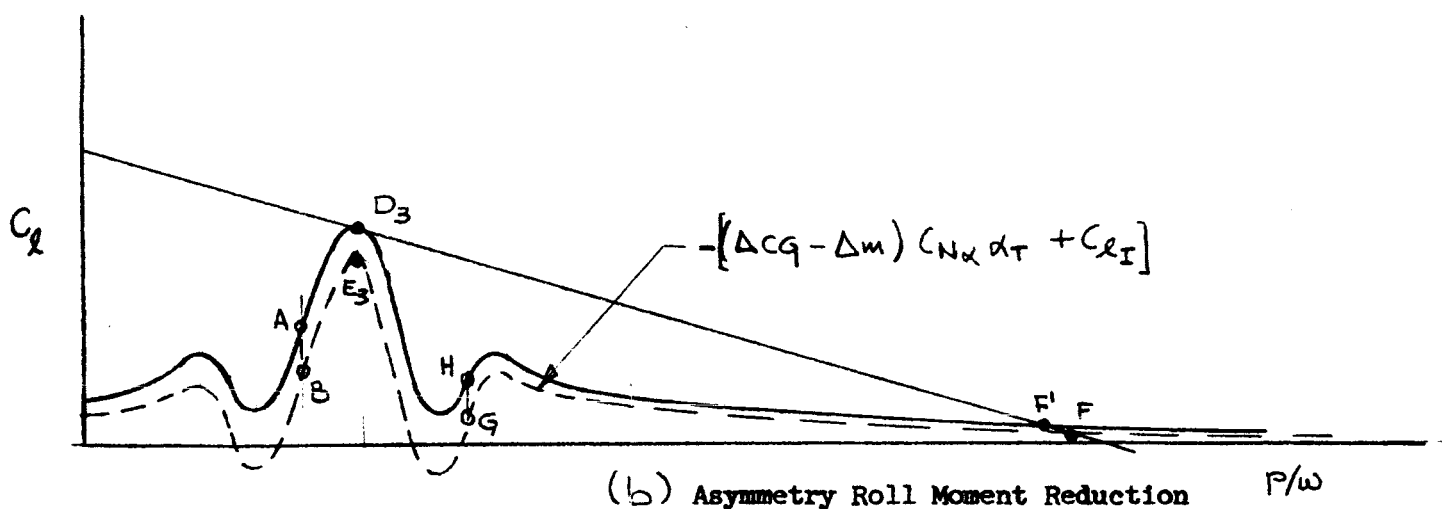
Fig. 2-2b



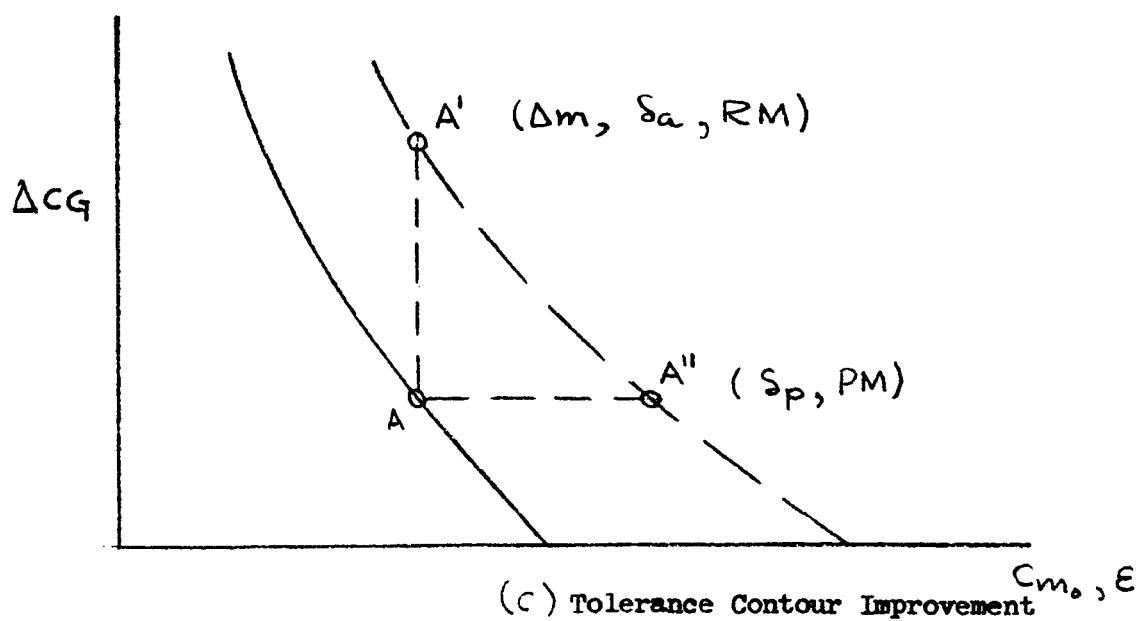
ROLL TRIM AND ASYMMETRY TOLERANCES



(a) Auxiliary Roll Control



(b) Asymmetry Roll Moment Reduction



(c) Tolerance Contour Improvement

ROLL LOCK-IN EQUILIBRIUM EQUATIONS

Lateral Center-of-Gravity Offset: $\Delta CG = \frac{12d}{\alpha_T C_{N\alpha}} \left(\delta C_{\ell\delta} + C_{\ell p} \frac{\omega d}{2V} - \eta_1 RC_{\ell_I} \sin 4\Gamma - \frac{Tca}{12\bar{q}Ad} + \frac{R}{q} \frac{Rm}{Ad} \right)$

Trim Angle of Attack: $\alpha'_T = \frac{1}{b} \left(\frac{RC_{m_0}}{-C_{m\alpha}} + \frac{r_e T\epsilon}{(-C_{m\alpha})\bar{q}Ad} - \frac{R}{(-C_{m\alpha})} \frac{Pm}{Ad} \right)$

Damping Factor: $b = \frac{R\bar{q}A}{mV\omega} \left[C_{L\alpha} (1 - \nu) - \frac{md^2}{I} (C_{m_q} + C_{n_{p\alpha}}) \right] + \frac{RT}{mV\omega} (1 - \nu) + \frac{RTr_o^2}{I g_{sp}^1 \omega}$

INTERCEPT SOLUTIONS ($\Delta CG \equiv 0$)

$$C_{m_0} = \frac{b\alpha_T^* (-C_{m\alpha})}{R}$$

$$\epsilon = \frac{b\alpha_T^{*\omega^2} I}{r_e TR^2}$$

Fig. 2-5

TOLERANCE CONTOUR COMPARISON

Aerodynamic Asymmetry

$\delta = 0.3 \text{ deg.}$

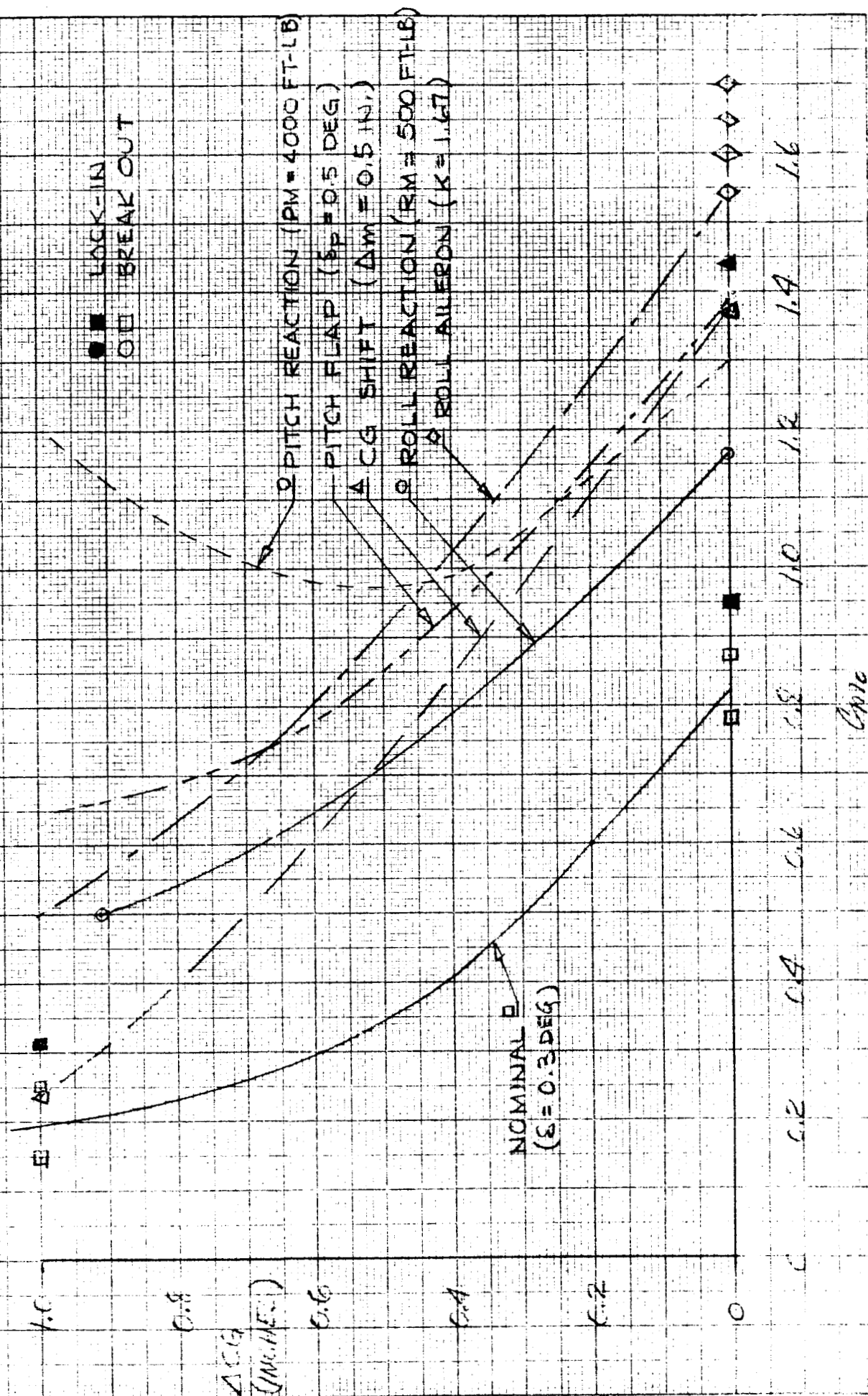
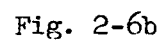


Fig. 2-6a



LIMITING TERM ASYMMETRY

RESONANCE
FOR $\delta = 0.3^\circ$

INTERCEPT

C_{m0}, E

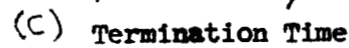
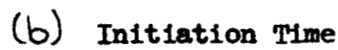
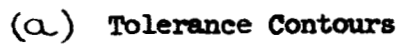
INTERCEPT OF $C_{m0} + E$ (DEG)

$\alpha_T = 14$

$\alpha_T = 0.7$

TIME (SEC)

Fig. 2-7



BREAKOUT DEMONSTRATION WITH ROLL REACTION IMPULSE

ANGLE OF ATTACK LOCUS WITH RESPECT TO BODY FIXED AXES

RUN NUMBER 939

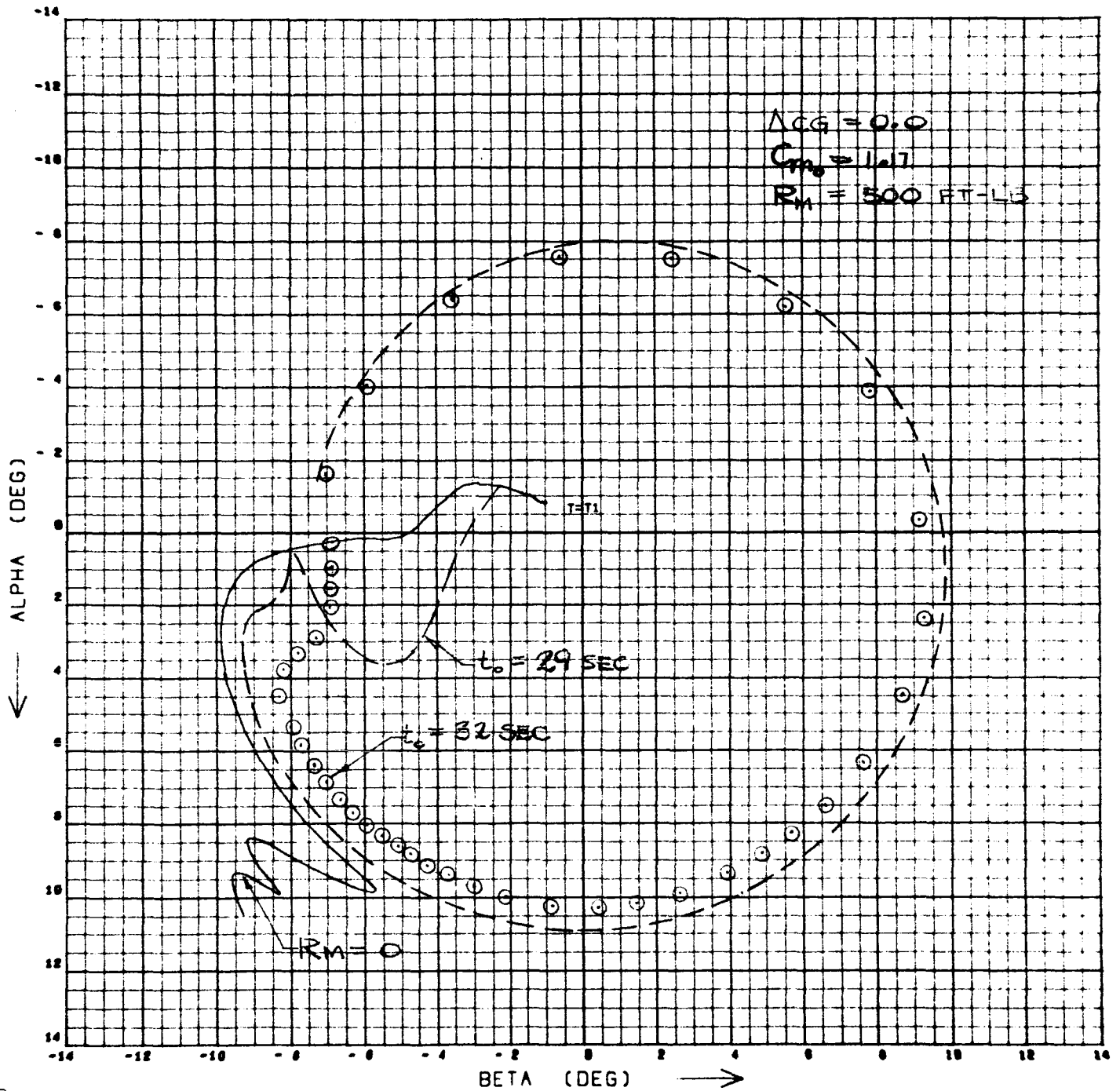


Fig. 2-9a

BREAKOUT DEMONSTRATION
ROLL REACTION IMPULSE

ROLL RATE TIME HISTORY

RUN NUMBER 939

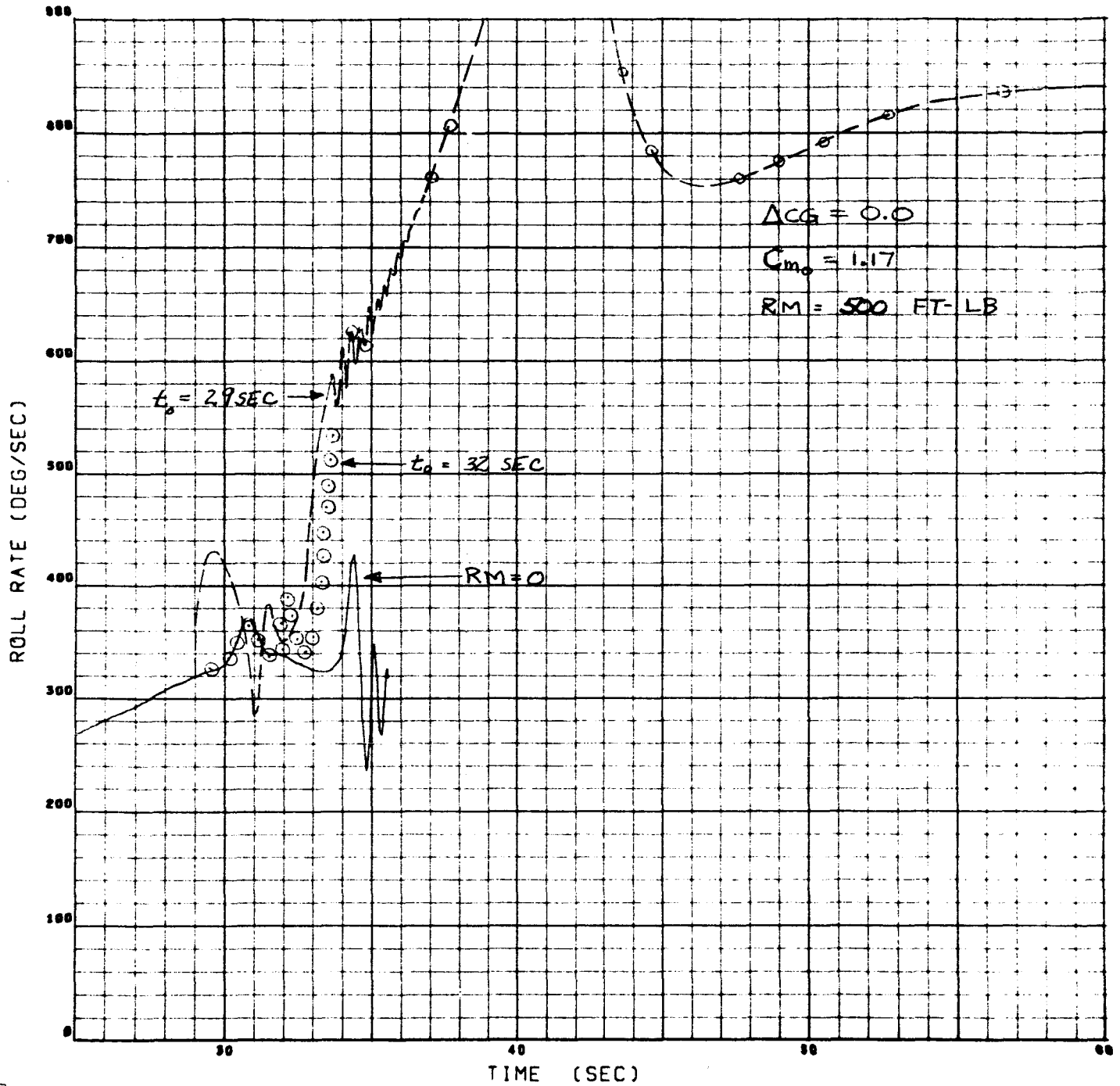


Fig. 2-9b

BREAKOUT DEMONSTRATION WITH TIPAILERONS

ANGLE OF ATTACK LOCUS WITH RESPECT TO BODY FIXED AXES

RUN NUMBER 10

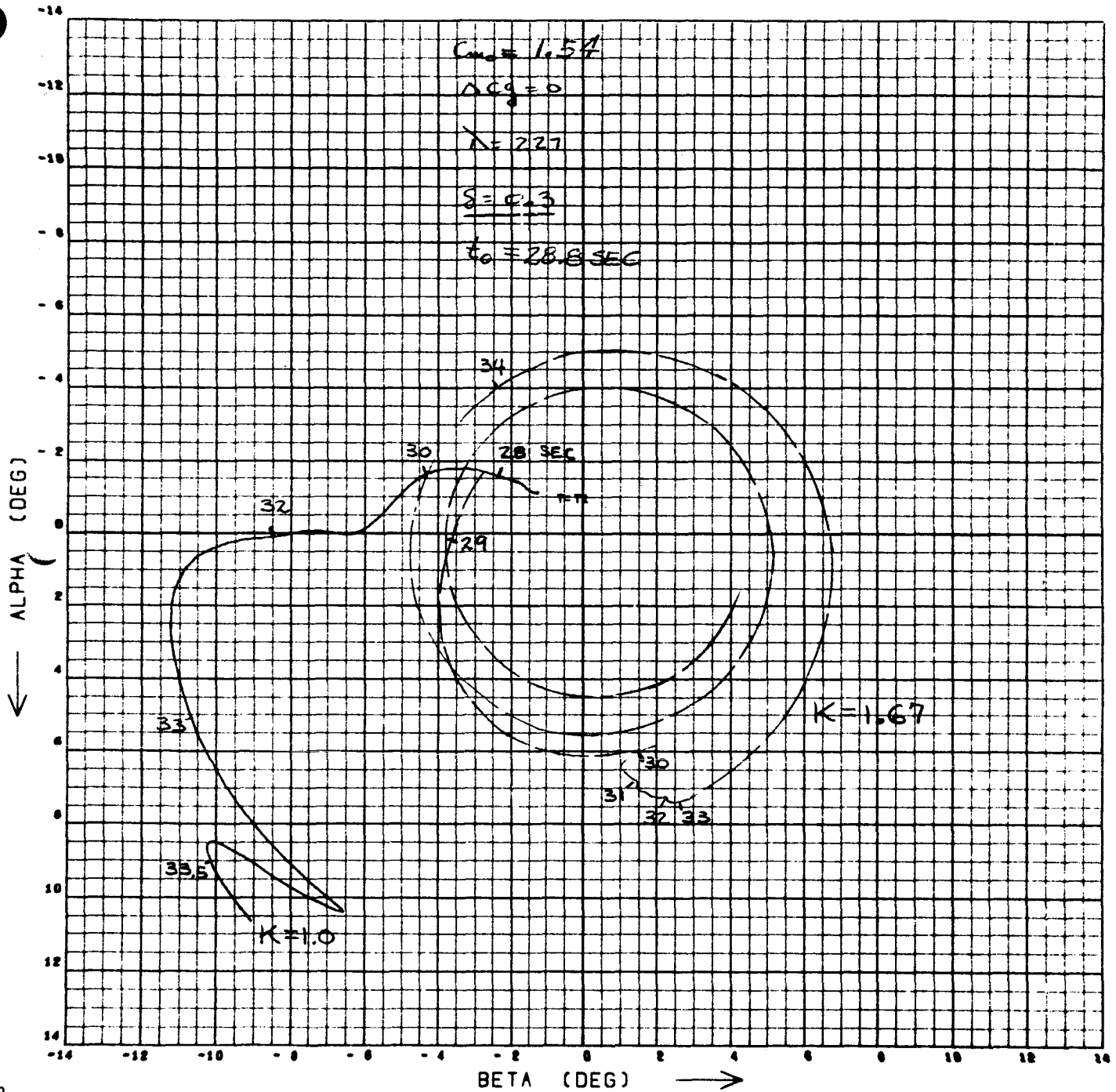


Fig. 2-10a

BREAKOUT DEMONSTRATION WITH TIP AILERONS

TOTAL ANGLE OF ATTACK TIME HISTORY

RUN NUMBER 10

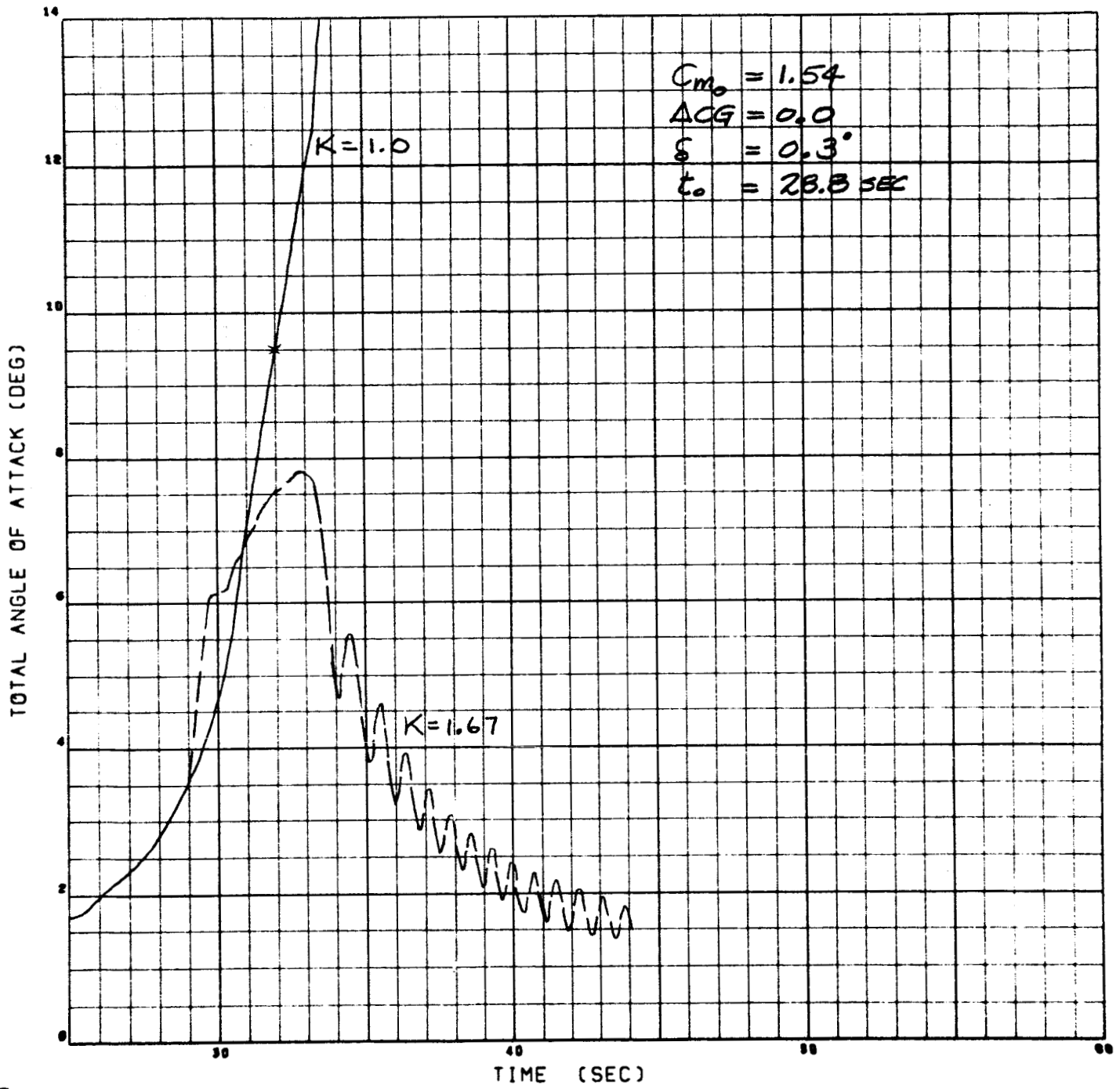


Fig. 2-10b

BREAKOUT DEMONSTRATION WITH TIP AILERONS

ROLL RATE TIME HISTORY

RUN NUMBER 10

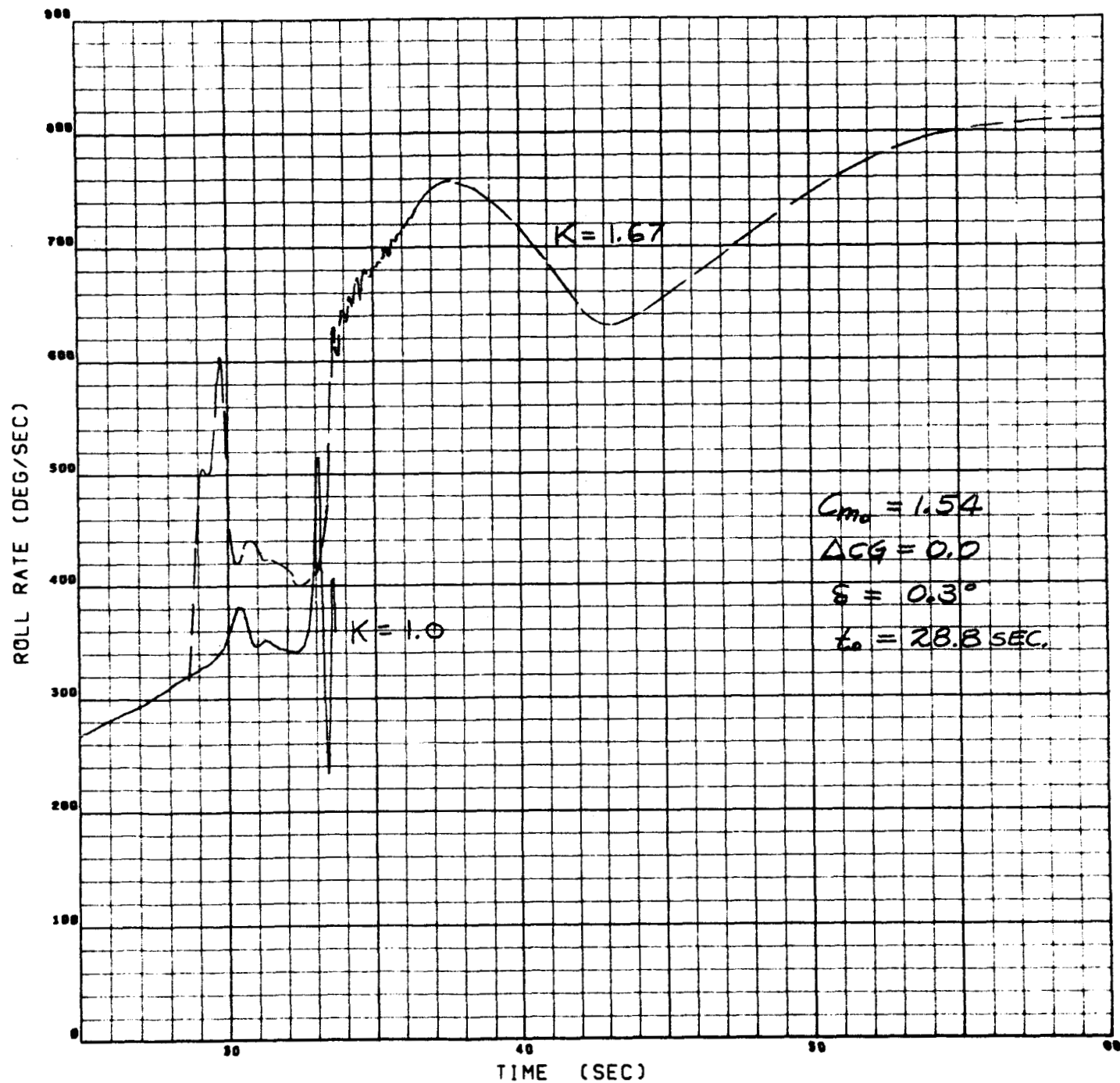


Fig. 2-10c

BREAKOUT DEMONSTRATION WITH C.G. SHIFT

ANGLE OF ATTACK LOCUS WITH RESPECT TO BODY FIXED AXES

RUN NUMBER 982

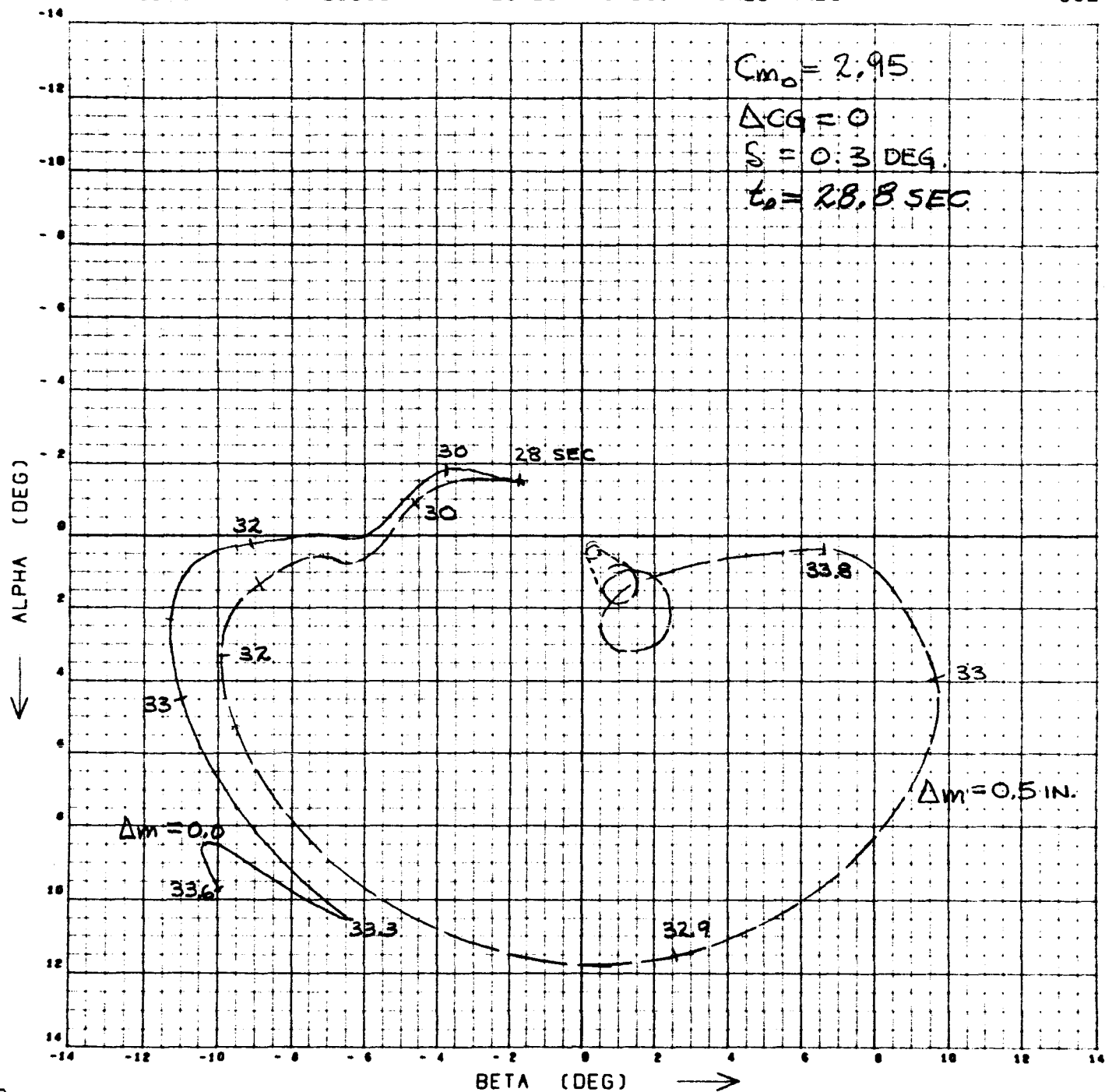


Fig. 2-11a

BREAKOUT DEMONSTRATION WITH C.G. SHIFT

TOTAL ANGLE OF ATTACK TIME HISTORY

RUN NUMBER 982

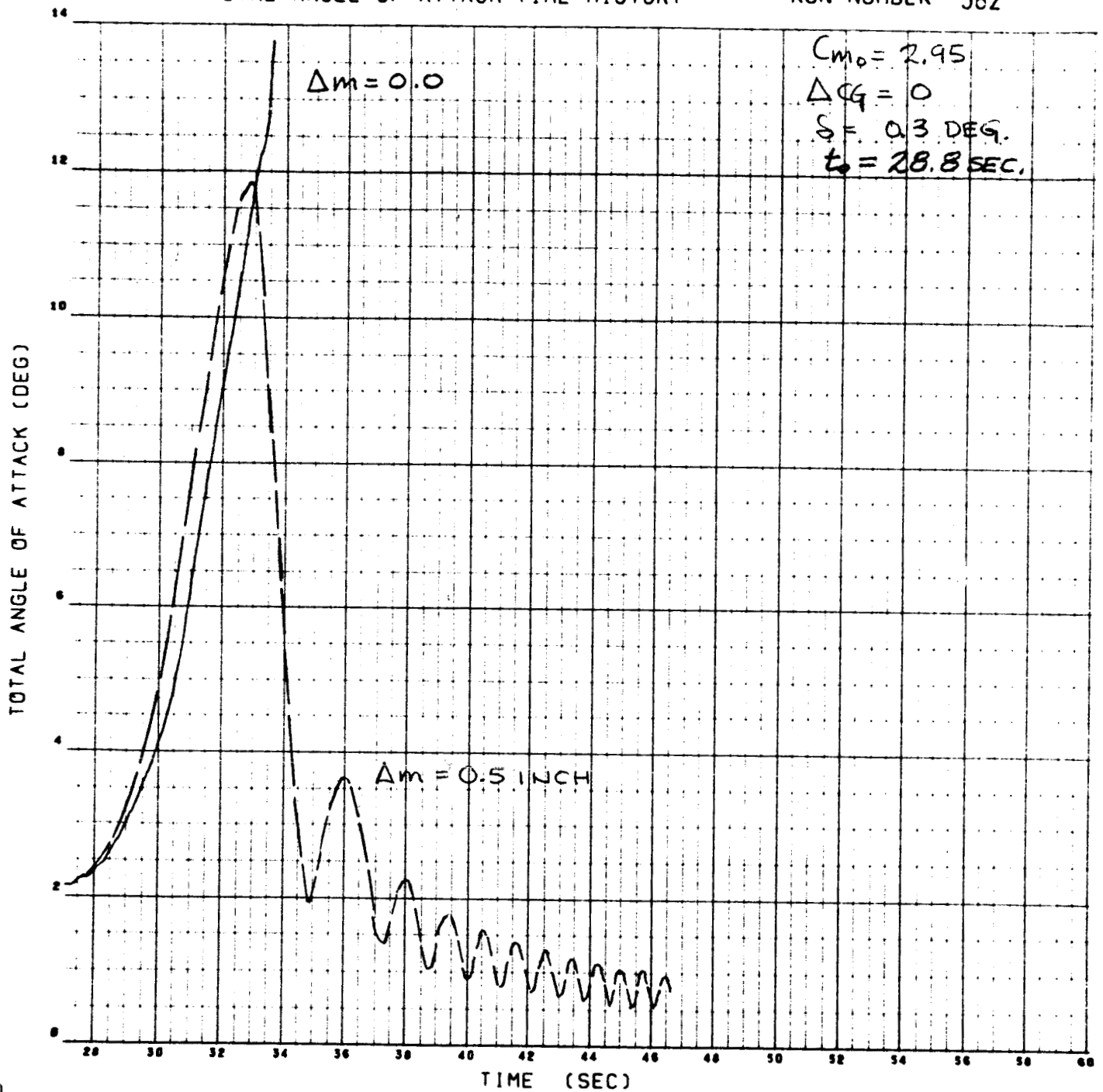


Fig. 2-11b

BREAKOUT DEMONSTRATION WITH C.G. SHIFT

ROLL RATE TIME HISTORY

RUN NUMBER 982

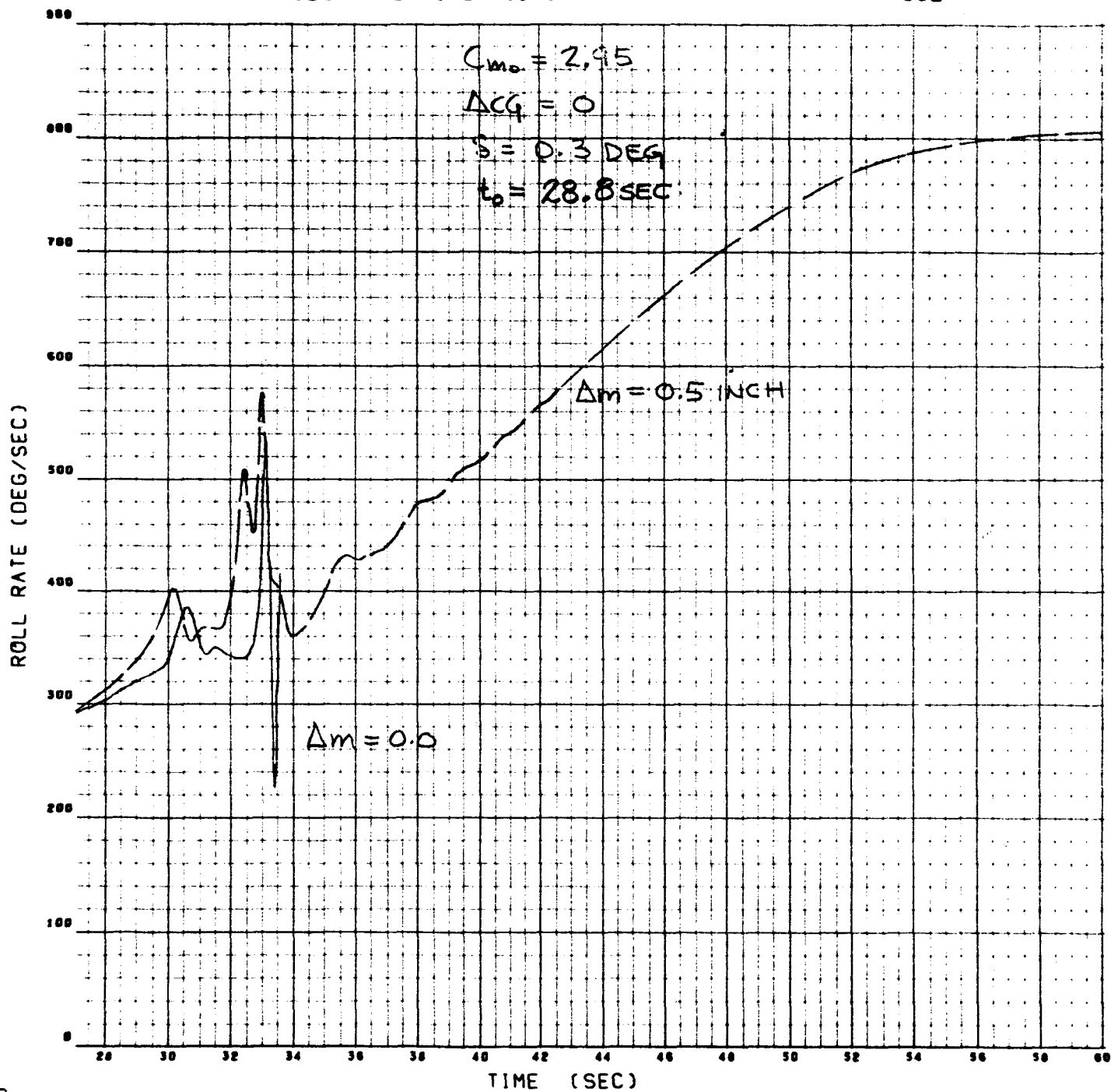
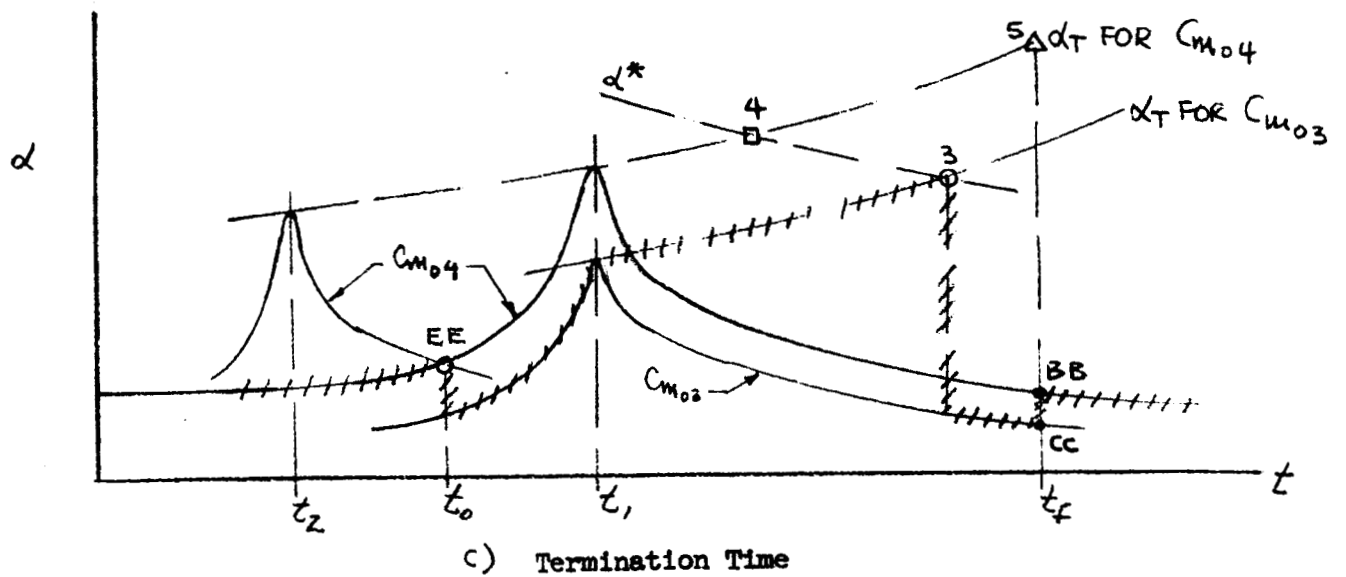
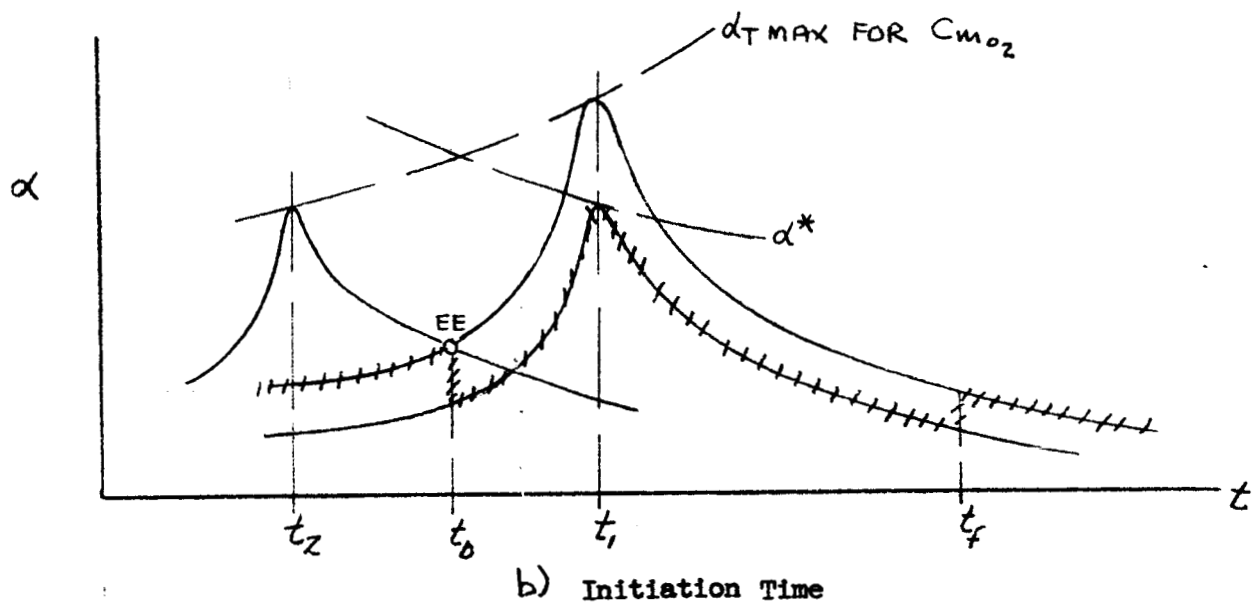
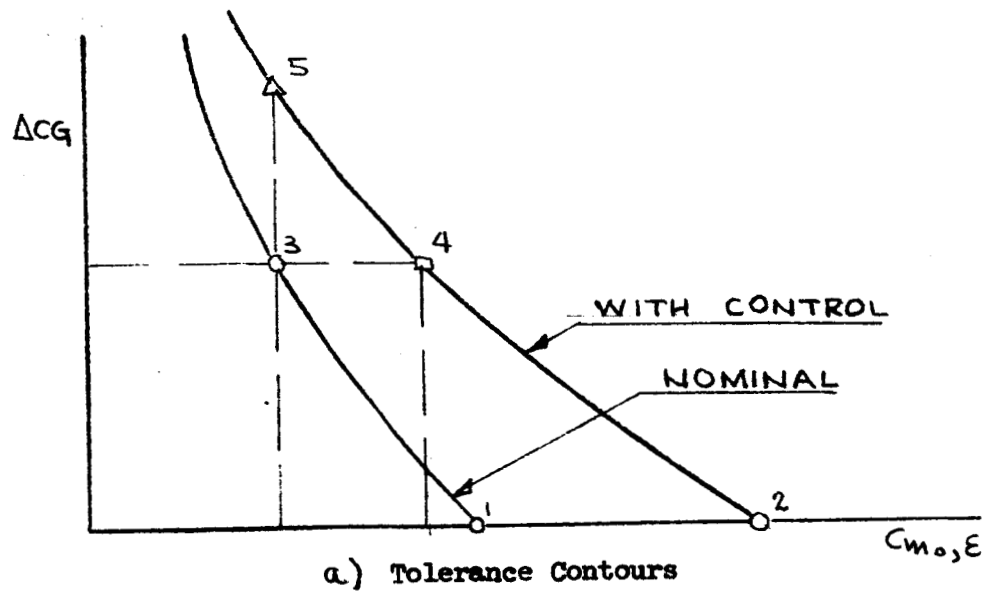


Fig. 2-11c



BREAKOUT DEMONSTRATION
WITH PITCH REACTION IMPULSE

ANGLE OF ATTACK LOCUS WITH RESPECT TO BODY FIXED AXES

RUN NUMBER 957C

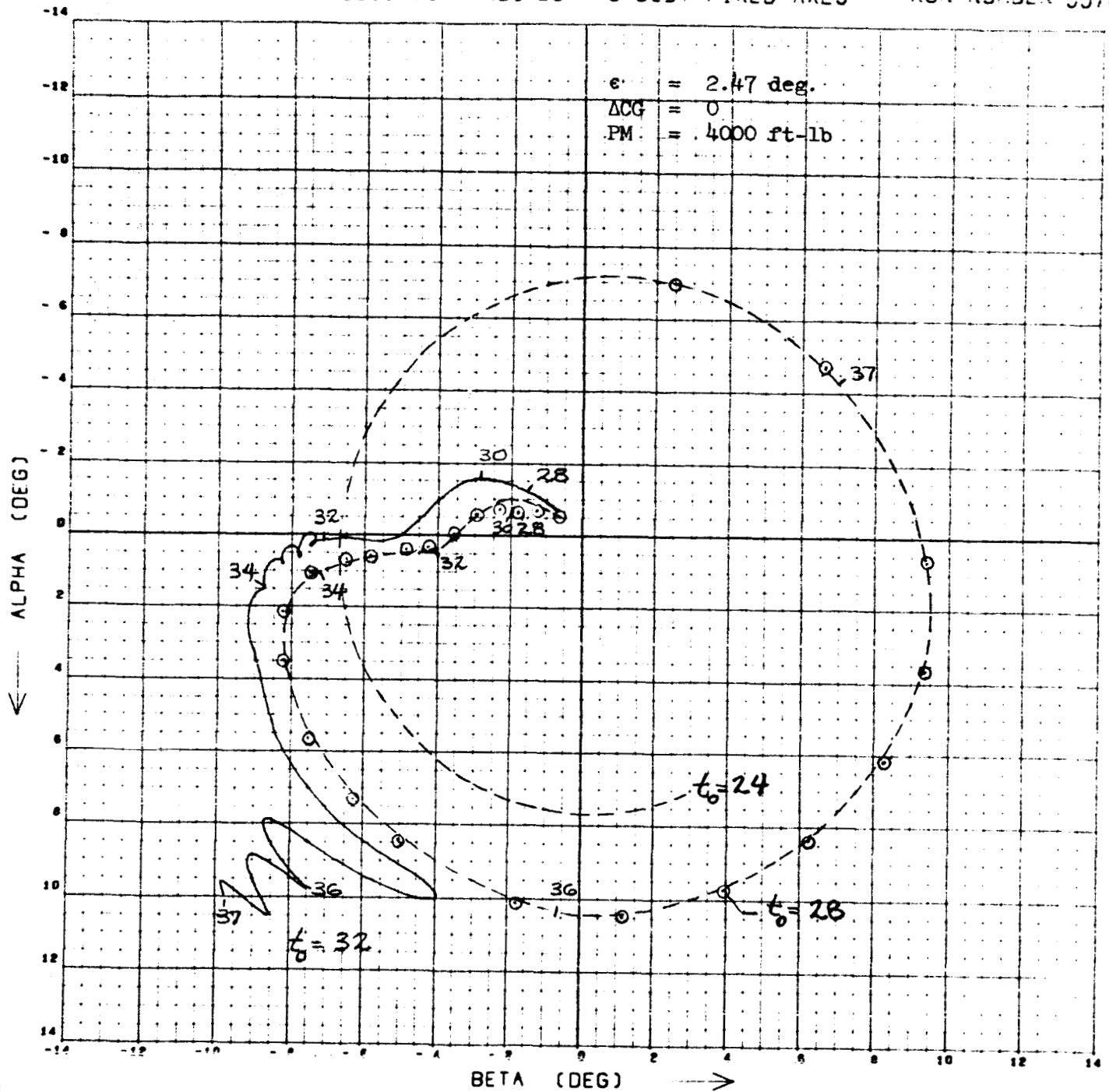


Fig. 2-13a

BREAKOUT DEMONSTRATION
WITH PITCH REACTION IMPULSE

TOTAL ANGLE OF ATTACK TIME HISTORY

RUN NUMBER 9570

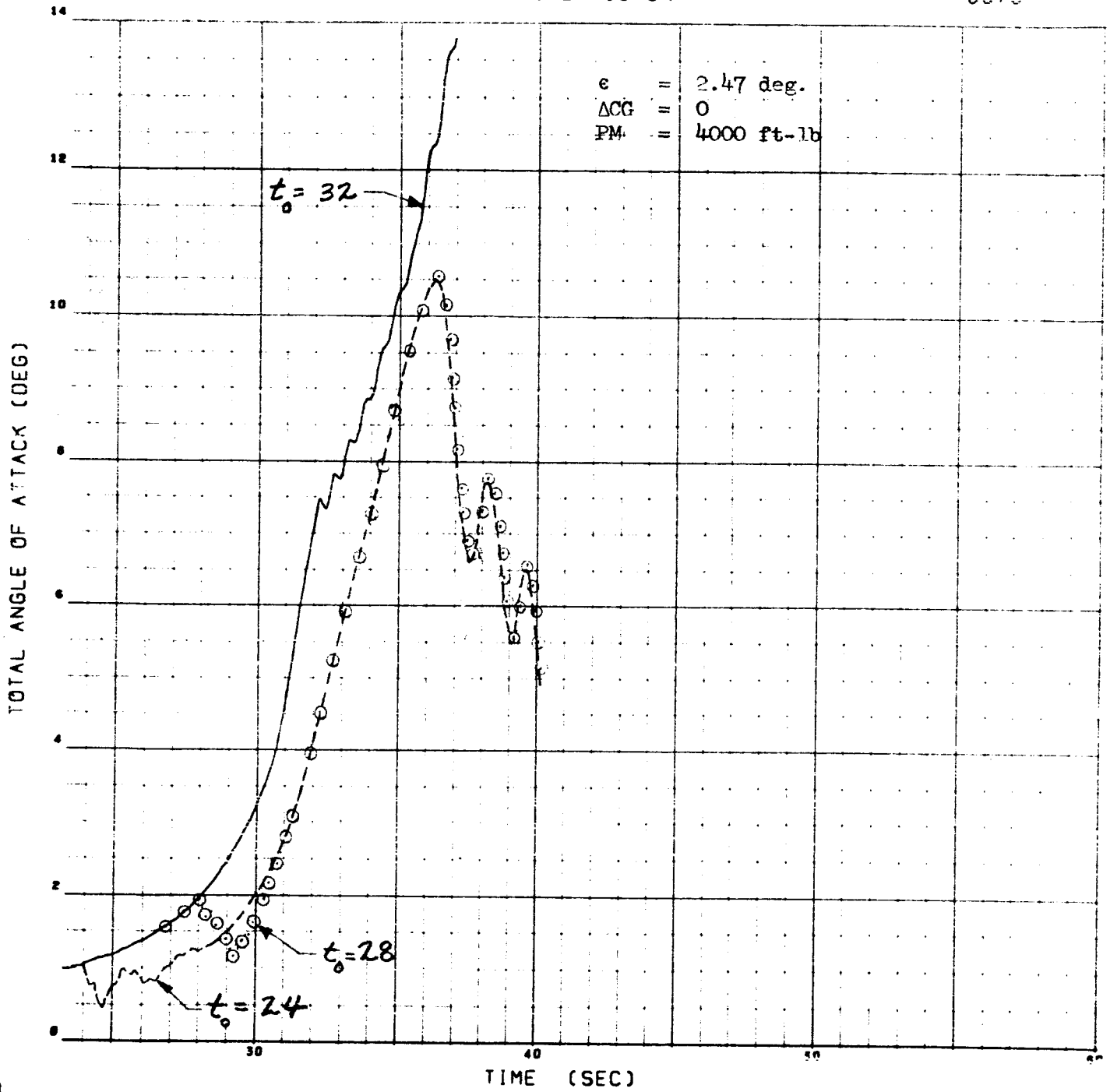


Fig. 2-13b

BREAKOUT DEMONSTRATION
WITH PITCH REACTION IMPULSE

ROLL RATE TIME HISTORY

RUN NUMBER 9570

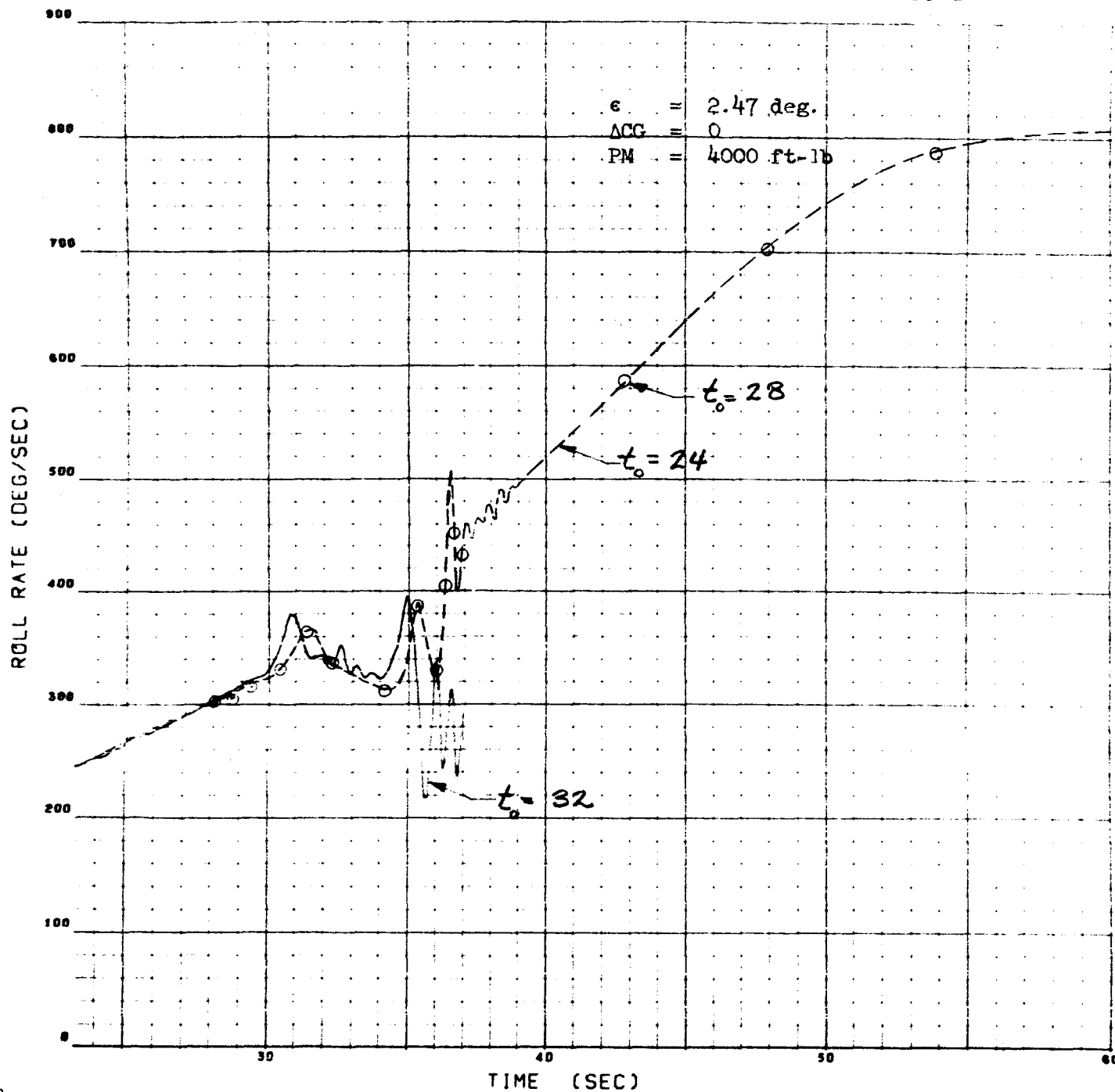


Fig. 2-13c

EFFECT OF RATE LIMIT

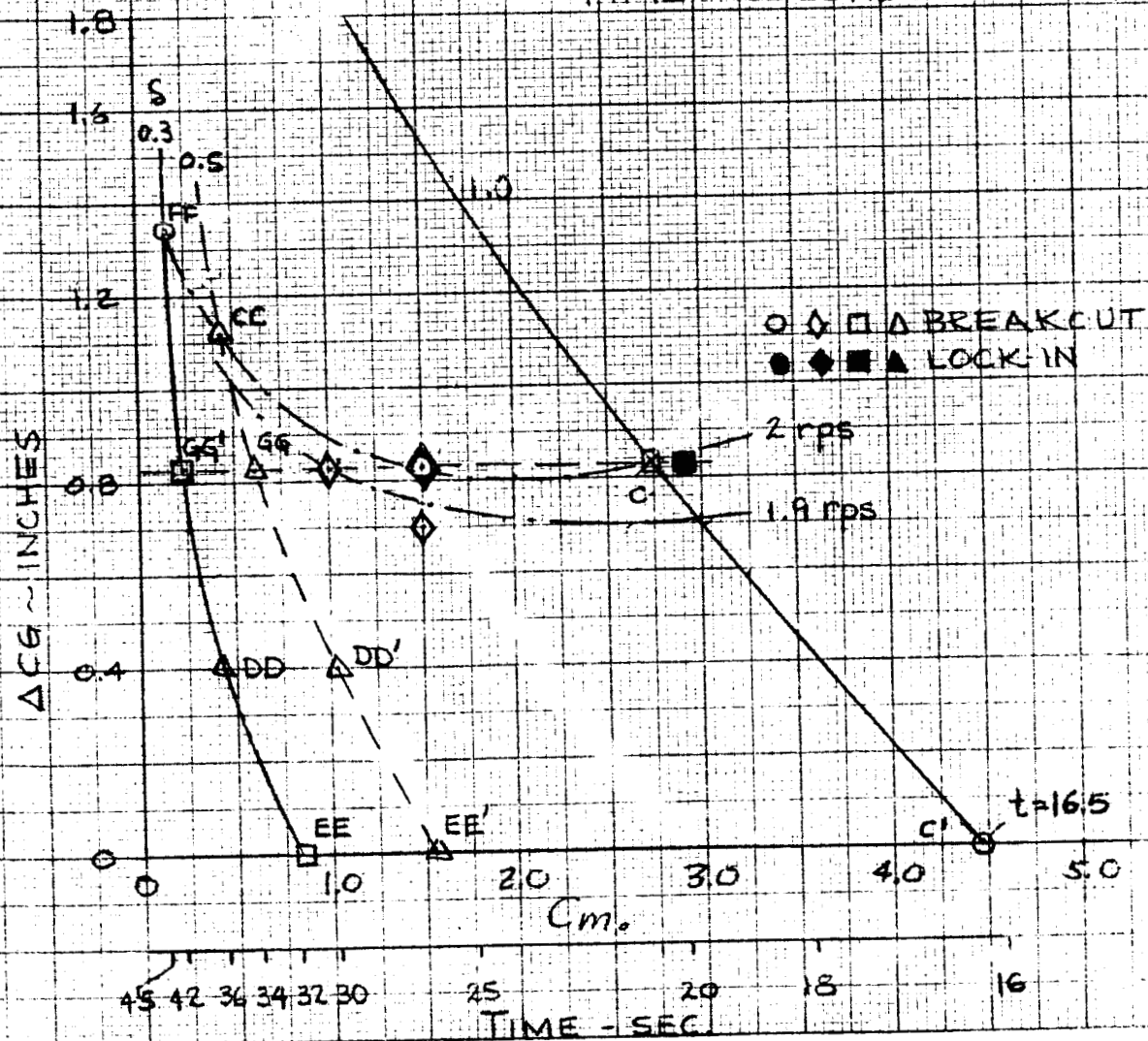
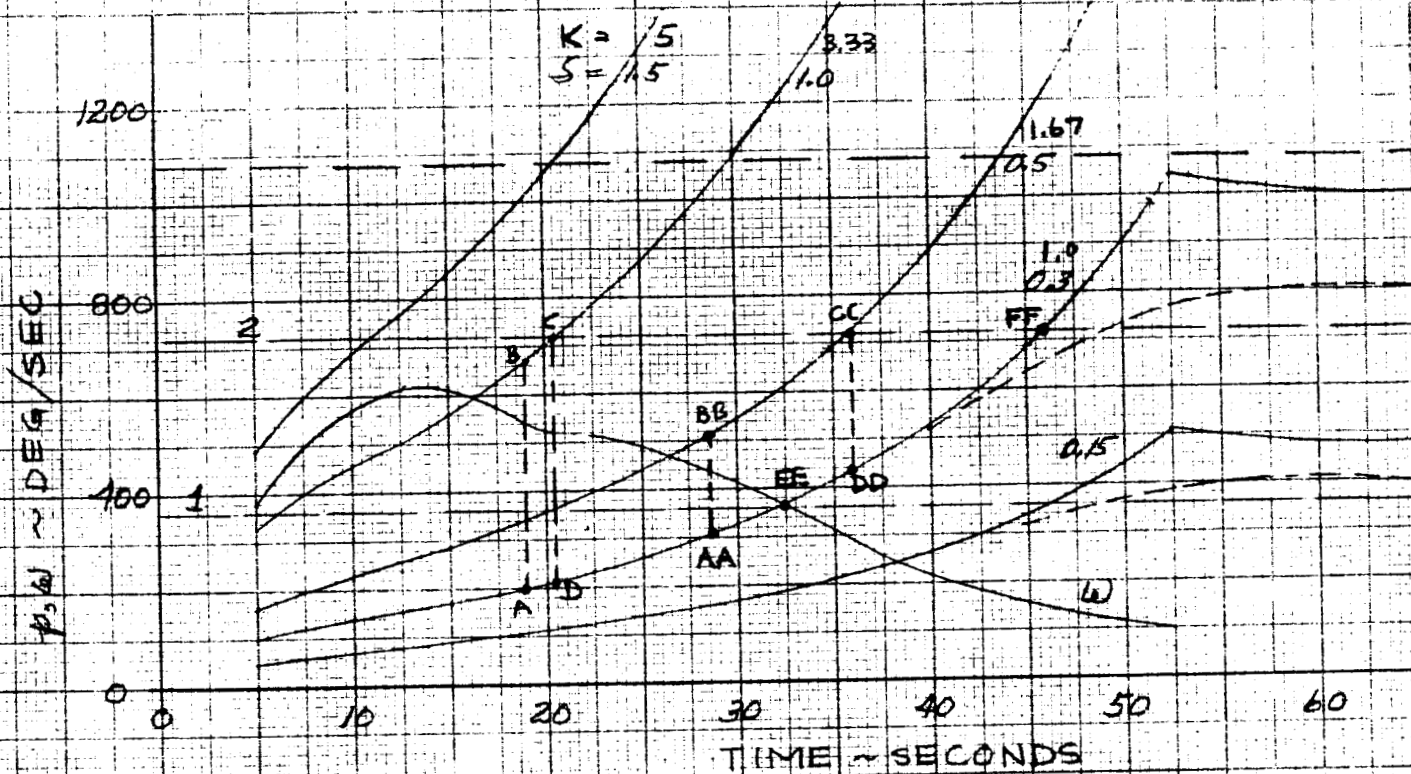


Fig. 2-14

VERIFICATION OF TOLERANCE CONTOURS
WITH TIP AILERON DEFLECTION

ROLL RATE TIME HISTORY

RUN NUMBER 306

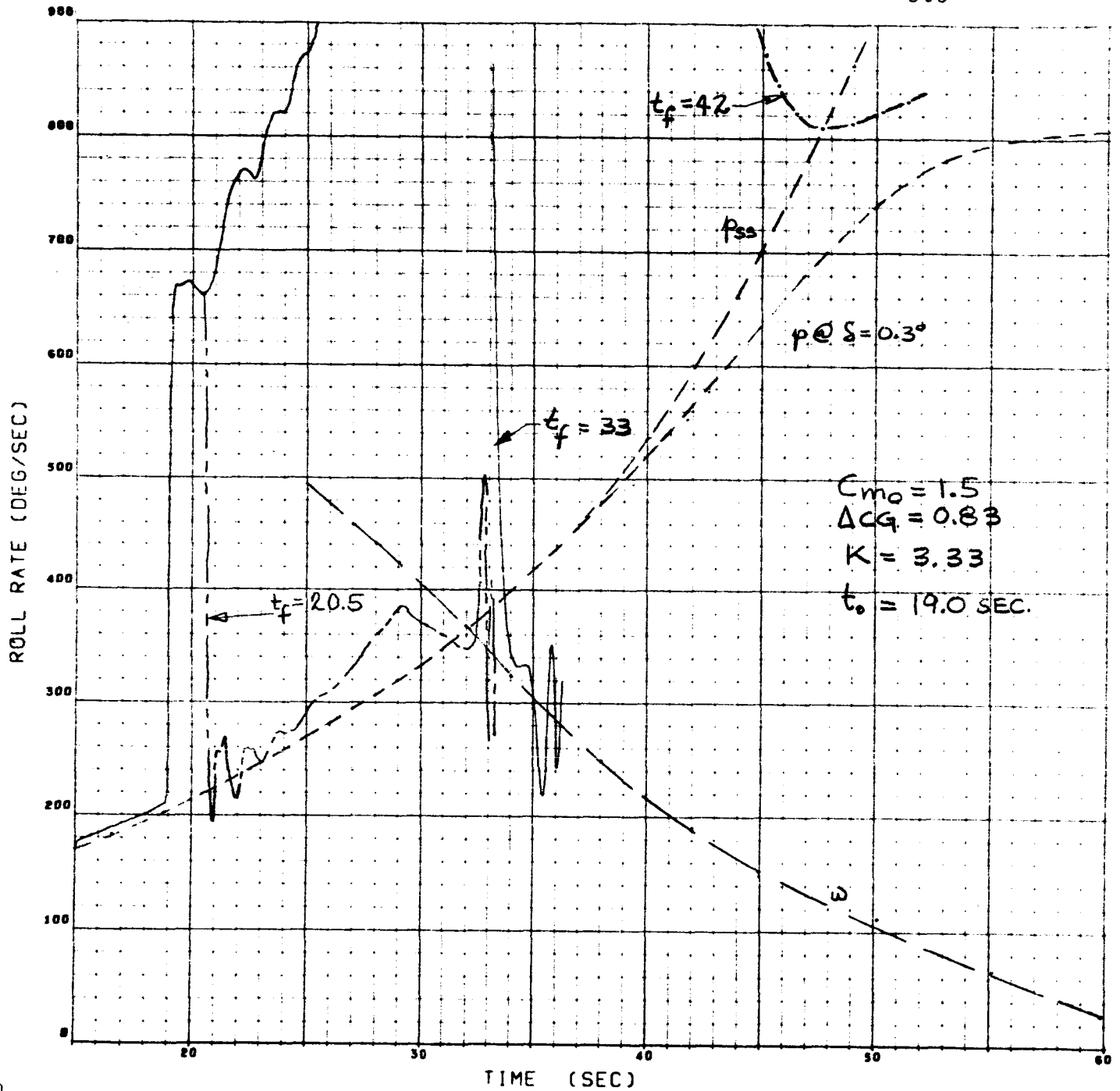


Fig. 2-15a

VERIFICATION OF TOLERANCE CONTOURS
WITH TIP AILERON DEFLECTION

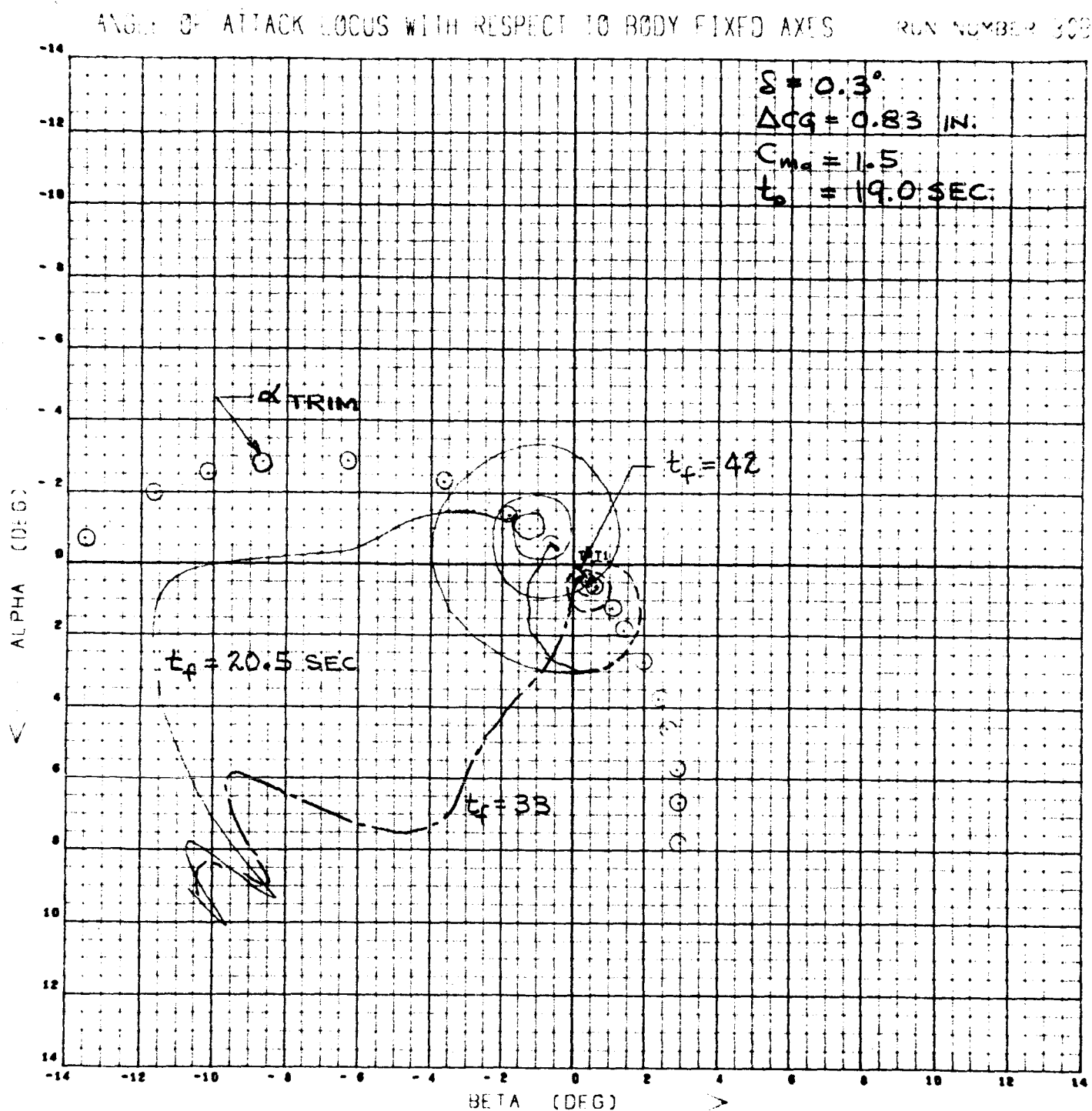


Fig. 2-15b

VERIFICATION OF TOLERANCE CONTOURS
WITH TIP AILERON DEFLECTION

TOTAL ANGLE OF ATTACK TIME HISTORY

RUN NUMBER 306

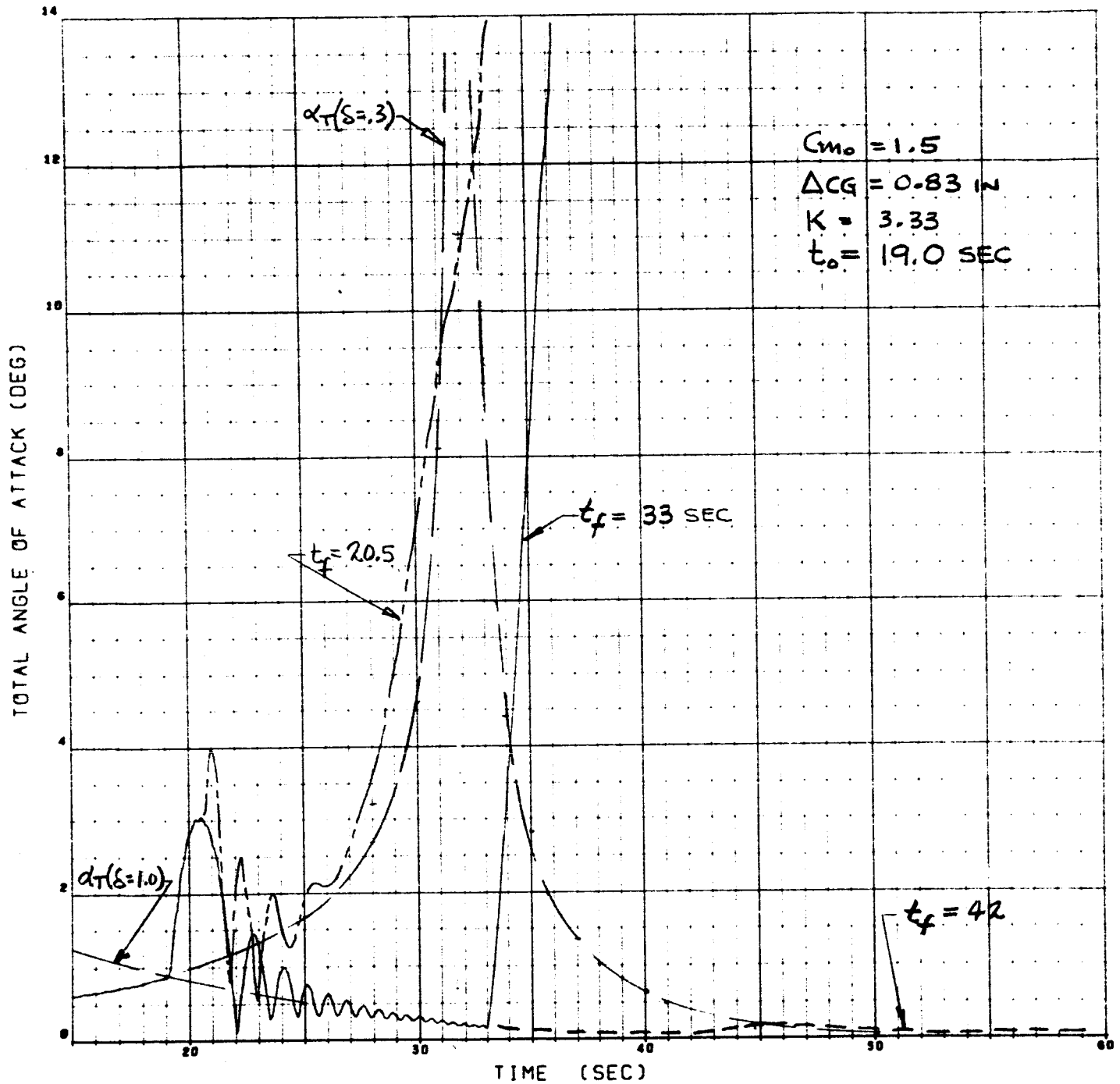


Fig. 2-15c

VERIFICATION OF TOLERANCE CONTOURS
WITH TIP AILERON DEFLECTION

δ_a Programmed for 2 rps

TOTAL ANGLE OF ATTACK TIME HISTORY

RUN NUMBER 30H

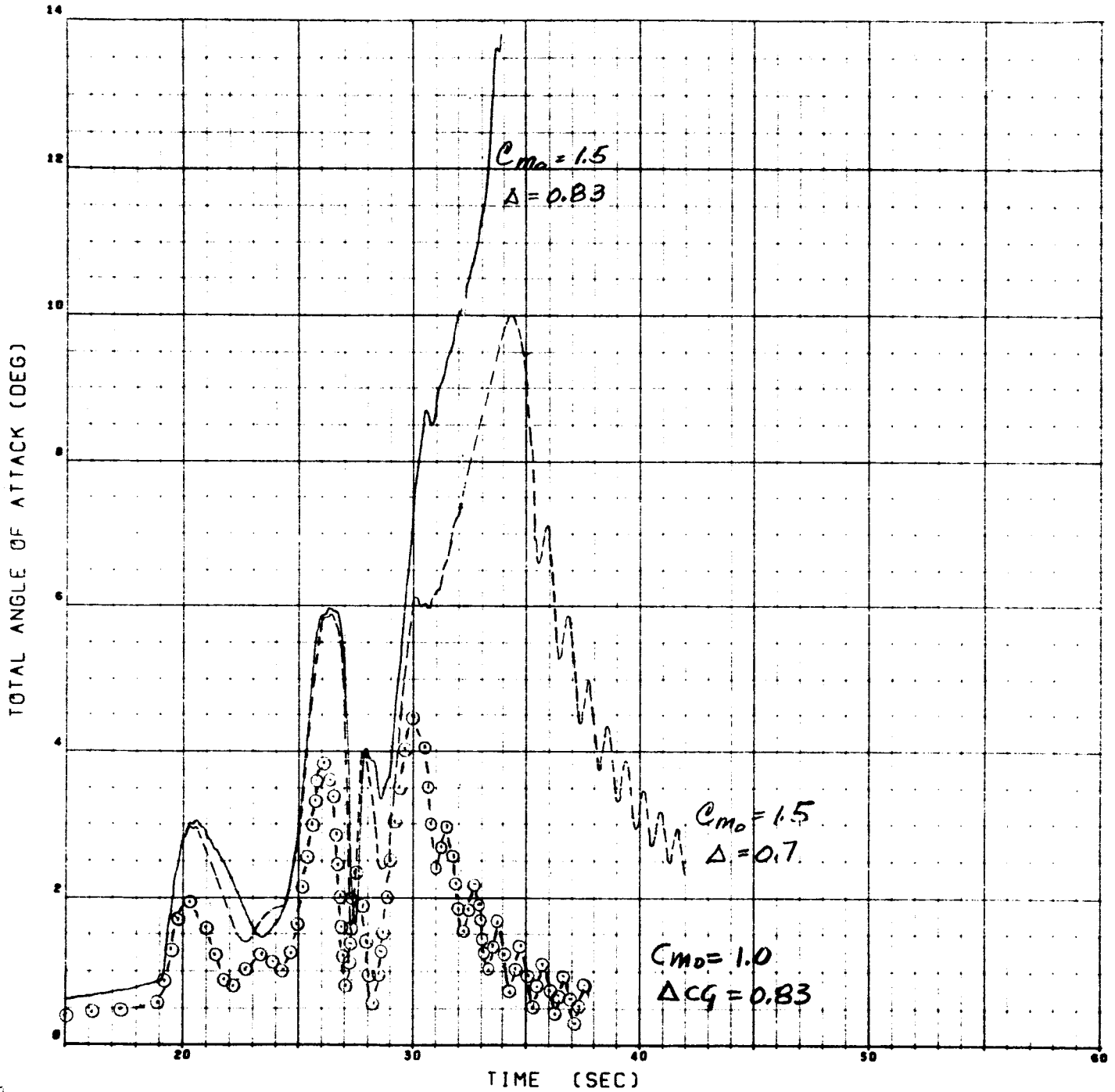


Fig. 2-16a

VERIFICATION OF TOLERANCE CONTOURS
WITH TIP AILERON DEFLECTION
ROLL RATE TIME HISTORY

RUN NUMBER 30H

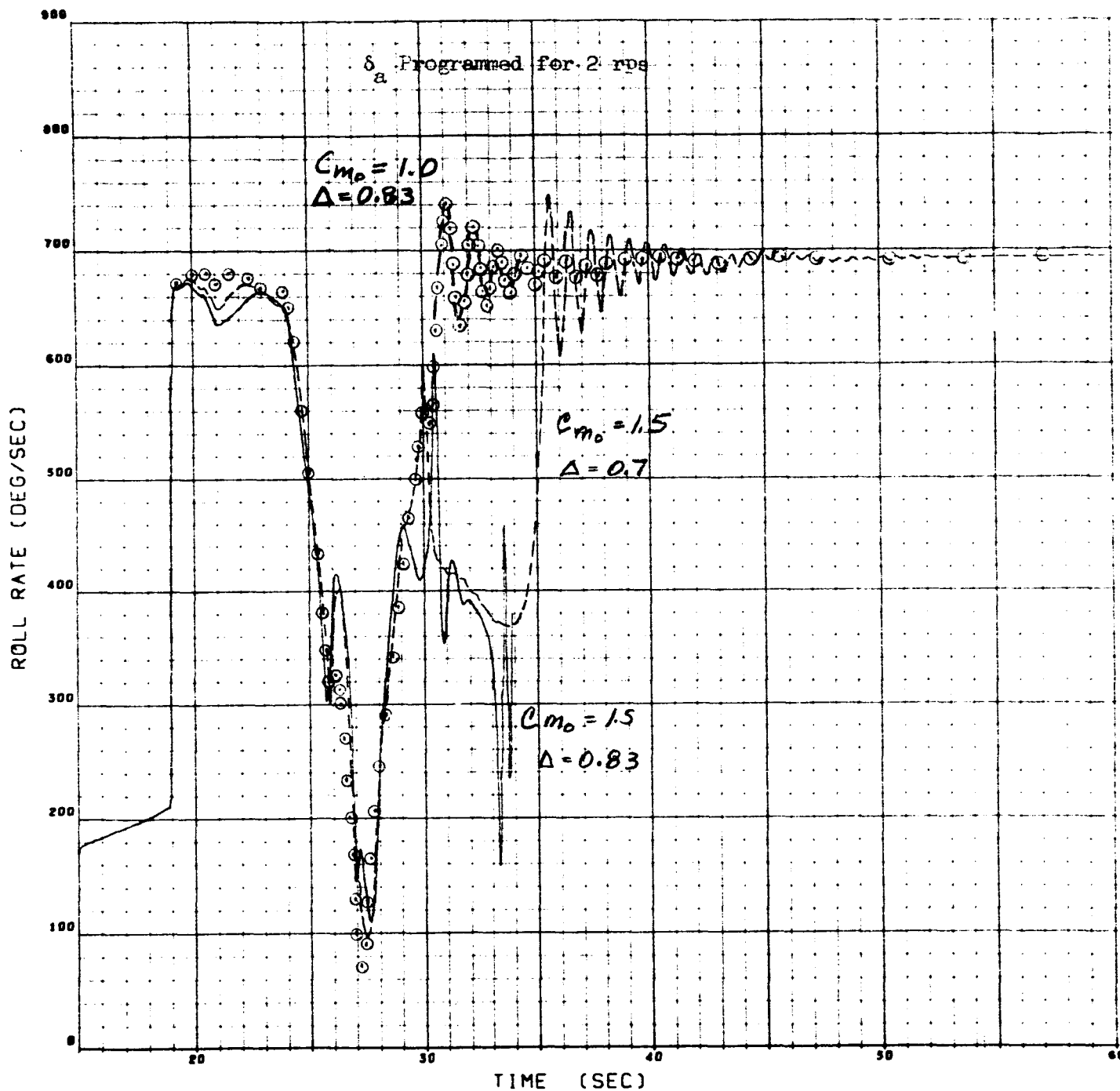


Fig. 2-16b

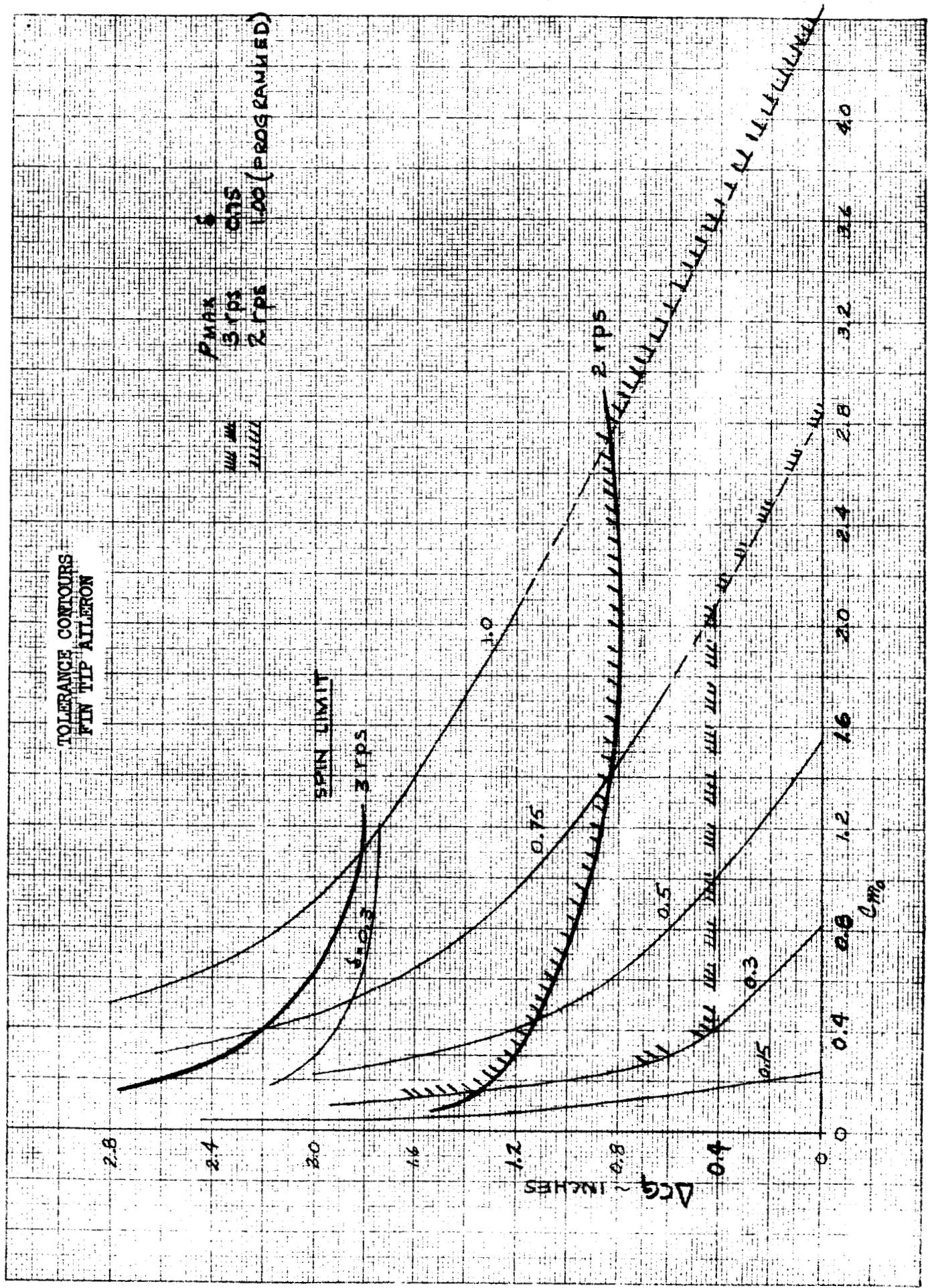


Fig. 2-17a

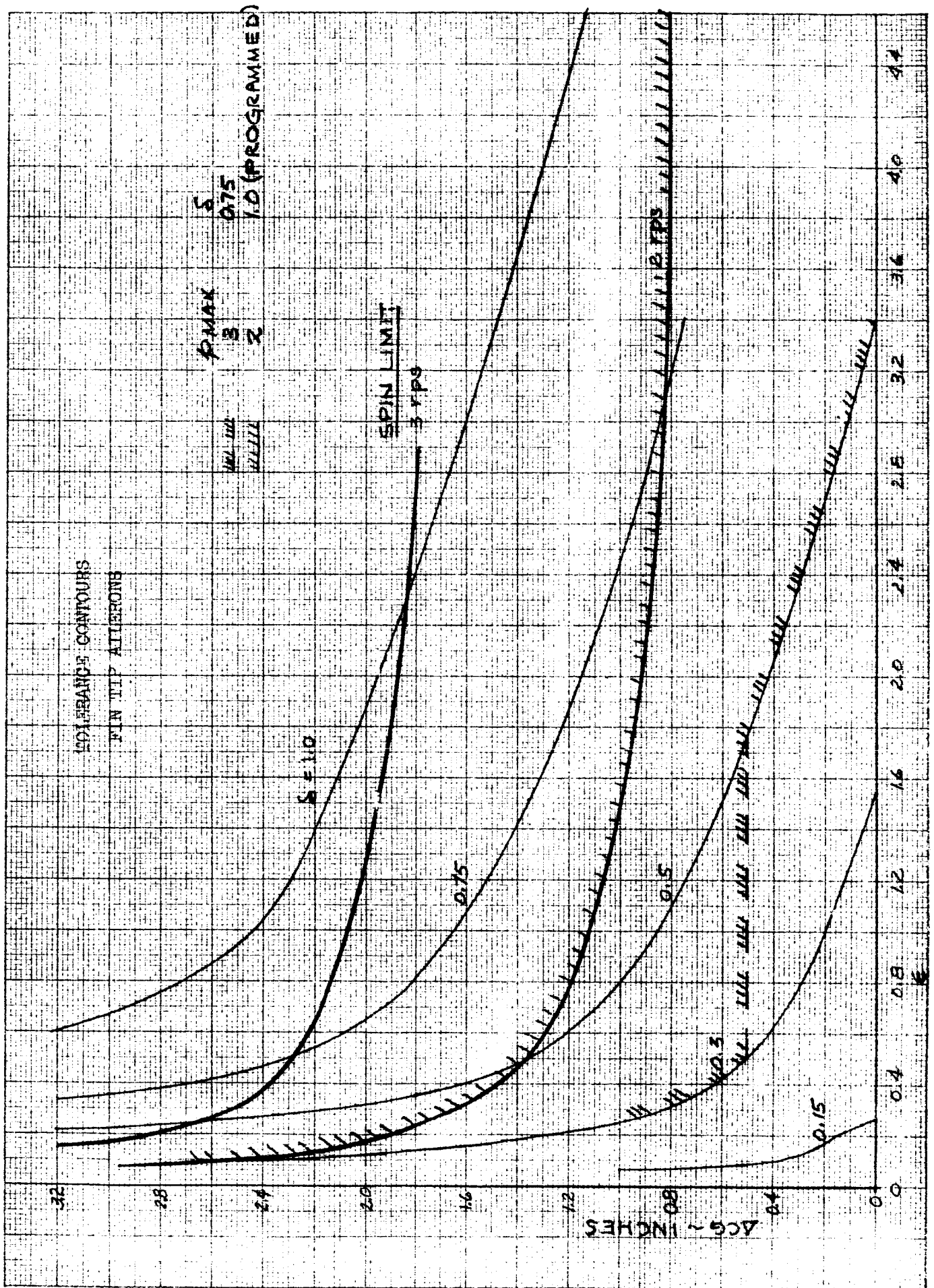


Fig. 2-17b

TOLERANCE CONTOUR BOUNDARY
PITCH REACTION CONTROL

$$\Delta C_G = 0.5 \text{ IN.}$$

$$\delta = 0.3 \text{ DEG.}$$

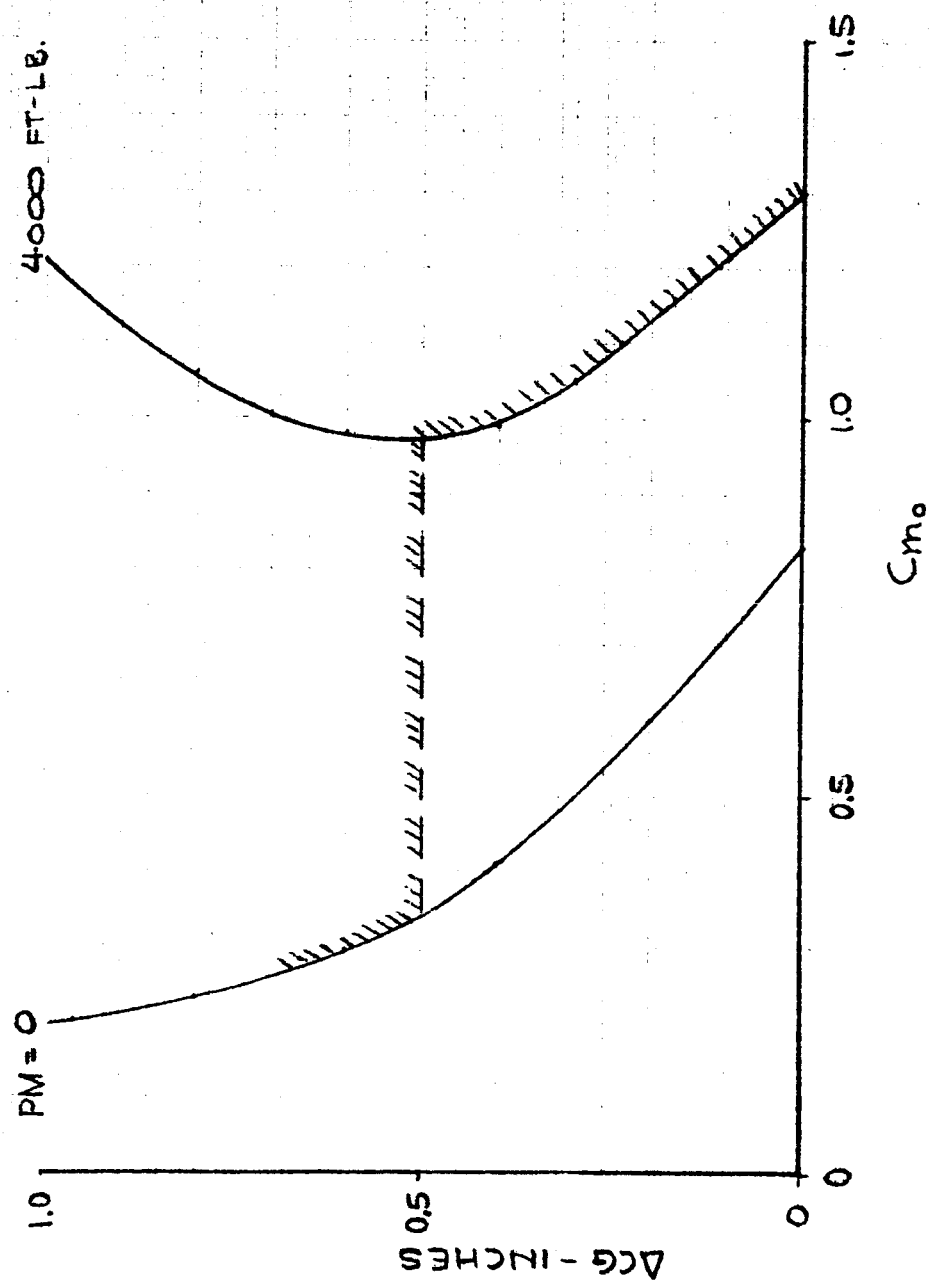


Fig. 2-18a

TOLERANCE CONTOUR BOUNDARY
PITCH REACTION CONTROL

$\Delta CG = 0.5$ IN
 $\delta = 0.3$ DEG

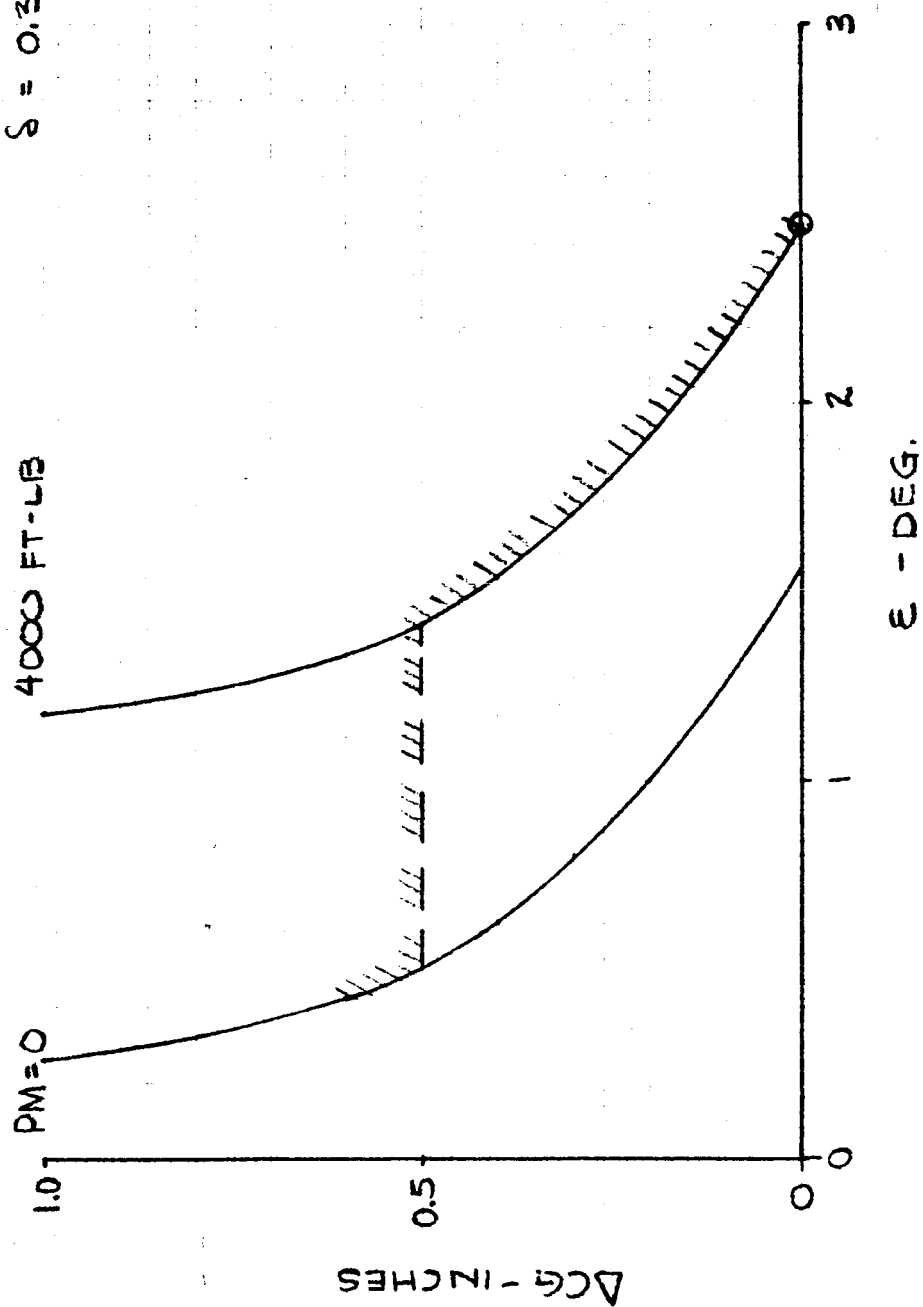


Fig. 2-18b

TOLERANCE CONTOURS FOR
TOTAL ANGLE OF ATTACK

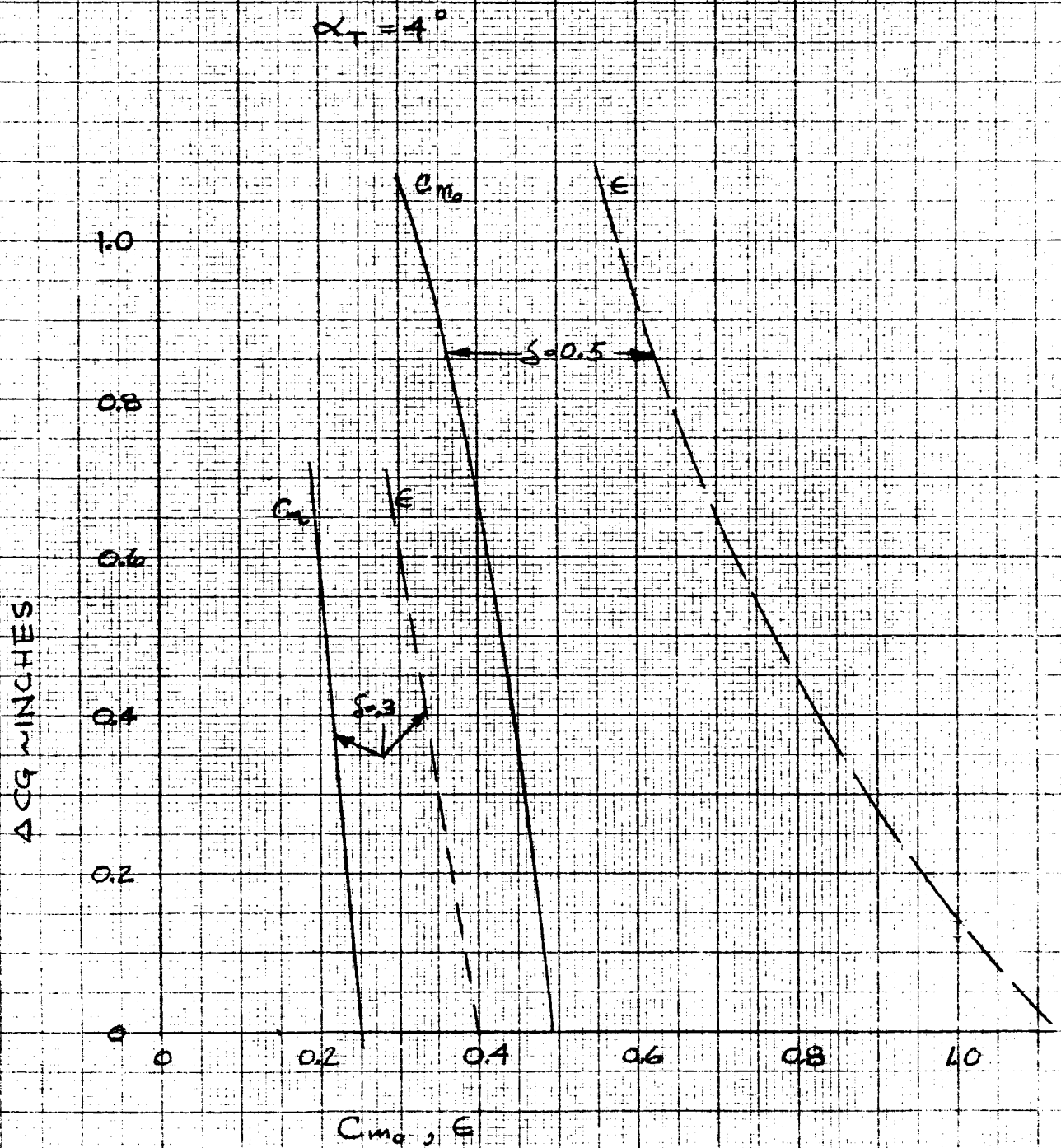


Fig. 2-19

DEMONSTRATION OF ANGLE OF ATTACK CONTROL

ANGLE OF ATTACK LOCUS WITH RESPECT TO BODY FIXED AXES

$\Delta CG = 0.0$
 $\delta_F = 0.3 \text{ deg}$
 $t_0 = 28.8 \text{ sec}$

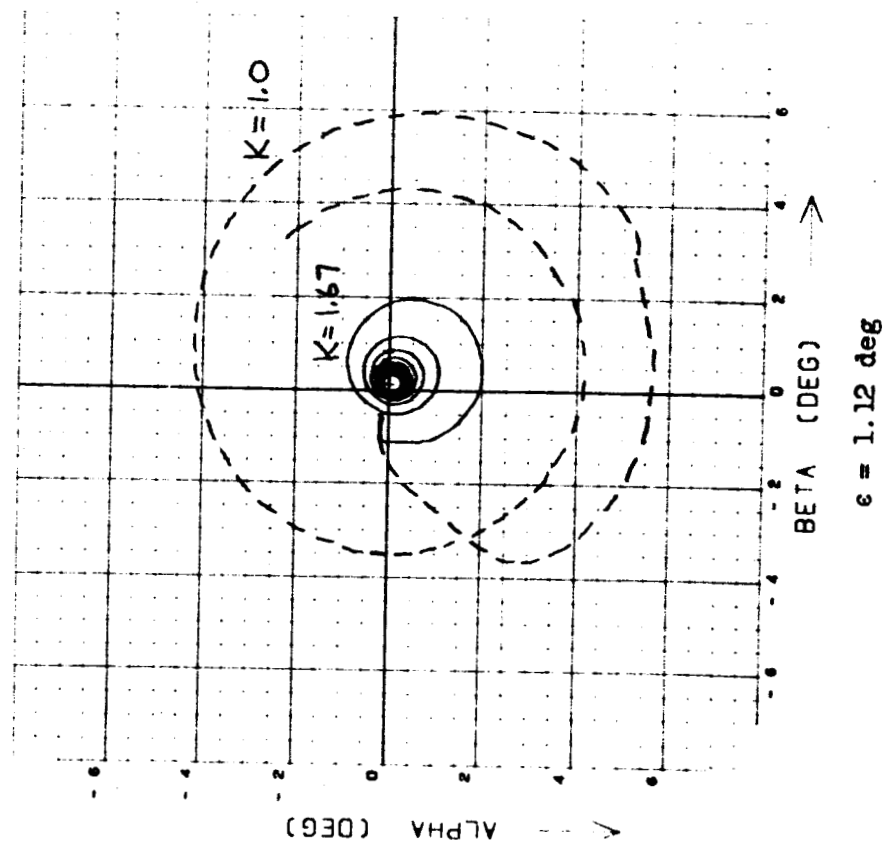
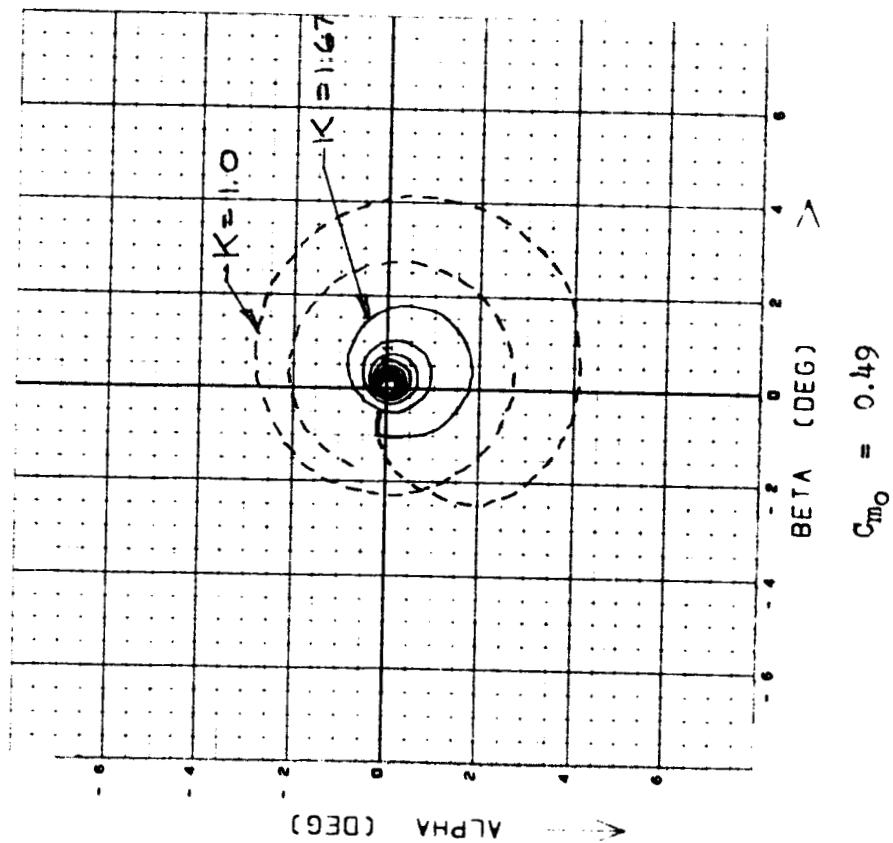


Fig. 2-20a

DEMONSTRATION OF ANGLE OF ATTACK CONTROL

TOTAL ANGLE OF ATTACK TIME HISTORY

RUN NUMBER 1020

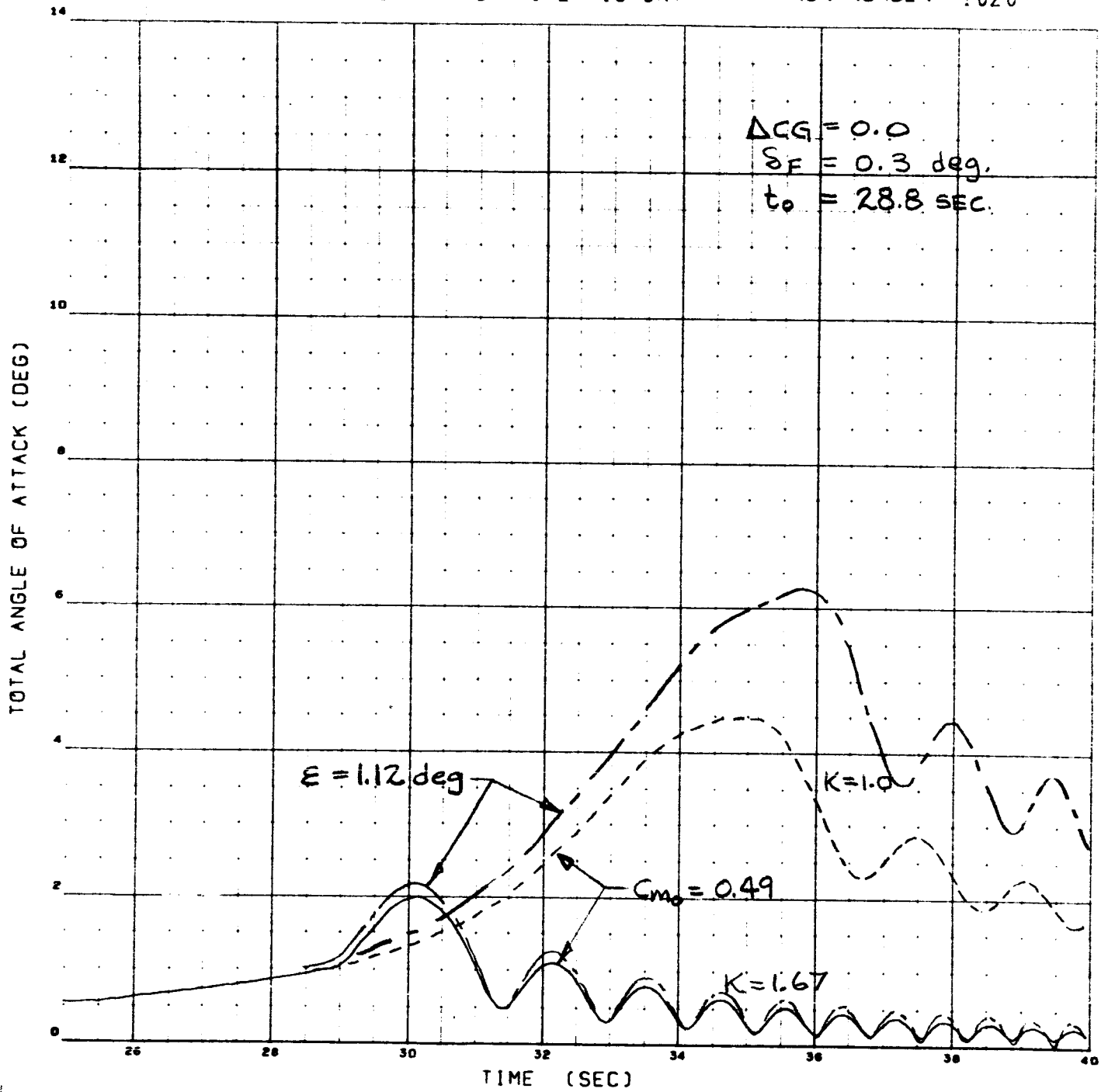


Fig. 2-20b

DEMONSTRATION OF ANGLE OF ATTACK CONTROL

ROLL RATE TIME HISTORY

RUN NUMBER 1020

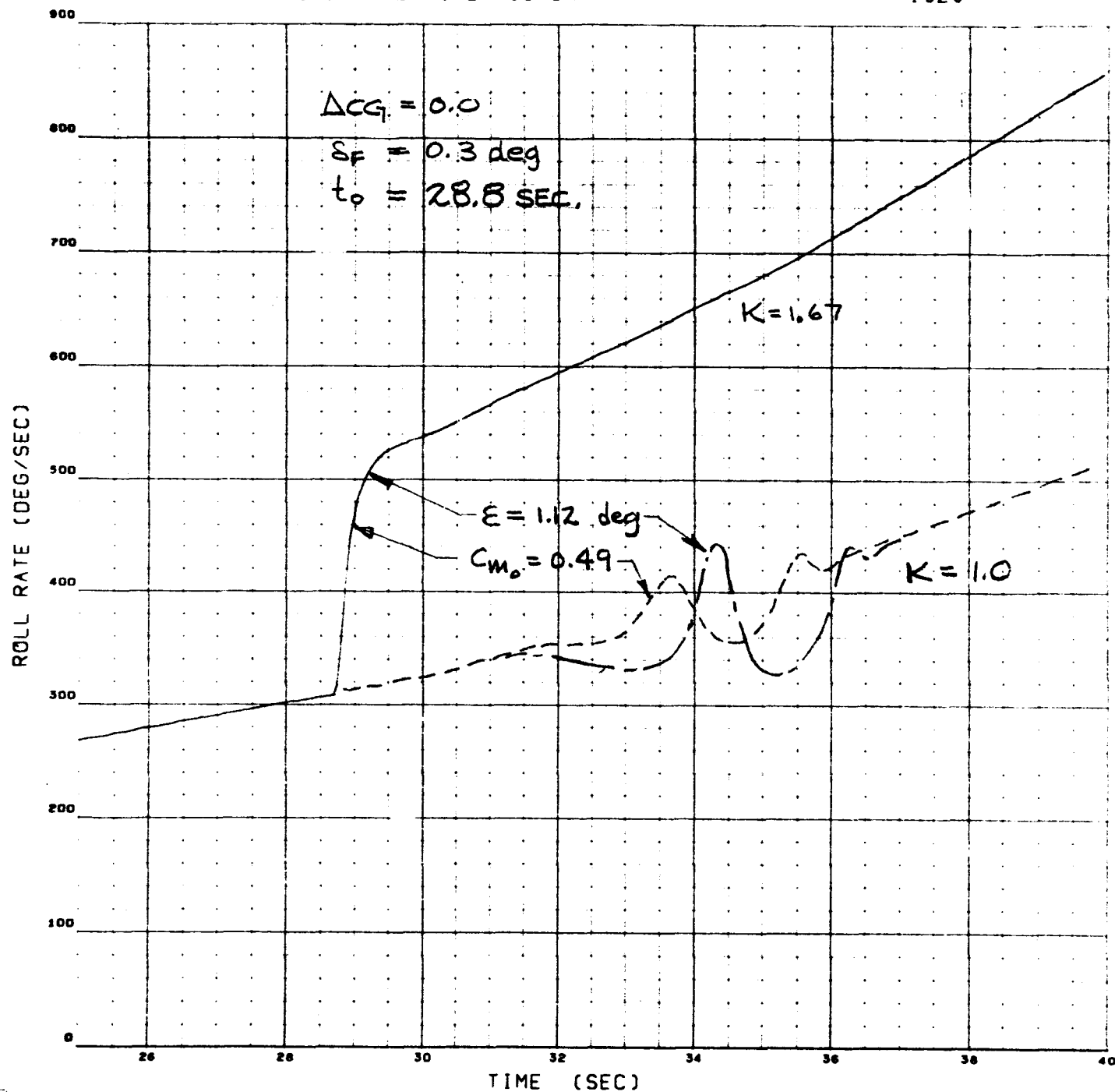


Fig. 2-20c

ACCELERATION ENVIRONMENT

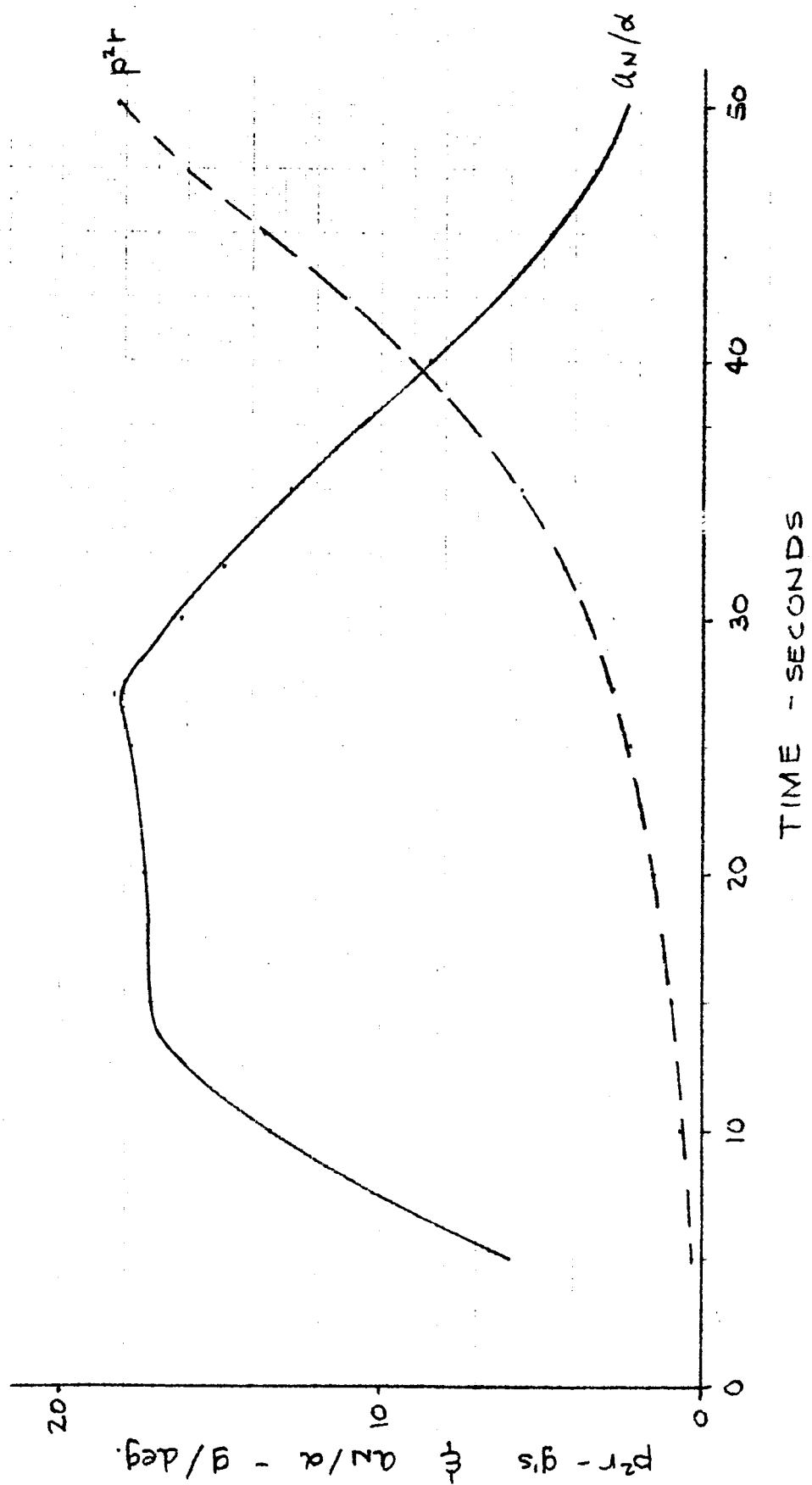
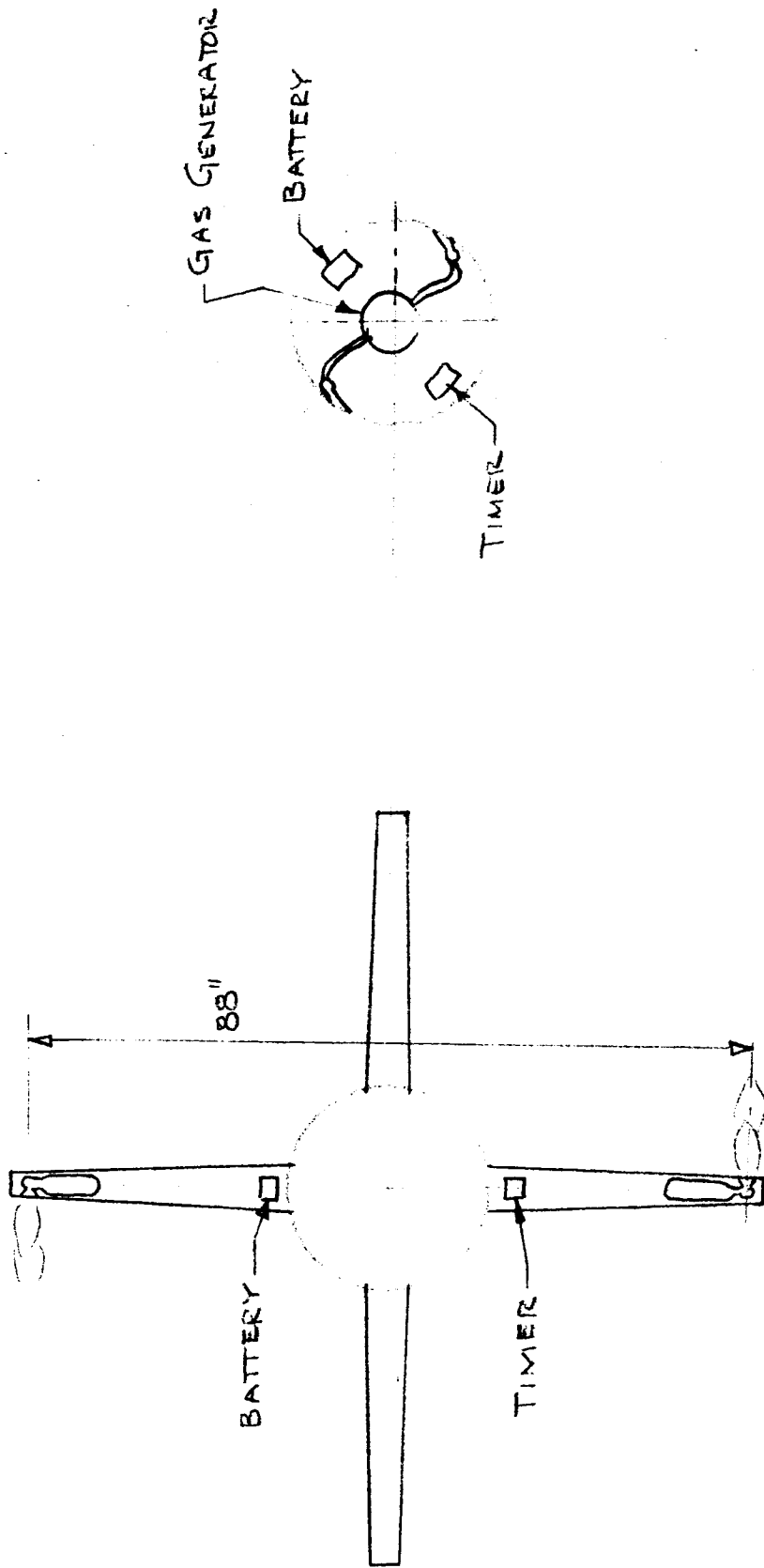
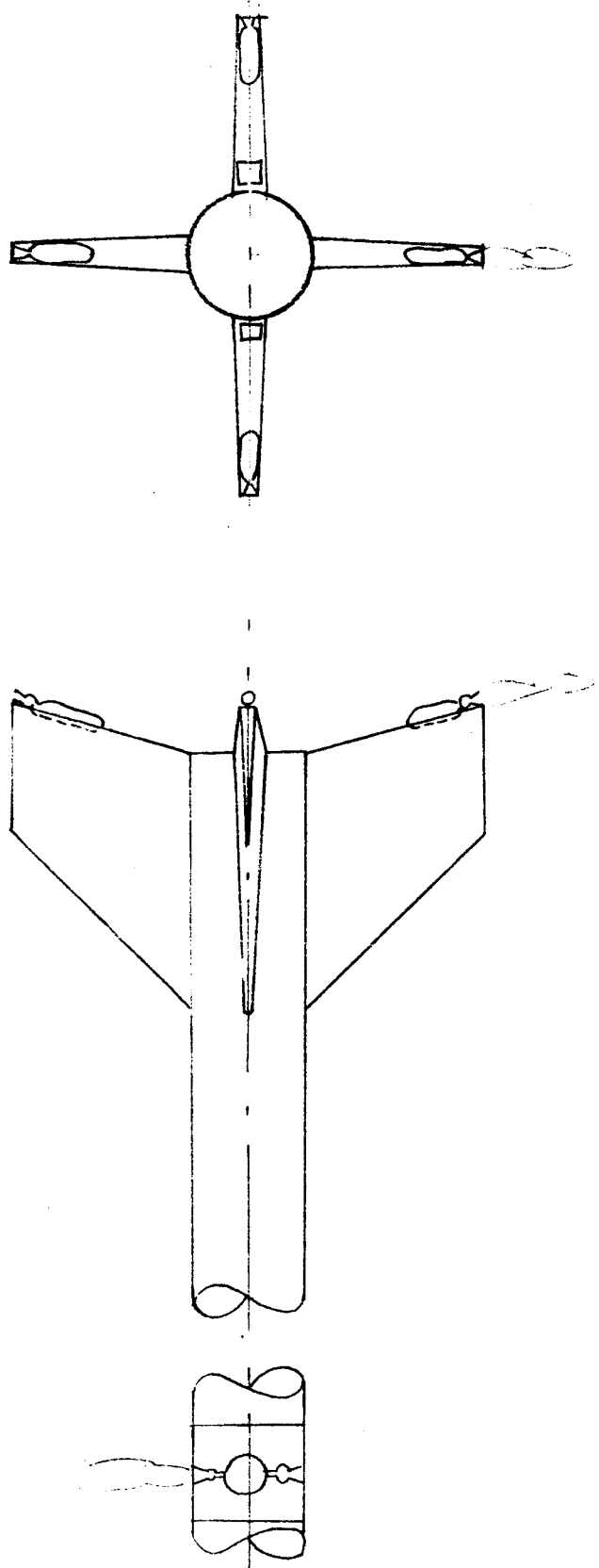


Fig. 3-1

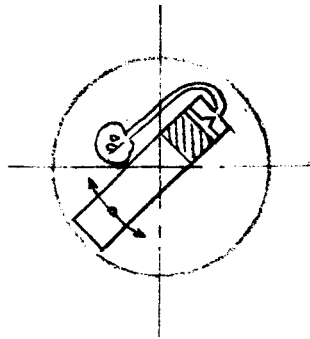


ROLL REACTION CONTROL MECHANIZATION

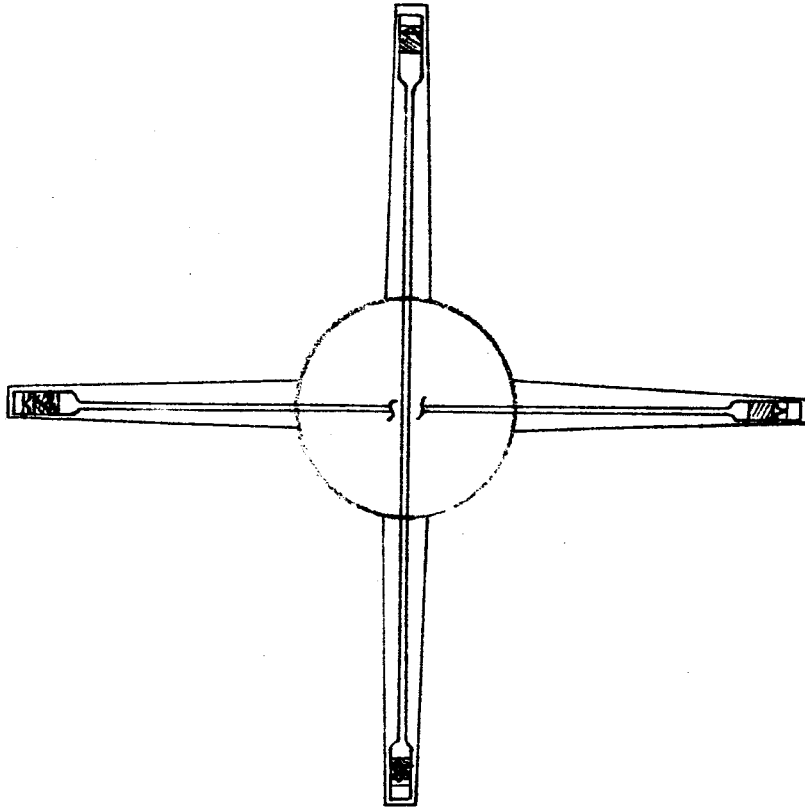


PITCH REACTION CONTROL MECHANIZATION

Fig. 3-2b

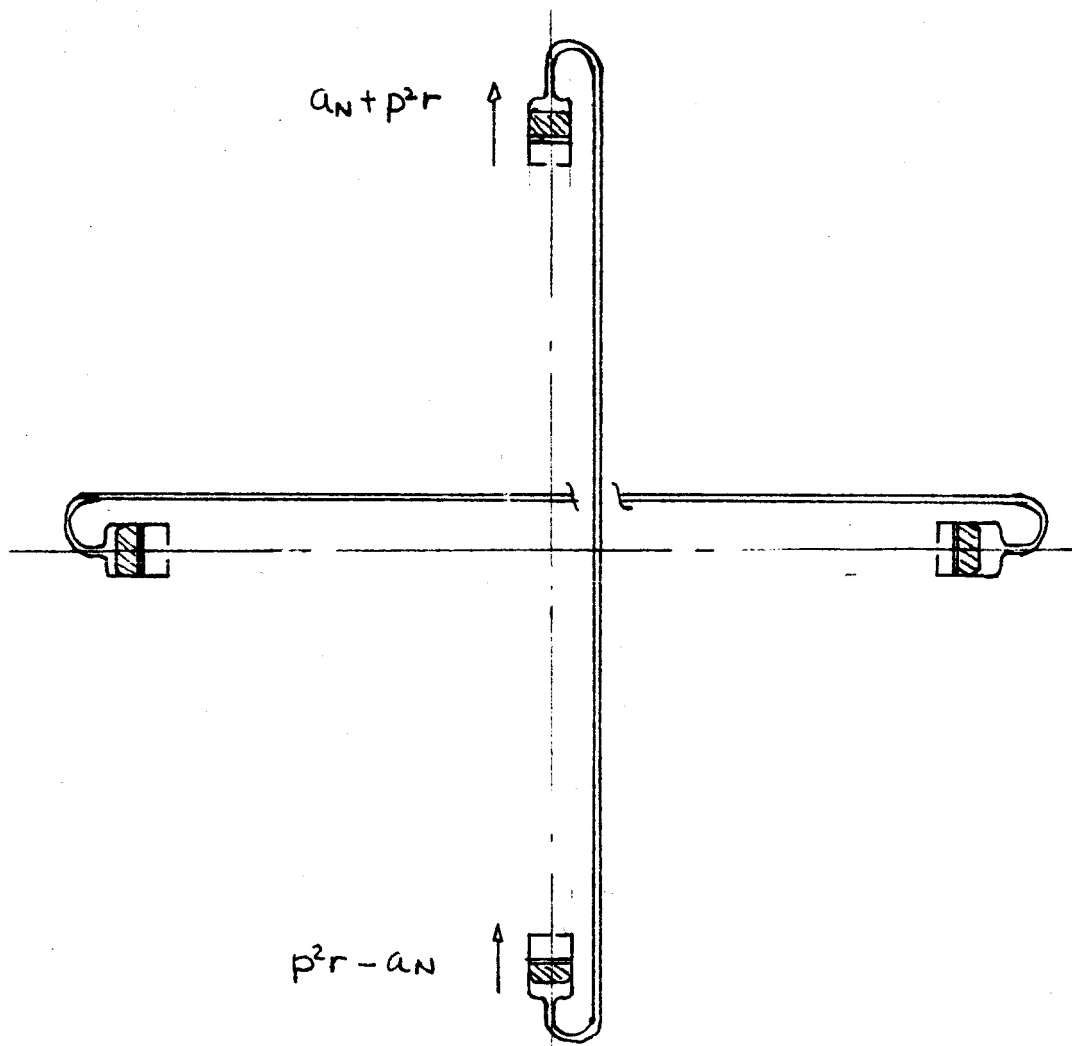


BODY MOUNTING

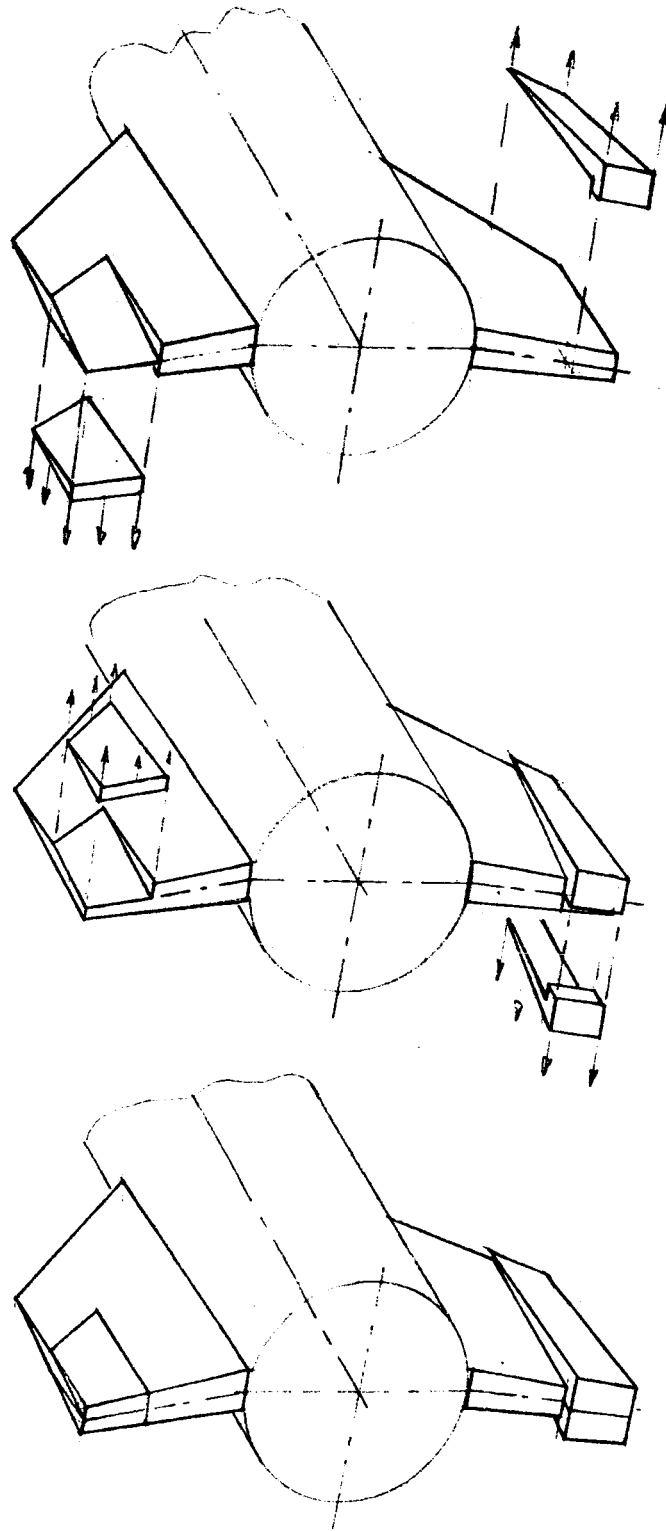


FIN MOUNTING

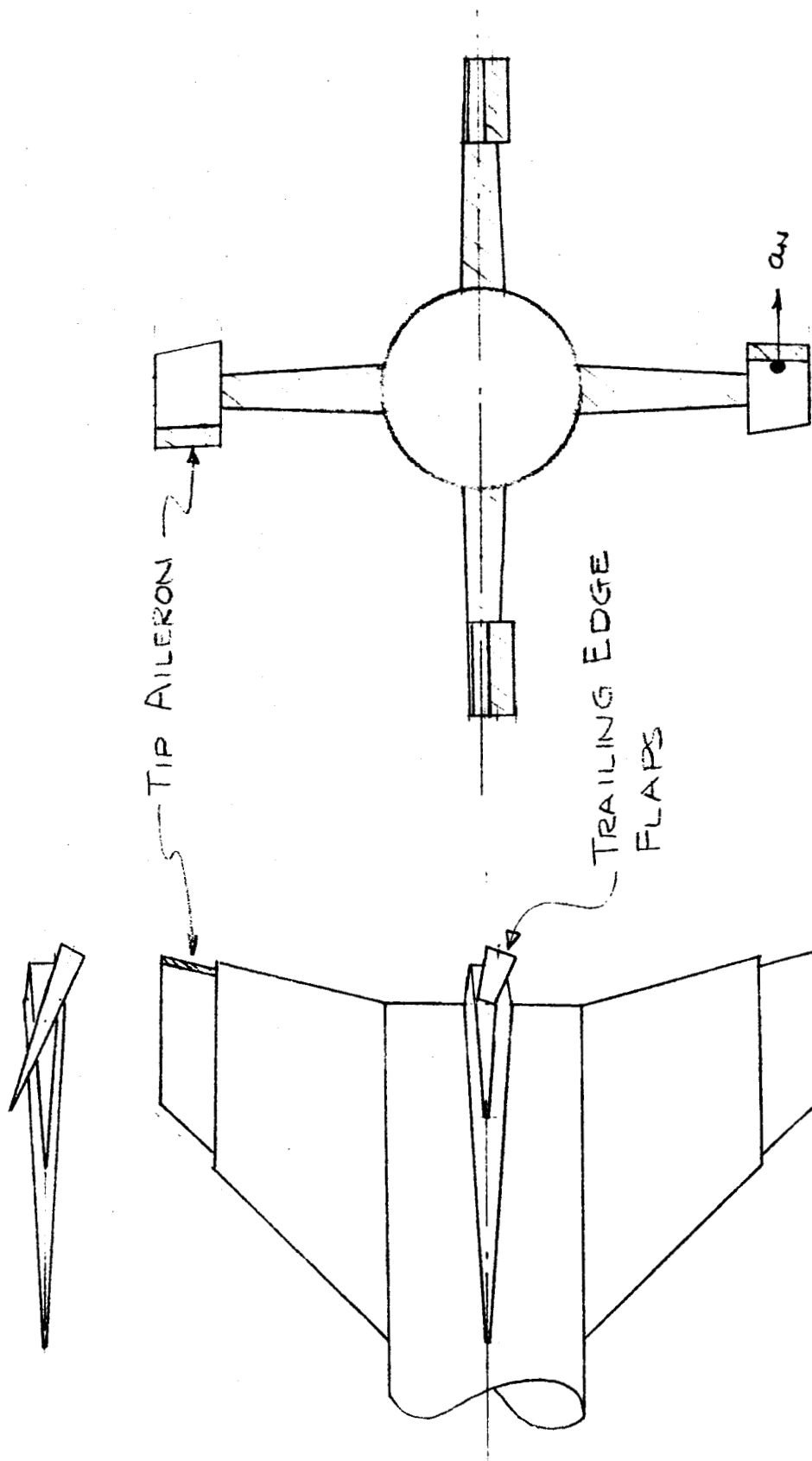
C. G. SHIFT ROLL CONTROL MECHANIZATION PRESSURE TRANSFER



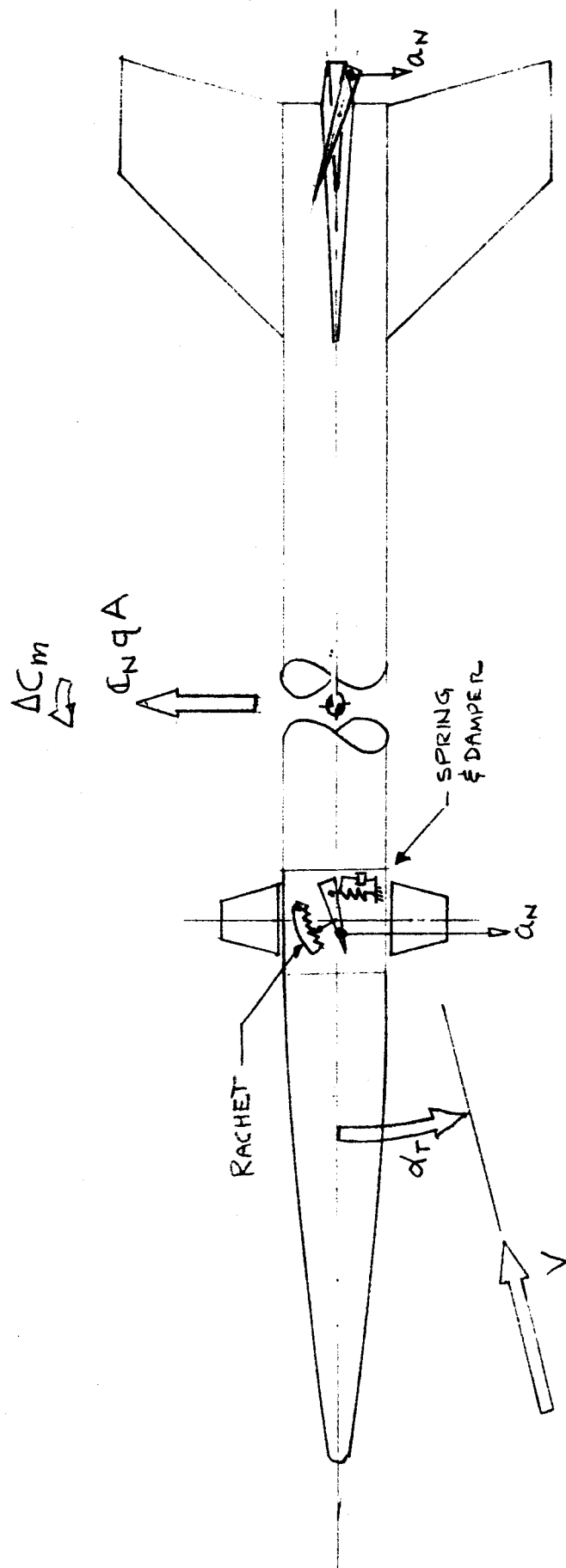
ACCELERATION TRANSFER



ROLL CONTROL GLOVE

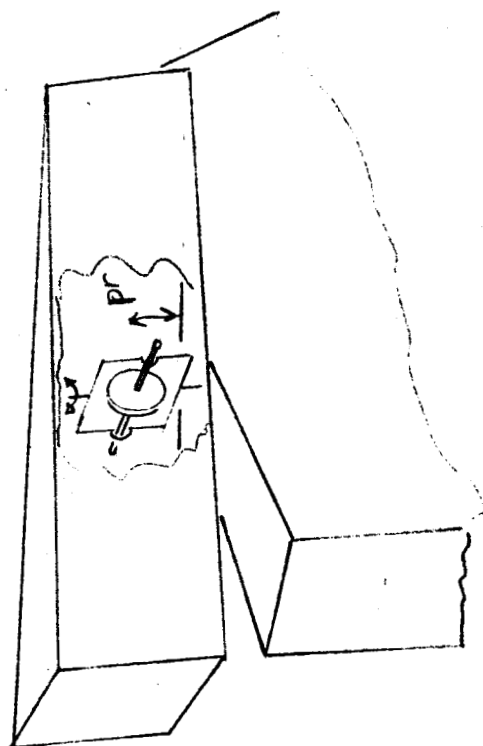


AERODYNAMIC ROLL CONTROL

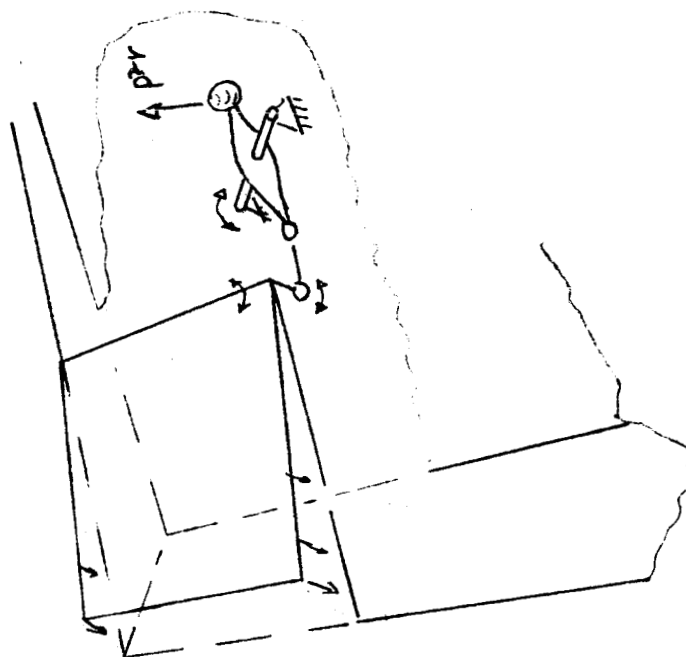


AERODYNAMIC PITCH CONTROL MECHANIZATION

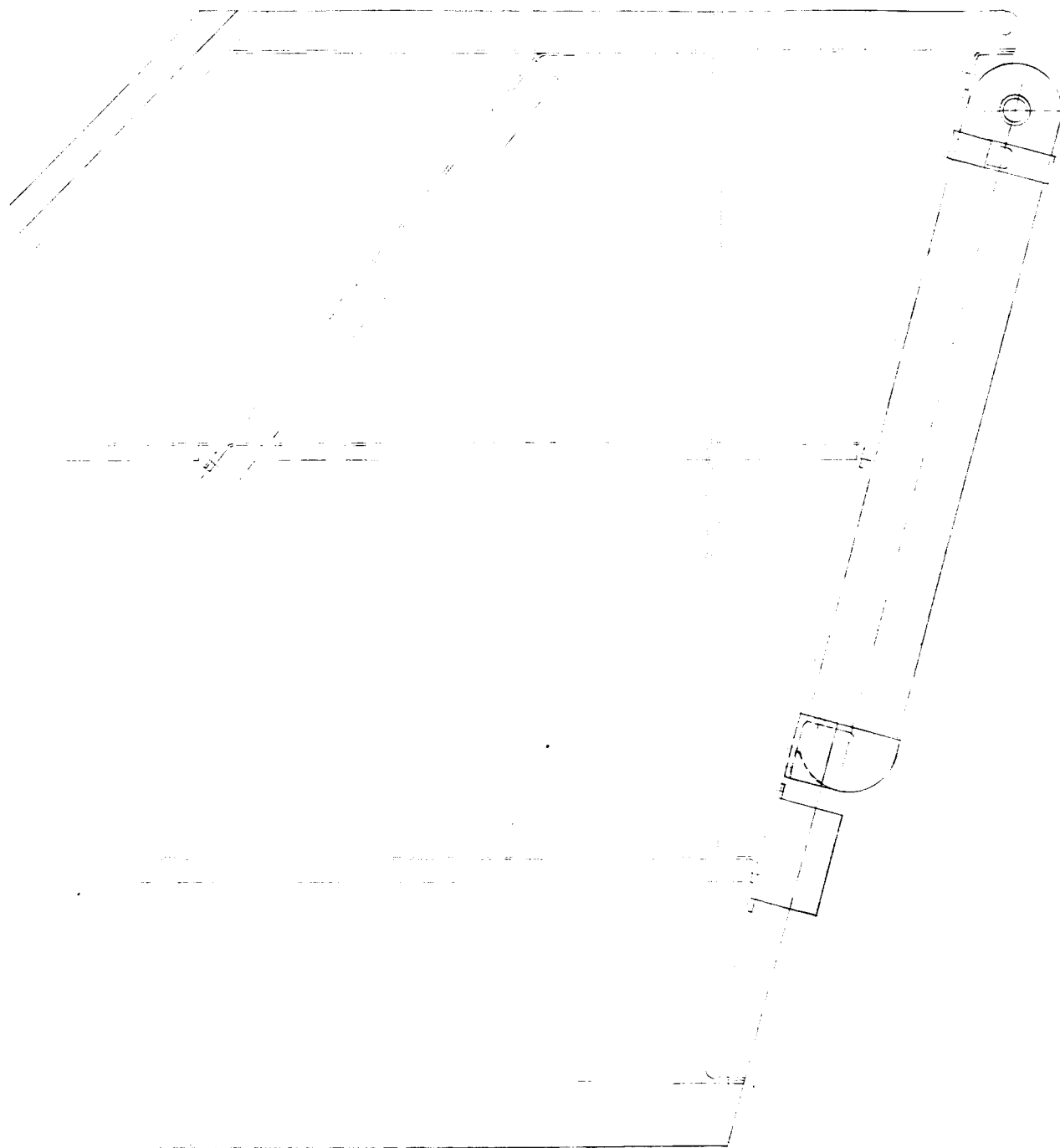
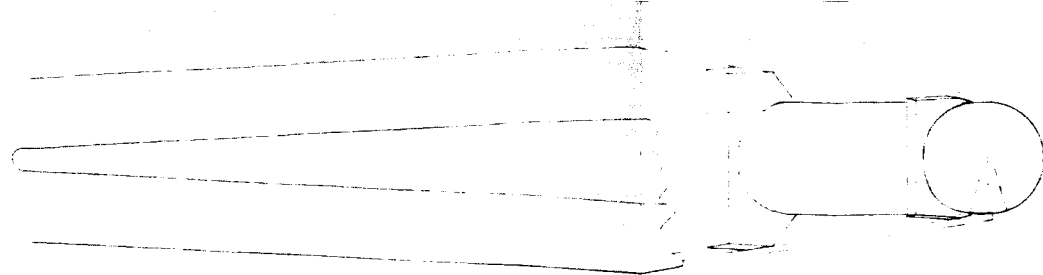
ROLL RATE PROGRAMMING



GYRO



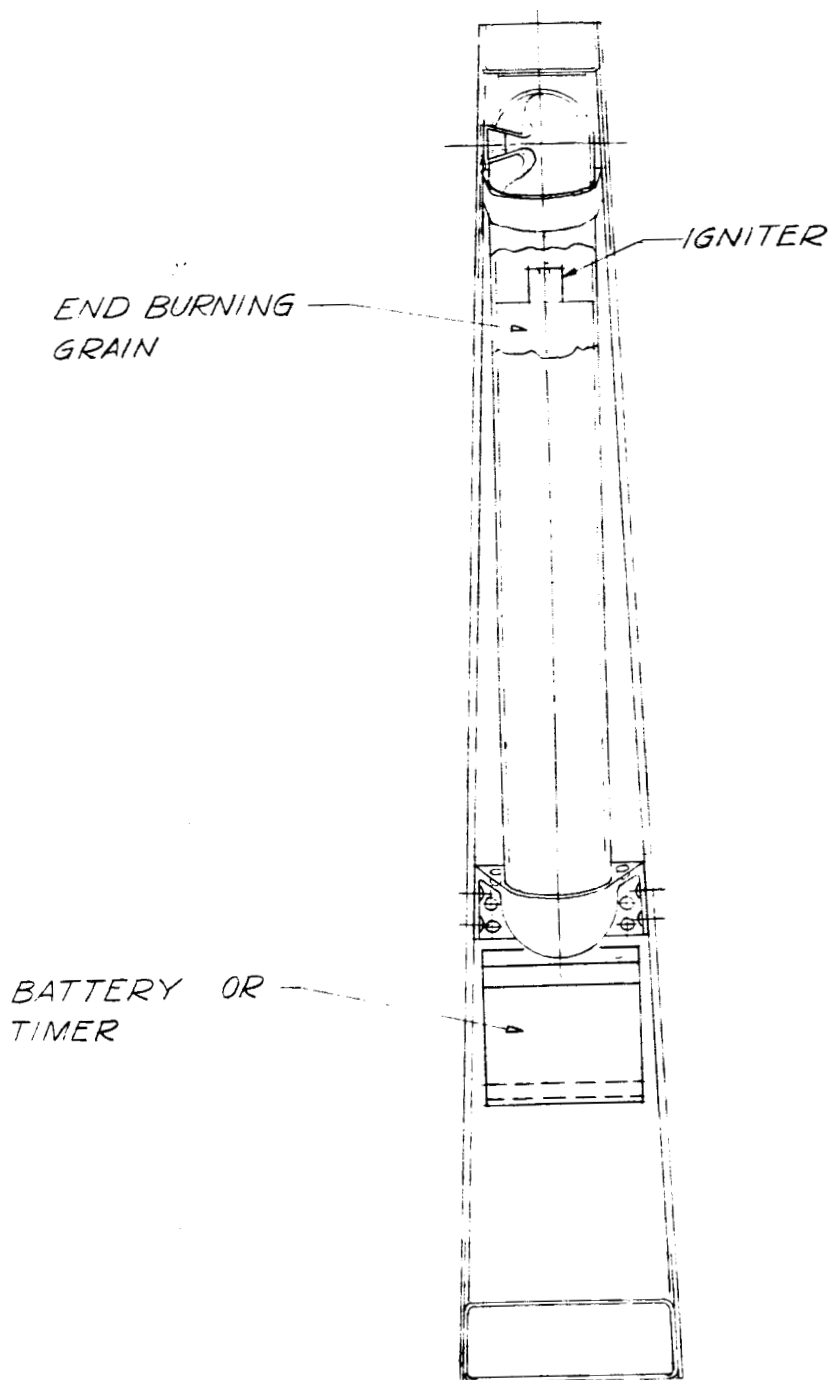
GOVERNOR



REACTION

1

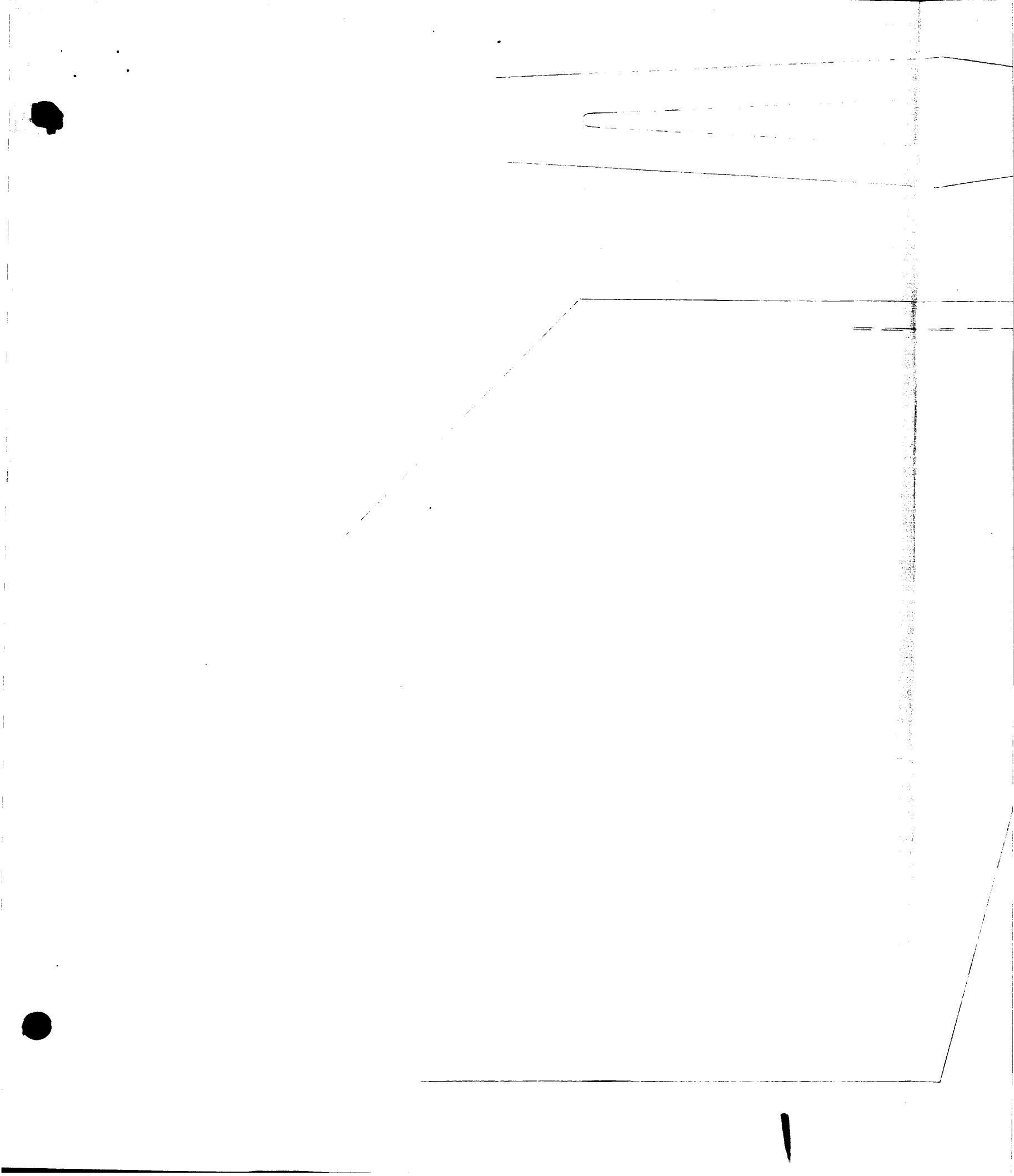
3.5 FT. MOMENT ARM

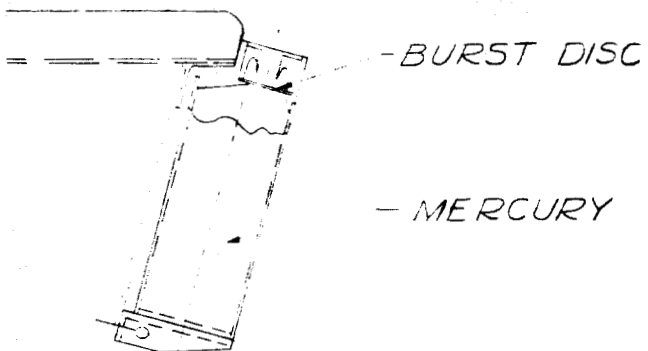
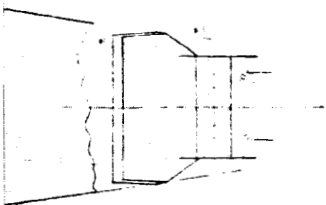


IMPULSE

2

FIG. 3-5

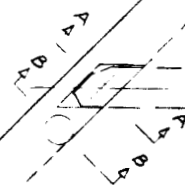
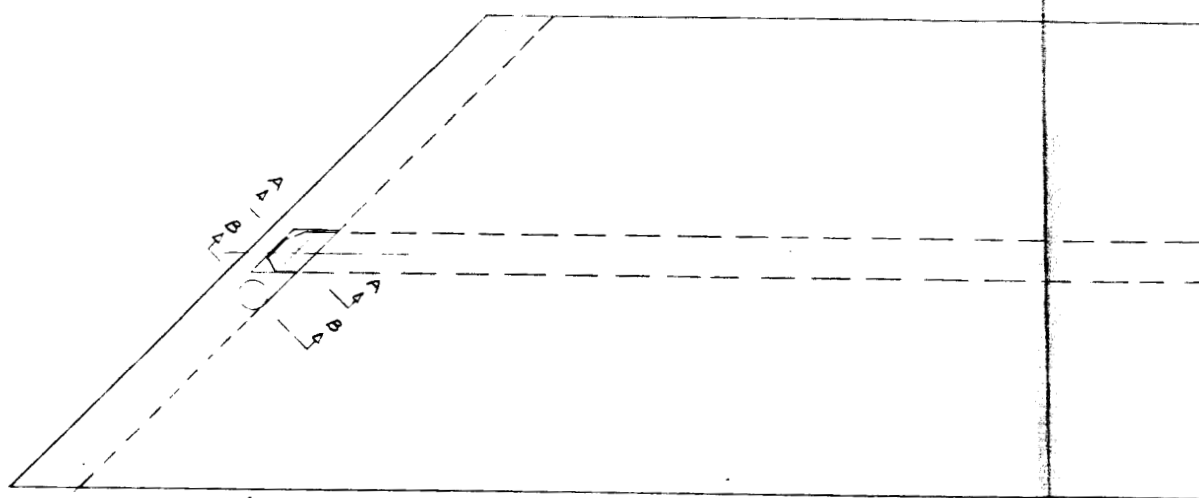
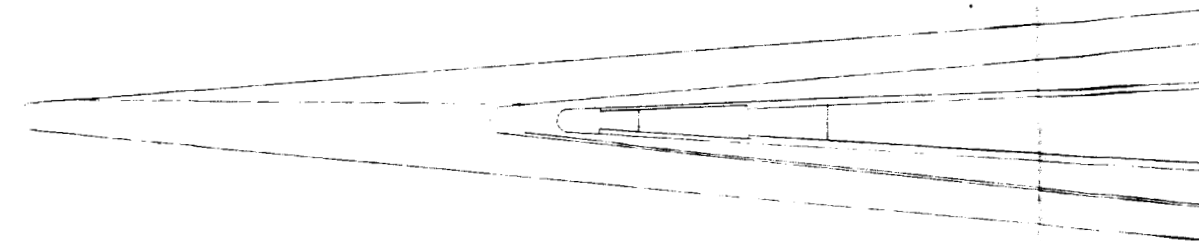




CG SHIFT 

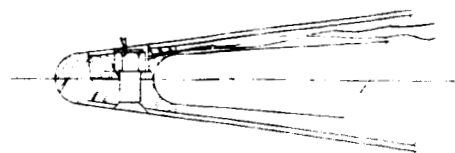
FIG. 3-6

GLOVE

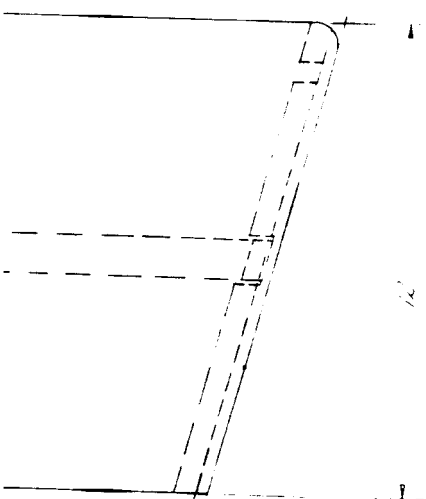
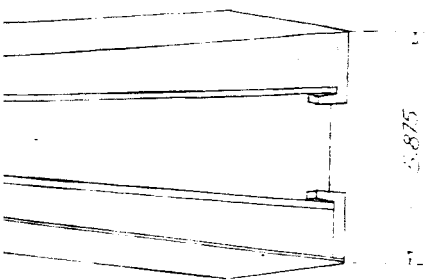


SEPARATION NUT

A-A



B-B



BATTERY or TIMER

2

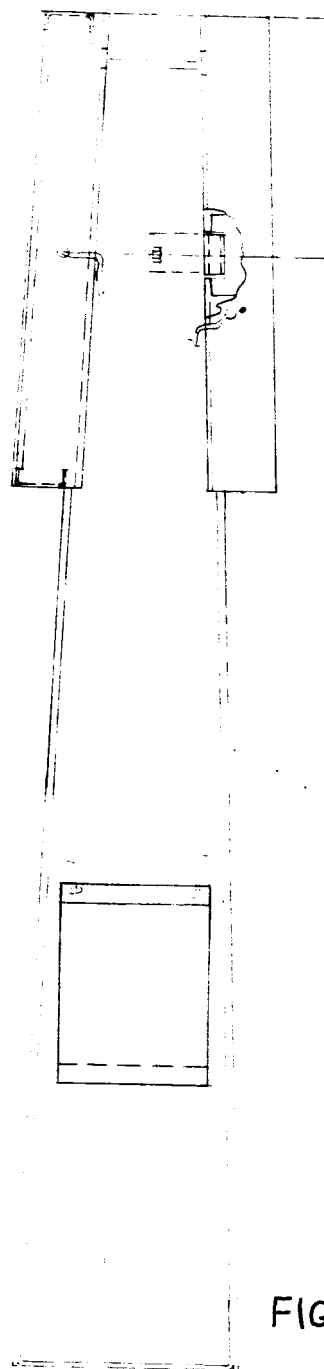
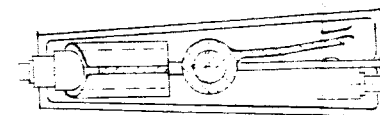
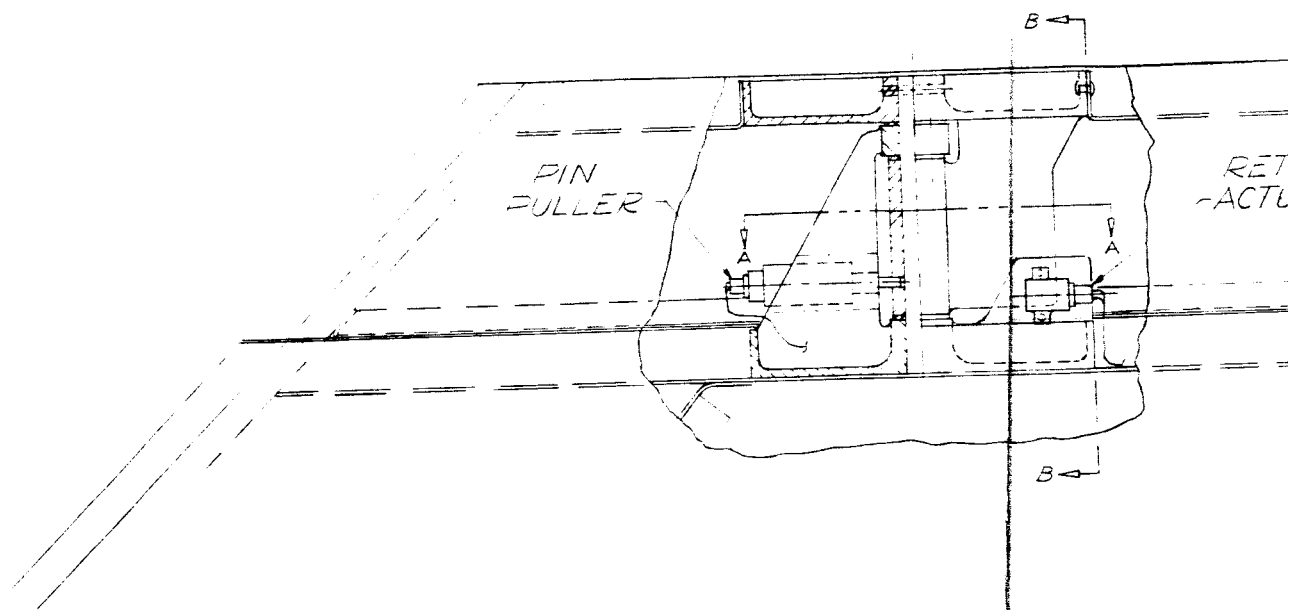


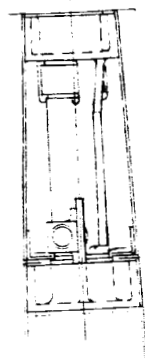
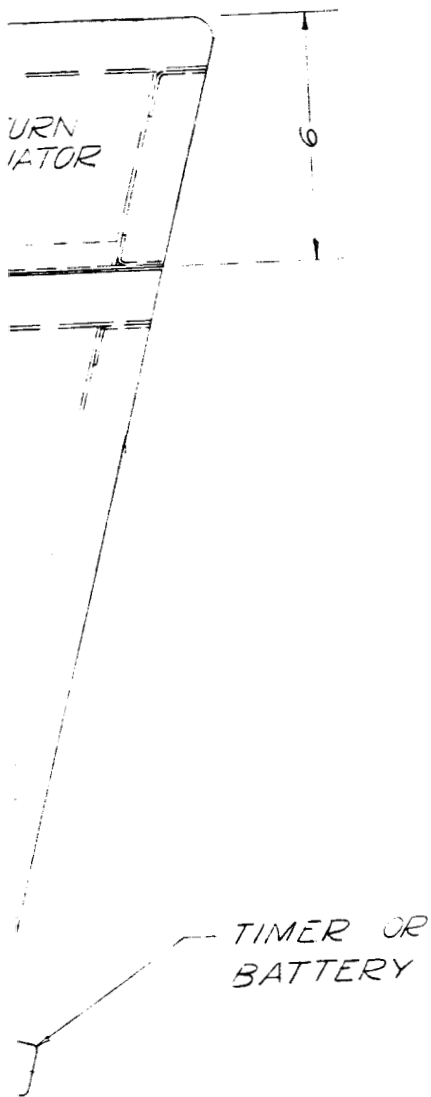
FIG. 3-7



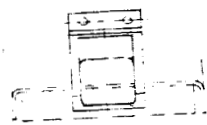
A-A



TIP AILERON



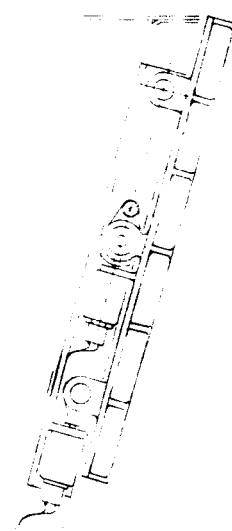
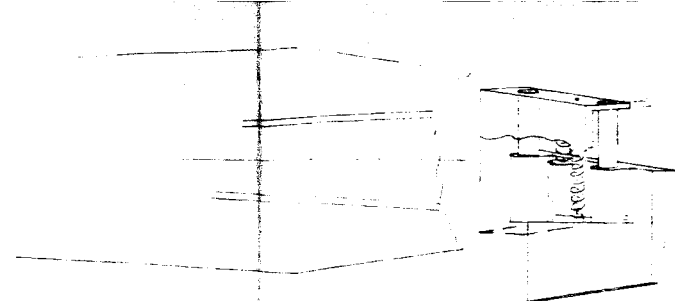
B-B



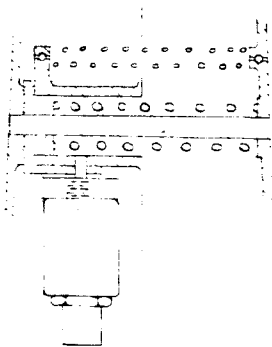
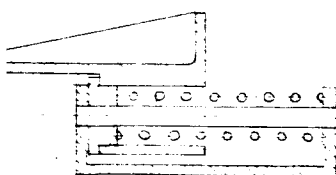
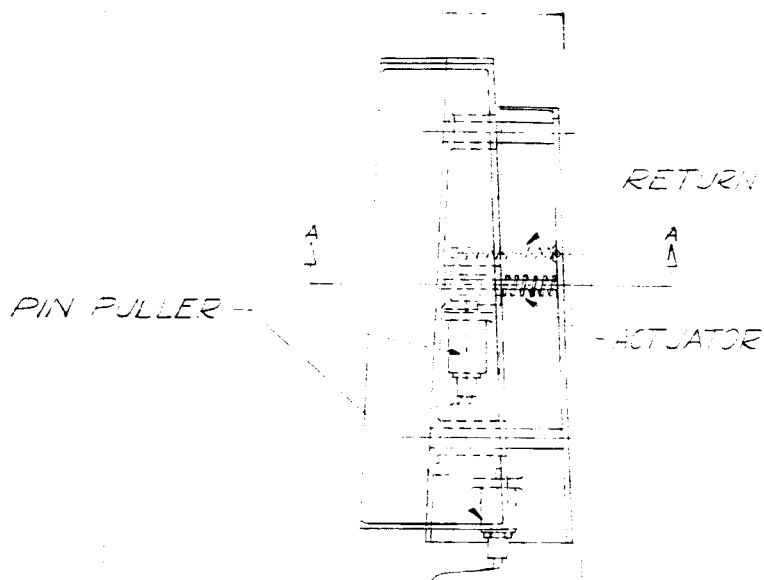
2

DN

FIG. 3-8



SPOILER



A-A

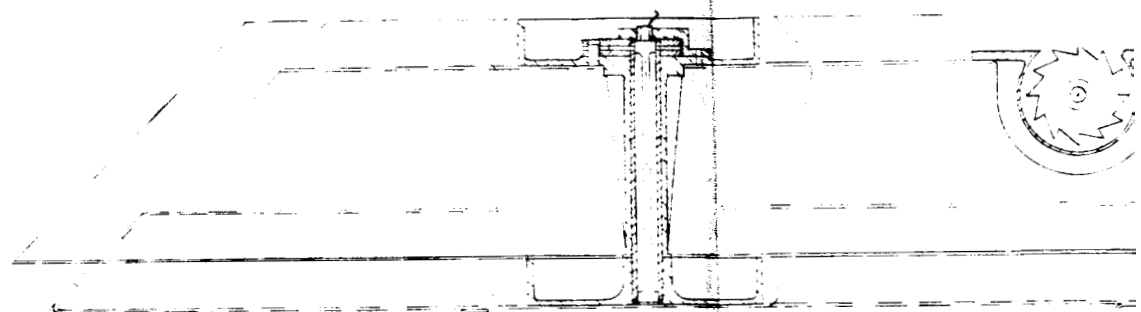
2

FIG. 3-9

LIMIT PIN --

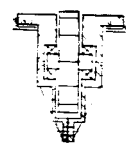
PRE-LOAD LEVER

TORSION SPRING



GYRO

— AIR DRIVEN
GYRO



ILERON

FIG. 3-10

SPIN RATE PROGRAMMING WITH GYRO AILERON

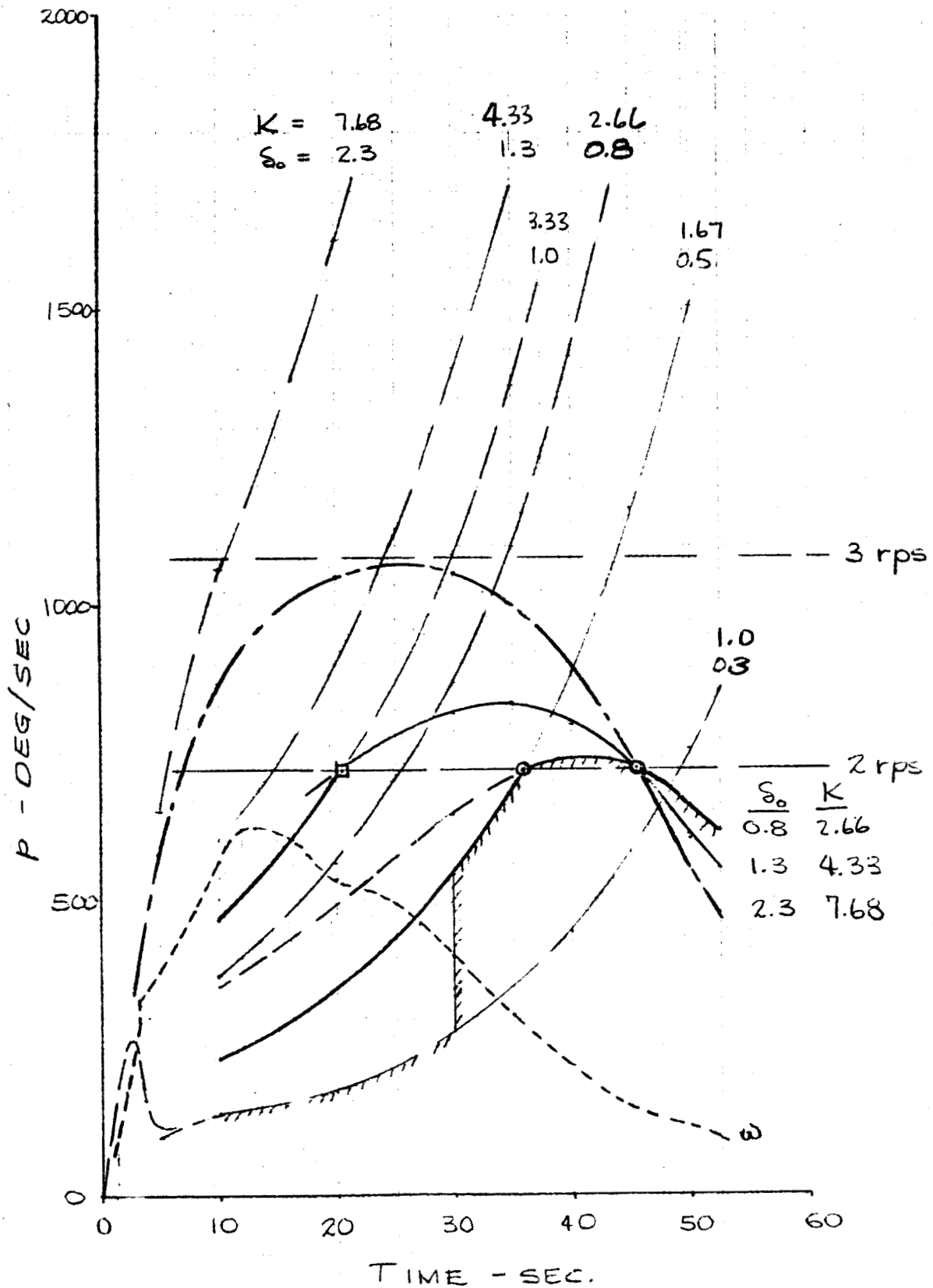


Fig. 3-11

DESIGN COMPARISON

Device	Number Required	Location	Weight (lb)	Timer Events	Power Watts (at 18.5 v DC)	Comments
Roll Reaction	2	Fins	17	1	0.5	Simple
Pitch Reaction	4	Fins	33	1	1.0	Sense Direction
C.G. Shift	4	Fins	101	0	0	Heavy - No Timing
Tip Glove	2	Fins	27	2	1.0	Increases Fin Thickness
Spoiler	2	Fins	6	2	1.0	Aeroelastic Reduction
Tip Aileron	2	Fins	10	2	1.0	Aeroelastic Increase
Gyro Aileron	2	Fins	13	0	0	Roll Programming No Timing